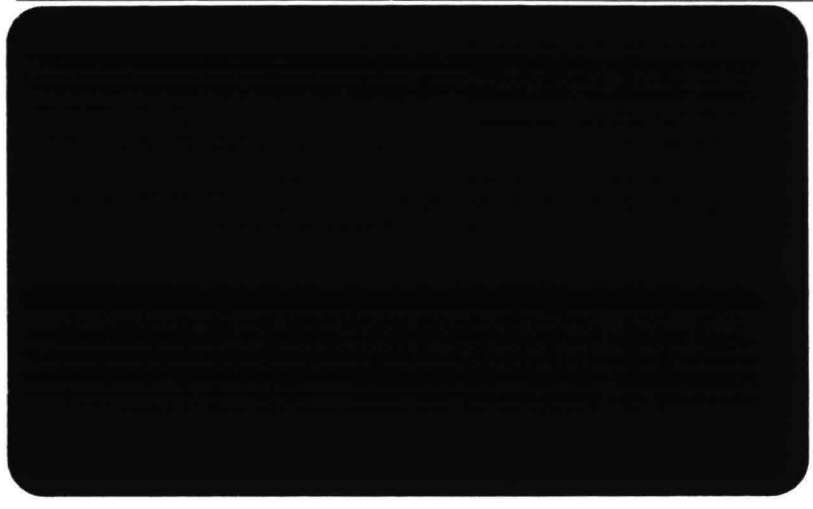

TU Delft
Delft University of Technology

Faculty of Civil Engineering
Department Hydraulic Engineering

Suspended-load experiments in a curved flume, run no. 3

A.M. Talmon and J. de Graaff

report no. 7-89, December 1989

part of:
STW-project; River bend morphology with suspended sediment.

Delft University of Technology
Faculty of Civil Engineering
Hydraulic Engineering Division

ABSTRACT

A laboratory experiment in a 180 degree curved flume with a mobile bed and suspended sediment transport is described. The flow is steady.

The bed topography is measured by means of a profile indicator. The bed topography is characterized by a slowly damped oscillation of the transverse bed slope. Downstream of the bend entrance a pool and a submerged point-bar are present, here the radial bed slope is maximal. Further downstream the transverse bed slope decreases and subsequently increases again. No axi-symmetrical part is present. The bed topography is very similar to the topography of an earlier experiment.

Suspended sediment concentrations are determined by the method of siphoning and by optical measurement. Concentration verticals are measured throughout the whole bend (at 1/4, 1/2 and 3/4 of the channel width). At one specific location a denser measuring grid is used.

CONTENTS

LIST OF TABLES

LIST OF FIGURES

LIST OF SYMBOLS

a	local ensemble mean water depth	[m]
a'	local fluctuation of bed level	[m]
a_0	mean water depth of cross-section 1 to 5 (in earlier reports: mean depth at cross-section 1)	[m]
$\hat{a}$	complex amplitude of bed oscillation	[-]
A	critical mobility number	[-]
B	mobility parameter; $B = \tau_{cr}/(\mu\tau)$	[-]
c	local concentration	[g/l]
c_r	concentration at reference level	[g/l]
$\bar{c}$	local depth averaged concentration	[g/l]
$\bar{c}_{tr}$	total transport concentration; $\bar{c}_{tr} = Q_s/Q_w \; 10^{-3}$	[g/l]
$\bar{c}_{trb}$	transport conc. of bed-load; $\bar{c}_{trb} = S_{s\ bed}/(\bar{u}a_0) \; 10^{-3}$	[g/l]
$\bar{c}_{trs}$	transport conc. of suspended-load; $\bar{c}_{trs} = S_{s\ sus}/(\bar{u}a_0) \; 10^{-3}$	[g/l]
C	parameter in Ackers White formula	[-]
C	Chézy coefficient, with $d=a_0$; $C = \bar{u}/\sqrt{(di)}$	$[m^{0.5}/s]$
d	a representative water depth	[m]
D_{gr}	dimensionless grain diameter; $D_{gr} = D_{50}(\Delta g/\nu^2)^{1/3}$	[-]
D_g	geometric mean grain diameter; $D_g = \sqrt{(D_{84}/D_{16})}$	[m]
D_p	grain size for which p% of the grains is smaller than D_p	[-]
D_{50}	median grain size	[m]
D_s	sedimentation diameter	[m]
F_g	grain Froude number	[-]
F_{g0}	critical grain Froude number	[-]
F_{gr}	grain mobility number	[-]
Fr	Froude number, with $d=a_0$; $Fr = \bar{u}/\sqrt{(gd)}$	[-]
G	coefficient in gravitation term	[-]
H	depth of the flume	[m]
i	water surface slope	[-]
k	complex wave number	[1/m]
k_b	wave number in transversal direction	[1/m]
k_{sn}	secondary flow convection factor	[-]
L_c	arc length of the bend	[m]
L_{cs}	length scale of adaptation of concentration	[m]
m	parameter in Ackers White formula	[-]
n	parameter in Ackers White formula	[-]
n	coordinate in transverse direction	[m]
P	wetted perimeter	[m]

Q_w	water discharge	[m³/s]
Q_s	sediment discharge	[g/s]
r_u	profile function of the velocity profile	[-]
r_c	profile function of the concentration profile	[-]
R_c	radius of curvature of axis of flume	[m]
R_g	grain Reynolds number; $R_g = \sqrt{(gD_{50}^3)}/\nu$	[-]
s	coordinate in streamwise direction	[m]
$S_{s\ sus}$	transport rate of suspended sediment, per unit width, in s-direc.	[g/m/s]
$S_{n\ sus}$	transport rate of suspended sediment, per unit width, in n-direc.	[g/m/s]
S_{tot}	total transport rate, per unit width	[g/m/s]
T	water temperature	[°C]
u	local depth averaged mean flow velocity	[m/s]
$\bar{u}$	overall averaged mean flow velocity: $\bar{u} = Q_w/(Wa_0)$	[m/s]
u_{cr}	critical depth averaged velocity	[m/s]
u_*	bed friction velocity, based on C : $u_* = \sqrt{(u/g)}/C$	[m/s]
W	width of the flume	[m]
w_s	fall velocity of sediment	[m/s]
Z	the Z parameter: $Z = w_s/(\beta\kappa u_*)$	[-]
z_r	reference level	[m]
z_s	surface level	[m]
β	ratio of exchange coefficients of sediment and momentum	[-]
β	coefficient in the bed shear-stress direction model	[-]
κ	von Karman constant	[-]
λ_c	adaptation length of concentration	[m]
λ_s	adaptation length of bed level	[m]
λ_{sf}	adaptation length of bed shear-stress	[m]
λ_w	adaptation length of velocity	[m]
μ	efficiency factor	[-]
ρ	density of water; ρ =1000 kg/m³	[kg/m³]
ρ_s	density of sediment; ρ_s=2650 kg/m³	[kg/m³]
σ_g	gradation of sediment; $\sigma_g = D_{84}/D_{16}$	[-]
τ	total drag	[N/m²]
τ'	effective grain-shear stress; $\tau' = \mu\tau$	[N/m²]
τ_{cr}	critical bed-shear stress	[N/m²]
ν_{tm}	turbulent diffusion coefficient of momentum	[m²/s]
ν_{tc}	turbulent diffusion coefficient of mass	[m²/s]

1. INTRODUCTION

The project at hand is directed towards the computation of river bend morphology in case of alluvial rivers transporting a significant part of their bed material in suspension.

In this report an experiment is described which will serve to calibrate and test morphological models for river bend flow with suspended sediment. The experiment is performed in the curved flume of the Laboratory of Fluid Mechanics. It is the third of a number of successive runs with suspended sediment transport. The steady state bed topography and local concentrations of suspended sediment are measured.

In chapter 2 the laboratory equipment is described briefly. In chapter 3 the properties of the sediment and the overall flow conditions are given. In chapter 4 the results of the measurements of bed topography and concentration are reported. In chapter 5 the results are discussed, attention is being paid to implications regarding the mathematical and numerical simulation of the experiment. In chapter 6 the conclusions are presented.

This research is a part of the project: 'River bend morphology with suspended sediment', project no. DCT59.0842. The project is supported by the Netherlands Technology Foundation (STW).

2. LABORATORY EQUIPMENT

2.1 The flume

The layout of the LFM curved flume is shown in figure 1. Water is pumped from an underground reservoir to an overhead tank and led to the flume. The water discharge is controlled by a valve in the supply pipeline. Sand is supplied to the model 2 m downstream of the entrance of the flume. The sand supply is effectuated by one small hole, 2.5 mm diameter, in the bottom of a container located 0.5 m above the water surface.
After passing the tailgate of the flume, by which the water level is adjusted, the water pours in a settling tank. After passing this tank the water flows back into the underground reservoir.
The dimensions of the flume are:

inflow section length	11.00 m
outflow section length	6.70 m
arc length of the bend	L_c = 12.88 m
radius of the bend	R_c = 4.10 m
width of the flume	W = 0.50 m
depth of the flume	H = 0.30 m

The bottom of the flume is made of glass and the side walls are made of perspex.

2.2 Measuring equipment

2.2.1 Discharge measurement

The discharge is controlled by a valve in the supply pipeline.
The discharge is measured by a volumetric method. A 150 liters barrel is partly filled during about 25 seconds at the downstream end of the flume. The volume is measured and divided by the filling time.

2.2.2 Slope and depth measurements

The measurements of the bottom and water level are performed with an electronic profile indicator (PROVO). From these measurements the longitudinal slope of the water level and the local depth are calculated. This device is traversed in cross-sectional direction. In each cross-section 9 equidistant measuring points are used. The carriage in which the PROVO is mounted is also traversed in longitudinal direction. In longitudinal direction 48 cross-sections are situated, they are indicated in figure 5. The distance between these cross-sections at the flume axis is 0.32 m. The profile indicator is continuously moved in cross-sectional direction, this is achieved by specially developed electronic hardware. The position of the profile indicator is measured electronically. The carriage is moved manually in longitudinal direction.

2.2.3 Concentration measurement by siphoning

Throughout the whole bend sediment concentrations are measured. The sediment concentration is determined from samples siphoned by a tube-pipette of stainless steel (Outside diameter 5 mm, inside diameter 3 mm) shaped much like a pitot tube. The tip of the sampler is flattened in order to minimize the vertical extended of the measuring volume.
To prevent sand to accumulate in the plastic tube it is necessary to increase the sampling velocity. This yields a non-isokinetic sampling velocity slightly higher then the local flow velocity. This does not seriously affect measurements (Talmon and Marsman, 1988).
Measuring periods of about 45 minutes are employed.

2.2.4 Optical measurement of concentration

The optical concentration meter OPCON has not been used.
Although, according to the manual, concentrations are within the measurement range, an electronic drift complicates the application use of the OPCON. Consequently a zero concentration adjustment is made prior to each (45 min) measurement.

The sensitivety of the OPCON is obtained by calibration:
$E = 2.24\ c$, c[g/l], E[V] at output 10x amplifier

2.2.5 Temperature measurements

Temperatures are measured by inserting a thermometer into the flow near the downstream end of the flume. The water temperature during the measurements was $23 \pm 0.5\ ^{o}C$.

2.3 Measuring procedures

The flume is partly filled up with sand. The thickness of the sand bed at the entrance of the flume is 0.11 m, at the exit the bed thickness is about 0.06 m.
The sand supply is measured daily. The sand settled in the settling tank is gathered at regular intervals (about 100 hours) and is weighed under water. The results are converted to equivalent weights of dry sand. The supply rate is adjusted such that the supply rate and the discharge rate balance approximately.
The water surface slope in longitudinal direction is measured daily. After about 250 hours of flow, measurement of the bed topography and the concentration are started when steady conditions are established. At that stage no significant changes of the water surface slope and differences between in and outflow of sand are measured.
The stationary bed topography is obtained by ensemble averaging of 10 measuring sessions. A measuring session consists of a water level - and a bed level measurement. The water level is measured during flow conditions. After closing the tailgate and filling the flume with water (about 100 mm above the bed level), the bottom is measured. This procedure to measure the bed topography is necessary, because the PROVO needs a minimal water depth of 25 mm. One measuring session takes about one hour. The average time interval between the first 5 sessions is about 5 hours. Time lapse between sessions 5 and 6 is 200 hours (during which the concentration measurements were performed.). The interval between the last 5 sessions is also 5 hours.

Each session consists of 2 * 48 cross-sectional traverses (one bed and one water level measurement). Within a cross-section 9 measuring points are used. The data are digitized and stored at a local data-acquisition system which uses a HP1000 mini computer. Next, the data are processed by a central main frame IBM computer of the Delft University. From the mean water level in each cross-section the longitudinal slope is determined. Comparing the results of each measuring session, only local differences in the water level slope are noticed.

Most sediment concentration profiles are taken at the cross-section numbers 1, 5, 10, 15, 20, 25, 30, 35, 40, 45 (see figure 5).
In a vertical, depending on the local water depth, 5 to 40 samples are taken. The samples are siphoned into buckets. With a measuring time of 45 minutes about 9 liters water are gathered. The sample is weighed to determine the volume. Then the water is separated from the sediment. The sediment is weighed under water with an electronic balance (Mettler PE 360). Weights are read with an accuracy of 10 mg. The results are converted to equivalent weights of dry sand.
Near the bed it is not possible to apply this method, because of propagating bed forms.

The OPCON is applied in cross-sections 1 to 25. With this apparatus concentration measurements somewhat closer to the sediment bed are possible. An eventual bed-form passing the probe blocks the ligth beam, which is immediately noticed by the experimentator because of an excessive high output voltage of the OPCON.

3. FLOW AND SEDIMENT CONDITIONS

3.1 The sediment

3.1.1 Sieve curve

The sediment used in the flume has also been used in the previous experiments: run no. 1 (Talmon and Marsman, 1988) and run no. 2 (Talmon, 1989a). At the end of the present experiment sediment samples were collected from three different sources: the sand supply container, the upper layer of the sediment bed and sediment which is transported in suspension. Figure 2 shows the cumulative probability distributions of the grain sizes of these sediment samples. Characteristic grain diameters are:

	D_{10}[μm]	D_{16}[μm]	D_{50}[μm]	D_{84}[μm]	D_{90}[μm]	D_g[μm]	σ_g
bed layer :	76	83	110	>150	>150	>110	>1.8
supply cont. :	69	74	90	113	122	91	1.53
suspended sed.:	62	65	81	101	108	81	1.55

The quantity D_p is defined as the grain size for which p % of the total mixture volume is smaller then D_p.
The geometric mean diameter is defined by: $D_g = \sqrt{(D_{84}D_{16})}$
The gradation of the sediment is defined by: $\sigma_g = D_{84}/D_{16}$
These results indicate that some grain sorting has taken place during the course of the experiments. The sediment of the bed layer has a relatively large amount of course particles. This could be due to the use of non-cleaned containers during the sand handling routine.

3.1.2 Fall velocity

The fall velocity of the suspended sediment is determined in a settling tube. This is a device to determine the fall velocity distribution of particles in a sample. At the lower end of the settling tube the sediment particles accumulate on a very sensitive weighing device. A cumulative weight distribution of the sample as a function of the measuring time is obtained. This distribution is converted into the fall velocity distribution of the sample using the height of the settling tube (Slot and Geldof, 1986).

A sample is extracted from the supply container and samples of suspended sediment are siphoned at cross-section 1. These are siphoned at the centerline 10, 20, 30 and 40 mm below the water level. The sediment is gathered during 24 hours. The samples are dried and split into amounts that can be used in the settling tube. The sample taken 40 mm below the water is discarded because some course material (bed layer material) is present.

Figure 3 shows the probability distribution of the fall velocity of sediment originating from the supply container.

The mean fall velocity, at 20^0C, of sediment origination from the supply container is: $w_s = 0.0080$ m/s. The mean fall velocity, at 20^0C, of suspended sediment is: $w_s = 0.0073$ m/s. At higher temperatures the fall velocity increases; 2% per ^{0}C. The sedimentation diameter is: $D_s = 96$ μm. (Slot, 1983)

3.2 Flow conditions

The flow conditions are given in table 3.1a and 3.1b. The values of parameters determined by measurement are given in table 3.1a. The values of parameters obtained by calculation are given in table 3.1b. The Vanoni and Brooks (1957) correction method for side wall effects is not applied because the parameters are hardly affected ($W/a_0 > 5$).

Table 3.1a Measured parameters

Q_w = 0.0050	[m^3/s]	
W = 0.50	[m]	
a_0 = 0.051	[m]	
i = 2.05 10^{-3}	[-]	
D_{50} = 90	[μm]	(supply)
w_s = 7.7 10^{-3}	[m/s]	(23^0C susp.)
Q_s = 0.53	[g/s]	
T = 23.5	[^{o}C]	

Table 3.1b Calculated parameters

$\bar{u} = Q_w/(Wa_0)$	= 0.196	[m/s]
$\bar{c}_{tr} = (Q_s/Q_w)10^{-3}$	= 0.106	[g/l]
$C = \bar{u}/\sqrt{(a_0 i)}$	= 19.2	[$m^{0.5}$/s]
$Fr = \bar{u}/\sqrt{(ga_0)}$	= 0.28	[-]
$\theta = a_0 i/(\Delta D_{50})$	= 0.70	[-]
$u_* = (\bar{u}\sqrt{g})/C$	= 0.032	[m/s]
D_s = 96 [μm]	(susp., sec. 3.1.2)	
$Z = w_s/(\beta\kappa u_*)$	= 0.33	(sec. 4.2.2)

4. RESULTS

4.1 Depth measurements

4.1.1 Mean depth

The ensemble relative water depth of the 10 measuring sessions are tabulated in appendix A. Figure 5 shows the ensemble averaged contour line map of the relative water depth (normalized with the mean water depth of cross-section 1). The contour lines are drawn at intervals of $\Delta a/a0 = 0.2$. The relative depth, at 0.3 W, 0.5 W and 0.7 W, as a function of longitudinal distance is depicted in figure 6. Figures 7a to 71 show the ensemble averaged flow depths of each cross section.

A maximum of the transversal bed slope occurs at cross sections 15 to 17. A minimum of the transversal bed slope occurs at cross sections 25 to 30. Further downstream the transversal bed slope increases again, up to cross-section 45, which is also the end of the bend. The bed topography of the bend is characterized by a slowly damped oscillation of the radial bed slope in downstream direction. The bed topography is comparable with run no.1 (Talmon and Marsman, 1988).

4.1.2 Bed form statistics

The bed consists of bed forms moving downstream. The height of the bed forms is a significant fraction of the flow depth. These bed forms cause a significant form drag. This is reflected in the low Chézy value; $C \approx 20\ m^{0.5}/s$. The large dimensions of the bed forms also affect the choice of reference level, i.e. the level above which the sediment is considered to be transported as suspended load and below which the sediment is considered to be transported as bed-load transport.
To guide the choice of reference level the probability distribution of bed form height is calculated. This is achieved as follow: In a selected region of the flume, the data of all individual local depth measurements is gathered and normalized with their local ensemble averaged value: a'/a. (at each location 10 data points are available.)

Two regions have been selected, each possessing local ensemble averaged water depths about equal to a_0.

- The inflow section, cross section 1 to 5; 450 data points
- The centerline of the channel ; 480 data points

The probability distributions of the water depth of both regions are shown in fig. 8. Both distributions are very similar. These distributions, assuming steady state of the bed, equal the bed form height distributions. In fig. 8 also the 5% and 10% exceedance levels of bed form height are indicated. These are within the range: 0.15a to 0.20a. (In run no. 1, which has a higher sediment transport rate, the bed form height is larger. The 5% and 10% exceedance levels are in the range: 0.20a to 0.30a.)

The bed form statistics are also calculated in the region cross-section 30 to 45. This is documented in appendix C, the results are depicted in fig. C1. These calculations serve to test two hypothesis (data from run 2 is also used):

A: The absolute bed form height is constant in transversal direction.

B: The relative bed form height is constant in transversal direction. The bed form height is normalized with the local mean water depth.

The conclusion is that both hypotheses can neither be affirmed or rejected.

4.2 Concentration measurements

4.2.1 Mean concentration

The mean concentrations are tabulated in appendix B.

The figures 9a - 9i show the concentration profiles of respectively the cross-sections 1, 5, 10, 15, 20, 25, 30, 35, 40, 45.

4.2.2. Curve fit of equilibrium concentration profile

The straight reach prior to the bend entrance serves to establish flow and sediment conditions which are in equilibrium with the local

conditions, i.e. the flow and concentration fields are independent of streamwise coordinates. The length of this reach is sufficient (Talmon and Marsman, 1988).

To establish the values of parameters of the concentration vertical at equilibrium conditions the measurements in the straight reach are used (cross-sections 1 and 5)
The Rouse concentration profile is fitted with the measurements. This profile is based on the parabolical function for the turbulent exchange coefficient over the vertical.
The parameters of the concentration vertical are:

- the choice of reference height z_r/a
- the concentration at reference height c_r
- The Z parameter, $w_s/(\beta\kappa u_*)$

The concentration profile is given by:

$$c = c_r\left(\frac{z_r}{a_0-z_r}\,\frac{a_0-z}{z}\right)^Z \qquad (4.1)$$

Curve fitting has been performed with the aid of a computer program which, given z_r, estimates the Z and c_r parameters of eq.(4.1). A least squares method is employed. Results are given in table 4.1. About 5% of the time the bed form height is larger than 0.20, see fig. 8. Therefore a reference height of $\gtrsim$ 0.15a should be appropriate. The curve fits of the concentration data at cross-sections 1 and 5 are given in fig. 10, a reference height of z_r/a_0=0.15 is applied. The relevant parameters are given in table 4.1.

Table 4.1 Parameter sets of the equilibrium concentration profile

	z_r/a_0[-]	c_r[g/l]	Z [-]	$\bar{c}$ [g/l]
cross-sec. 1	0.15	0.18	0.33	0.096
cross-sec. 5	0.15	0.18	0.33	0.096

The estimated Z parameter of the concentration vertical is: Z=0.33. The standard deviation is: σ_Z= 0.02. The reference concentration will vary with the choice of reference level. The depth-averaged concentration

given in table 4.1 is the integral of the concentration curve eq. (4.1) , section 4.2.3.

4.2.3. Depth-averaged concentrations

The results of the experiment will be used to test depth-averaged mathematical models. To that purpose depth-averaged values of concentration have to be computed. The depth-averaged value of the concentration is defined by:

$$\bar{c} = \frac{1}{a-z_r} \int_{z_r}^{a} c \, dz \qquad (4.2)$$

with: a = local flow depth

z_r = reference level, close to the bed

The choice of reference level is uncertain. This level will be located near the top of the bed forms. Concentration measurements below $z/a \lesssim 0.10$ were troubled by the presence of bed forms. Consequently depth-averaged concentrations have been computed for $z_r/a = 0.10$, 0.15 and 0.20

The depth-averaged concentration of a vertical is computed by:

$$\bar{c} = \frac{1}{j_{max}} \sum_{j=1}^{j_{max}} c_j \qquad (4.3)$$

with j_{max} the number of measurements above z_r

For a very large number of data points, uniformly distributed over the depth, the summation series converge to the definition (4.2). The available number of data points is, however, limited. Measurements are taken with a vertical increment in vertical direction of 5 mm. At each x,y,z location two or more measurements have been performed.

The depth-averaged concentration data, for $z_r/a = 0.10$, 0.15, and 0.20 are given in table 4.2. The depth-averaged concentration as function of the longitudinal coordinate, for $z_r/a = 0.15$ is given in figure 12.

Table 4.2 Depth-averaged concentrations in the 180 degree bend

cross-sec. no.	$\bar{c}$ (1/4 W)	$\bar{c}$ (2/4 W)	$\bar{c}$ (3/4 W)	
1	0.000	0.096	0.000	reference level at:
5	0.000	0.095	0.000	$z_r/a = 0.10$
10	0.089	0.102	0.102	
15	0.087	0.100	0.104	
20	0.060	0.137	0.103	
25	0.039	0.077	0.088	
30	0.048	0.091	0.115	
35	0.061	0.099	0.096	
40	0.058	0.076	0.097	
45	0.078	0.074	0.096	
1	0.000	0.093	0.000	reference level at:
5	0.000	0.093	0.000	$z_r/a = 0.15$
10	0.087	0.102	0.094	
15	0.087	0.095	0.093	
20	0.060	0.128	0.087	
25	0.039	0.077	0.088	
30	0.048	0.085	0.103	
35	0.052	0.096	0.096	
40	0.054	0.076	0.097	
45	0.041	0.074	0.096	
1	0.000	0.093	0.000	reference level at:
5	0.000	0.093	0.000	$z_r/a = 0.20$
10	0.087	0.102	0.091	
15	0.087	0.095	0.088	
20	0.060	0.128	0.087	
25	0.039	0.071	0.086	
30	0.048	0.136	0.103	
35	0.052	0.085	0.096	
40	0.054	0.076	0.097	
45	0.041	0.074	0.096	

4.2.4 The concentration field at cross-section 40

The bed topography of the experiment is less damped than in the preceeding experiment: run no. 2. In run no. 2 cross-section 40 was considered axi-symmetrical. Extended measurements of the concentration field at cross section 40 are performed. Although the bed-topography indicates that the axi-symmetrical case has not been reached at this location the concentration field could probably be considered as close to axi-symmetrical.

In fig. 11a and 11b the concentration verticals of cross section 40 are given. The concentration verticals have been measured at 1/8, 2/8, 3/8, 4/8, 5/8, 6/8 and 7/8 of the channel width.

An iso-concentration contour representation of the concentration field at cross-sections 40 is given in figure 11c. The contour plot is made by linear interpolation between the data points. The contour interval is 0.02 g/l.

The lowest concentrations are found in the inner part of the bend. In the upper part of the flow up to Y = 0.75 W the concentrations remain almost constant in transversal direction (a slight increase is noticed). In the region Y > 0.75 W the concentrations decrease with Y.
Unfortunately in the region 0.5 < Y/W < 0.8, near the bed, concentration data is lacking. The near bed concentration in the inner part of the bend is circa 1/2 of the near bed concentration in the outer part of the bend.

5 DISCUSSION

5.1. Introduction

The general purpose of the experiment is to provide data on which numerical and analytical morphological models, including suspended sediment transport, can be calibrated and verified.

Important input parameters of morphological models are:

- The percentage of suspended sediment transport
- The shape of the equilibrium concentration profile
- A transport formula

These subjects are discussed in sections 5.2, 5.3, 5.4 and 5.5. The bed form classification is investigated in sec. 5.6. Adaptation lengths of flow, bed level and concentration are calculated in sec. 5.7. The bed topography is discussed in sec. 5.8. Also a mathematical approximation of the bed topography is given. The concentration field at cross-section 40 is discussed in sec. 5.9. When a depth averaged morphological model is used, which will be the case at the present state (1989) of computer facilities, depth averaged concentrations are of interest. The depth averaged values of concentration are calculated in sec. 5.10.

5.2. The Z parameter

Curve fitting of the concentration profile prior to bend entrance yields a Z parameter of 0.33 (sec. 4.2.2.). The Z parameter is defined by: $Z = w_s/(\beta\kappa u_*)$. The Z parameter is a measure of the ratio of the downward flux by the fall velocity w_s and the upward flux by turbulent diffusion. Turbulent diffusion of sediment is modelled by:

$\nu_{tc} = \beta\, \nu_{tm}$, with ν_{tm} = turbulent diffusion of momentum

ν_{tc} = turbulent diffusion of mass (sediment)

It is generally accepted that the turbulent diffusion coefficient of mass is greater than of momentum (Csanady 1973). Consequently $\beta>1$. In the experiment, upward of the bend entrance the wall shear velocity is

equal to $u_* = 0.032$ m/s while the fall velocity of the suspended sediment is: $w_s = 0.0077$ m/s (sec. 3.1.2.). This yields $\beta \approx 1.8$

Based on a large data set van Rijn (1982) has calculated β by fitting the data with concentration verticals which are based on a parabolical-constant profile for the turbulent diffusion coefficient ν_{tc}. (The present curve fitting is based on a parabolical profile for ν_{tc}). For $w_s/u_* = 0.0077/0.032 = 0.24$ van Rijn reports effective β values of 1.0 and 1.7 for the experiments of Coleman (1970).
Hinze (1959) reports values of the turbulent Prandtl number $Pr_{turb} = 1/\beta$ of 0.65 to 0.72 (β=1.4 to 1.5) for various measurements on the distribution of heat and matter in pipe flow and two-dimensional channels.

5.3. Percentage of suspended sediment transport

The percentage of suspended sediment transport upstream of the bend is an important physical parameter in the experiment.
The division between bed and suspended load transport is somewhat arbitrary and is effected by the choice of reference level. The amount of suspended sediment transport per unit width is defined by:

$$S_{s\ sus} = \int_{z_r}^{z_s} u\ c\ dz \qquad (5.1)$$

Two methods will be employed to estimate the suspended sediment transport:

1 - Based on curve fitting of the concentration profile upstream of the bend entrance. By integration of the product of the mathematical functions of u and c, over the suspended load region, the suspended sediment transport is calculated.

2 - Based on an estimate of the depth-averaged concentration, multiplied by the depth-averaged velocity.

Method 1

The suspended sediment transport rate per unit width is equal to:

$$S_{s\ sus} = \bar{u}\,\bar{c}\int_{z_r}^{z_s} r_u r_c\,dz = (a_0-z_r)\bar{u}\,\bar{c}\int_0^1 r_u r_c\,d\zeta = (a_0-z_r)\bar{u}\,\bar{c}\,\alpha_s \qquad (5.2)$$

with: r_u, r_c shape functions of velocity and concentration

The total transport rate per unit width is equal to:

$$S_{tot} = a_0\bar{u}\,\bar{c}_{tr} \qquad (5.3)$$

in which: $\bar{c}_{tr}$ = the transport concentration defined by eq.(5.3)

The results for $0.1 < z_r/a_0 < 0.2$ are given in table 5.1.

Table 5.1 Fraction of suspended sediment transport in cross section 1, by method 1

	Z=0.33		
z_r/a_0	$\bar{c}$ [g/l]	$S_{s\ sus}/S_{tot}$	$S_{s\ sus}/S_{tot}$
0.10	0.102	0.87	0.96
0.15	0.099	0.77	0.85
0.20	0.091	0.68	0.75
		$\alpha_s = 1$	$\alpha_s = 1.1$ (Z=0.35, C=20 $m^{0.5}/s$)

Method 2

The suspended sediment transport per unit width is approximated by:

$$S_{s\ sus} \approx \frac{1}{z_s-z_r}\int_{z_r}^{z_s} u\,dz \int_{z_r}^{z_s} c\,dz \approx (z_s-z_r)\,\bar{u}\,\bar{c} \qquad (5.4)$$

The depth-averaged concentration $\bar{c}$ is computed by the method outlined in subsection 4.2.3. Dividing the suspended sediment transport by the total sediment discharge at channel exit, yields the fraction of suspended sediment transport (table 5.2).

Table 5.2 Fraction of suspended sediment transport, in cross section 1, by method 2

z_r/a	$\bar{c}$[g/l]	$S_{s\ sus}/S_{tot}$
0.10	0.096	0.82
0.15	0.093	0.75
0.20	0.093	0.70

Both methods involve some disadvantages.
Method 1 is based on curve fitting of the concentration profile. This fitting will be affected by the non-homogeneous distribution of measuring points in the vertical. Consequently the integral of the concentration profile will be affected also, even though by integrating the profile all points in the vertical are weighed equally.
Method 2, which yields a rough estimate of the depth-averaged concentration, favours the region were many measuring points are taken. In computing the depth integrated suspended transport the shape of the concentration and velocity profiles are neglected.
Based on the results given in table 5.1 and 5.2 it is concluded that the percentage of suspended transport is within the range: 70...80 % .

5.4 Transport formulae

To simulate the experiment numerically or analytically a transport formula is necessary to predict concentration and sediment transport rates. In this section the overall transport rate of the experiment is compared with some transport formulae known from literature. It is common practice to express the total sediment transport rate in the transport concentration: $\bar{c}_{tr} = Q_s/Q_w$ ($S_{tot} = \bar{c}_{tr} \bar{u}\, a_0$ [g/m/s]). The measured transport concentration is equal to: $\bar{c}_{tr} = 0.106$ g/l.
The sediment transport in the experiment is about 1/6 of the transport in run no. 1 which has a comparable bed topography.

The transport formulae of Engelund and Hansen (1967), Ackers and White (1973), Brownlie (1981) and Van Rijn (1984c) will be evaluated.
These formulae are often employed outside their range of applicability, yielding reasonable results. The Ackers White and Brownlie formulae are

based on data sets which include data of laboratory flumes with fine sediments.

The Engelund Hansen formula reads:

$$\phi = \frac{0.05}{1-\Gamma} \frac{C^2}{g} \theta^{2.5}, \quad \text{with } \theta = \frac{di}{\Delta D_{50}}, \; \phi = \frac{S}{\sqrt{(\Delta g D^3)}}, \tag{5.6a}$$

$$\text{or: } \bar{c}_{tr} = \rho_s \frac{1}{\bar{u} a_0} 0.05 \sqrt{(\Delta g D_{50}^3)} \frac{C^2}{g} \theta^{2.5} \tag{5.6b}$$

The predicted transport concentration is: $\bar{c}_{tr} = 0.63$ g/l
(for D_{50} the value of the supply container is used)

The Ackers White formula reads:

$$\bar{c}_{tr} = \rho_s \frac{D_{50}}{a_0} \left(\frac{\bar{u}}{u_*}\right)^n C \left(\frac{F_{gr}}{A} - 1\right)^m \tag{5.7}$$

with: $F_{gr} = \frac{1}{\sqrt{(\Delta g D_{50})}} u_*^n \left(\frac{\bar{u}}{\sqrt{32} \log (10 a_0 / D_{50})}\right)^{1-n} = 0.73$

$A = 0.23/\sqrt{D_{gr}} + 0.14 = 0.294$

$n = 1.00 - 0.56 \log D_{gr} = 0.806$

$m = 9.66/D_{gr} + 1.34 = 5.69$

$C = 10^{(2.86 \log D_{gr} - \log^2 D_{gr} - 3.52)} = 0.0022$

$D_{gr} = D_{50} (\Delta g/\nu^2)^{1/3} = 2.22$

According to White (1972) the formula is fitted to data for which no side wall correction method has been employed, i.e. $d=a_0$. In the publication of Ackers and White (1973), however, d is defined by d=A/P, while the same transport formula is reported. (P = wetted perimeter) Following the original work of White (1972) $d=a_0$ is used in eq.(5.7). This yields a transport concentration equal to: $\bar{c}_{tr} = 0.29$ g/l

The Brownlie formula reads:

$$\bar{c}_{tr} = 7115 (F_g - F_{g0})^{1.978} i^{0.6601} (r_b/D50)^{-0.3301} \quad [\text{mg/l}] \tag{5.8}$$

with: $F_g = \frac{\bar{u}}{\sqrt{(\Delta g D_{50})}}$ grain Froude number

$F_{g0} = 4.596 \, \theta_{cr}^{0.5293} \, i^{-0.1405} \, \sigma_g^{-0.1606}$ critical grain Froude number

$\theta_{cr} = 0.22 \, Y + 0.06 \, (10)^{-7.7 \, Y}$ critical Shields number

$Y = (\sqrt{\Delta} \, R_g)^{-0.6}$

$R_g = \sqrt{(gD_{50}^3)}/\nu$ grain Reynolds number

r_b = 0.051 [m], hydraulic radius related to the bed according to Vanoni and Brooks (1957), here a_0 is used.

Prediction with this formula yields: $\bar{c}_{tr}$= 0.062 g/l

The Van Rijn (1984c) formulae read:

bed-load: $$\bar{c}_{trb} = \rho_s \, 0.005\left(\frac{u-u_{cr}}{\sqrt{(g\Delta D_{50})}}\right)^{2.4} (D_{50}/a_0)^{1.2} \qquad (5.9a)$$

suspended-load: $$\bar{c}_{trs} = \rho_s \, 0.012\left(\frac{u-u_{cr}}{\sqrt{(g\Delta D_{50})}}\right)^{2.4} D_{50}/a_0 \; d_*^{-0.6} \qquad (5.9b)$$

total load: $\bar{c}_{tr} = \bar{c}_{trb} + \bar{c}_{trs}$

with: $d_* = D_{50}\sqrt[3]{(\Delta g/\nu^2)}$

$u_{cr} = 0.19 \, D_{50}^{0.1} \log (12r_b/(3D_{90})) = 0.251$ m/s

The transport predicted with these formulae is equal to: $\bar{c}_{tr} = 0$

This is caused by: $u_{cr} > u$

Unfortunate none of these transport formulae predicts the actual transport concentration of the experiment. It can be argued that Engelund Hansen and Van Rijn are applied outside their ranges of applicability. The Ackers White and Brownlie formulae, however, are applied within their ranges of application.

The Ackers White formula overpredicts the transport concentration by a factor 2, whereas the Brownlie formula underpredicts the transport concentration by a factor 0.5.

Prediction of the ratio of suspended-load and total-load can be accomplished by the equations of Van Rijn eq.(5.9a,b). Due, however, to $u_{cr} > u$ this is impossible.

Van Rijn (1984b) has calculated the ratio of suspended-load and total-load of measurements reported by Guy et.al. (1966). It is noticed that for $u_*/w_s > 3$ more than 50% suspended-load is present. This is in accordance with the results of the experiment: u_*/w_s= 4.2, $S_{s\,sus}/S_{tot} \approx$ 0.75

The performance of the transport formulae with regard to this experiment is comparable to the performance of the formulae in case of the suspended load experiment run no. 1 and 2.

5.5. Bed-shear stress and sediment transport

In case of a dune covered bed the bed resistance consist of bed shear stress (friction drag) and of a pressure gradient generated by the dunes (shape drag). The total drag (which actually consist of friction and shape drag) is defined by: $\tau=\rho gai$

The process of sediment transport is caused by the shear stress acting on the grains. The shear stress related to sediment transport is given by: $\tau'=\mu\tau$

in which: μ - efficiency factor

τ' - effective grain-shear stress

τ - total drag.

To initiate sediment transport the shear stress has to exceed a critical value: τ_{cr}.

In the experiment both μ and τ_{cr} are unknown.

One of the reasons of the poor performance of the transport formulae could be caused by the relatively high resistance ($C\approx 20\ m^{0.5}/s$). The data on which the transport formulae have been developed generally relate to less resistance ($C\gtrapprox 30\ m^{0.5}/s$). The transport formulae implicitly, or explicitly, contain the ratio of friction and total drag. This ratio could differ under the present conditions (the relatively large bed form height is quite exceptional). Consequently the effective grain-shear stress will differ also.

In the following sediment transport related parameters μ and θ_{cr} are estimated with the aid of some empirical formulae known from literature.

The transport formulae which incorporate the critical bed-shear stress are generally proportional with:

$$\left(\frac{\mu\tau-\tau_{cr}}{\tau_{cr}}\right)^b = \left(\frac{\mu\theta-\theta_{cr}}{\theta_{cr}}\right)^b = \left(\frac{1-B}{B}\right)^b \qquad (5.10a)$$

or:

$$(F_g - F_{g0})^b = \left(\frac{u - u_{cr}}{\sqrt{(g\Delta D_{50})}}\right)^b = (1-\sqrt{B})^b \left(\frac{C}{\sqrt{g}}\sqrt{\theta}\right)^b \qquad (5.10b)$$

in which: $B = \frac{\tau_{cr}}{\mu\tau}$, mobility parameter (5.10c)

Both unknown parameters are now incorporated in the B parameter.

Three methods are used to estimate B. The methods are:

1)- The set of transport formulae by Van Rijn (1984c), eq.(5.9a,b), is used to relate the total transport concentration c_{tr} and the B parameter. Substitution of the calculated c_{tr} value yields B.

2)- The bed load transport formula by Van Rijn (1984a), eq.(5.10) is used to relate the bed-load transport concentration and the B parameter. Substitution of the calculated c_{trb} value yields B.

$$c_{trb} = \frac{\rho_s}{a\ u}\ 0.053\ \sqrt{(\Delta g)}\ \frac{D_{50}^{1.5}}{d_*^{0.3}}\ \left(\frac{1-B}{B}\right)^{2.1} \quad [g/l] \qquad (5.11)$$

3)- A relation to estimate the critical Froude grain number by Brownlie (1981) is used.

$$F_{g0} = 4.596\ \theta_{cr}^{0.5293}\ i^{-0.1405}\ \sigma_g^{-0.1606} \qquad (5.12)$$

This relation has been obtained by Brownlie by manipulation of an empirical function which was derived to predict the flow depth. (The Brownlie depth prediction for this experiment is 140 % too large). With the aid of eq.(5.10b) B is calculated.

According to the Shields diagram the critical Shields number of the sediment is: $\theta_{cr} = 0.11$ (smaller θ_{cr} values have also been reported; Mantz (1977), $D_{50} = 77, 93\ \mu m$, $\theta_{cr} = 0.096$).

The methods are applied to the data of the present experiment and of the previous experiments run no. 1 and run no. 2. The results are given in table 5.3. A median grain diameter of $d_{50} = 90\ \mu m$ is applied.

Table 5.3 The mobility number B

run no. 1	method 1	method 2	method 3
B	0.29	0.29	0.20
μ (at θ_{cr}=0.11)	0.33	0.33	0.48
remark		60 % susp. transp.	depth prediction 60 % too large

run no. 2	method 1	method 2	method 3
B	0.44	0.32	0.30
μ (at θ_{cr}=0.11)	0.29	0.41	0.43
remark		65 % susp. transp.	depth prediction 30 % too large

run no. 3	method 1	method 2	method 3
B	0.51	0.54	0.36
μ (at θ_{cr}=0.11)	0.31	0.29	0.44
remark		75 % susp. transp.	depth prediction 140 % too large

The third method, Brownlie's method, is closely related to Brownlie's water depth prediction. Considering the large error in the depth prediction, in at least the present experiment, the estimate of μ is questionable. The results of the first two methods are comparable. The μ parameter is calculated by eq.(5.10c). The μ parameter of all three experiments is within the range: $0.3 < \mu < 0.4$. The Van Rijn (1984a) model for μ, which is applied in the Van Rijn transport formulae, yields a distinct result: $\mu = (C/C')^2 = (20/60)^2 = 0.11$. These results indicate that the estimate of μ, implicitly or explicitly contained in the transport formulae, could be erroneous.

The estimated value of μ indicates that in this experiment about 30 % of the total drag is available for sediment transport.

5.6. Bed form classification

The structure of the sediment bed is known to depend on many variables. In order of increasing flow velocity the bed forms are nowadays usually classified in the following range: plane bed, ripples, dunes, transition, plane bed, anti dunes.
In 1966 the definitions of these bed forms have been set by the ASCE task force on bed forms ASCE (1966). In Vanoni (1977, p 119) a summary is given. In case of bed material greater than 0.45 mm the ripple phase does not exist (Simons and Richardson 1961). The plane bed occurs under two different circumstances. At relatively low flow velocities, which yield small sediment transport rates, and at relatively high velocities for which the Froude number is near Fr=1.
The experiment's Froude number is Fr=0.4, consequently the bed forms should be classified either ripples or dunes.

The observed bed form length, by visual inspection, in the experiment is in of order 0.10 to 0.20 m. The bed form height is about 0.02 m (It is not possible to determine the average height of the bed forms on basis of fig. 8, because it is only a statistical manipulation of a quasi random sampled water depth data).

A classification diagram has been given by Simons and Richardson (1966) (also Vanoni, 1977 p 165). The bed form classification is given as a function of the diameter of the bed material and the stream power (τU).

The bed form classification employed by Barton and Lin (1955) is slightly different than the 1966 definitions. In order of increasing flow velocity, dunes, sandbars, plane bed and anti-dunes develop.
Dunes are more or less like fish scales or a shingled roof when looked upon from above. The dunes in their experiments have a typical length of less then 2 times the water depth. The dune height was in the order of 1/16 to 1/6 of the water depth.
A sandbar is referred to as a large wave which is distinctly higher and many times longer than the dunes. The wave front is in general not perpendicular to the flow. Typical dimensions of these sand bars are: length 1.8 to 3 m, height 0.1 m . The water surface is affected by the sand bars.

Vanoni and Brooks (1957) neither employ the 1966 classification. They use the same terminology as Barton and Lin (1955).
In Guy et al (1966) a phenomenological description of the bed form geometry in their laboratory experiments is given. They use the ripples and dune classification but do not give definitions. Some of the bed form patterns of the rippled bed experiments bear much resemblance with the pattern observed in the present experiment.
The photo's of the bed forms published by Barton and Lin (1955), Vanoni and Brooks (1957) and Guy et al (1966), indicate that the dunes reported in the early publications are the same features as the ripples of Guy et al (1966). After 1966, when the bed form definitions were established, the dunes of these early investigations were indeed classified as ripples (c.f. Van Rijn (1984c), Yalin (1984)).
Barton and Lin's sandbars are probably equivalent to dunes.

According to Engelund and Hansen (1967) the ripple shape is triangular, its maximal length is about 6 m and the maximal height is 60 mm. These dimensions probably refer to prototype situations. Van Rijn (1984c) reports a maximal ripple length of the order of the water depth and a height much smaller than, and independent, of the water depth.
Simons and Richardson (1961) indicate that ripples will exists also for small water depths. In that case small waves will be generated on the water surface by the sand ripples. In the experiment such small waves are present. Vanoni (1977, p162) remarks that ripples may be of mayor importance in movable bed hydraulic models.

The dune dimension is larger than ripple dimension. The dune length is larger than the water depth. Some reported values on dune length are:
Yalin (1964): $\Delta \approx 5a$, Hino (1969): $\Delta \approx 7a$, Yalin (1977): $\Delta \approx 2\pi a$,
Yalin (1985): $\Delta \approx 6a$, van Rijn (1984c): $\Delta = 7.3a$.
According to Yalin (1985) the dune length corresponds with the mean interval of the outer-layer turbulent bursting process. Ripples are suggested to be unaffected by the turbulent bursting process because the bed is protected by a viscous sublayer. The mean ripple length is suggested to correspond with the average wave length of the low- high-speed streak pattern, which scales on the inner-layer variables.
The basic idea of Yalin that the bed form shape is governed by the interaction of coherent turbulent stuctures and the sediment bed is

quite acceptable. It has to be pointed out, however, that the views presented by Yalin are based on a rather simplified and incomplete sketch of the coherent structure of turbulent flow. He, for instance, ignores the transversal distance of the low-speed streak pattern, which is about a factor 1/10 smaller than its length. This would yield elongated ripples in main stream direction. The contrary is the case; ripples are often observed elongated in transversal direction. Further, a simple decoupling of inner-layer and outer-layer features is questionable. A strong interaction has been proven to exist between the bursting process and the low-speed streaks (Talmon et al. 1985).

The dune height is strongly dependent on the water depth (van Rijn 1984c). The dune height can be of the order of the water depth.

Next to the data concerning the dune length and height some other quantitative data on ripple and dunes exist.

Engelund and Hansen (1967) suggest the ripples to exist in case the grain Reynolds number is less than 11.6. In that case the sediment particle dimension is equal to the thickness of the viscous sublayer. For the experiments of Guy et al (1966) with 190 μm material a maximal value of Re = 7.3 is found. Yalin and Scheuerlein (1985) indicate ripples to exist for Re < 10. The grain Reynolds number of the experiment is Re = $u_* d_{50}/\nu$ = 3.1, which indicates the sediment bed to consist of ripples.

Van Rijn (1984c) has modified the classification diagram of Simons and Richardson (1966) and has included more data, especially prototype data. Instead of the stream power van Rijn uses the transport stage parameter (T) as a classification parameter. When $d_* < 10$ ripples exist for $T < 3$, dunes exist for: $3 < T < 15$. When $d_* > 10$ ripples do not develop, dunes exist for $T < 15$.
The experiment's transport parameter is estimated to be: $T \approx 1$
(the efficiency factor μ is estimated to be: $\mu = 0.3$)
This also indicates the bed to consist of ripples.

According to the above arguments it has to be concluded that the bed form geometry is to be classified as ripples. The relative large height

of the bed forms in the experiment, however, suggests the bed forms to be associated with outer-layer flow structures. These outer-layer structures (bursts) were, however, associated with dunes by Yalin (1985b).

The same arguments apply to the previous suspended sediment experiments; run no. 1 (Talmon and Marsman, 1988) and run no. 2 (Talmon 1989a). The bed forms in these experiments should also be classified as ripples.

5.7 Adaptation lengths

In order to formulate mathematically the interaction of flow and sediment adaptation lengths of flow velocity, bed level and concentration have been defined: Struiksma et.al. (1986) and Olesen (1987). These adaptation lengths are defined as follows:

adaptation length of flow: $$\lambda_w = \frac{C^2}{2g} a_0 \qquad (5.13a)$$

adaptation length of bed level: $$\lambda_s = \frac{1}{\pi^2} \left(\frac{W}{a_0}\right)^2 \frac{1}{G} a \qquad (5.13b)$$

adaptation length of concentration: $$\lambda_c \approx a\bar{u}/w_s \qquad (5.13c)$$

in which: G = coefficient of the gravitational term in the bed-load sediment direction model

The adaptation lengths for flow and bed level in the experiment are:

λ_w = 0.96 m, based on C

λ_s = 0.33 m (for G=1.5)

The adaptation length of concentration depends mainly on the choice of boundary condition for the concentration at reference level (Talmon, 1989b). The adaptation length depends further on the value of the Z parameter, the reference height and the Chézy value. The adaptation lengths are calculated based on the assumption of a logarithmic velocity profile and a Rouse distribution for the concentration. To this purpose software which is used in Talmon (1989b) has been employed.

Curve fitting of the concentration profile yields: Z = 0.33

The Chézy value of the experiment is about: C = 20 $m^{0.5}/s$

The reference height should be chosen near the top of the dunes, consequently z_r will be in the range: $0.1 < z_r/a < 0.2$, (fig. 8)

Taking into account these ranges, the adaptation length of the concentration becomes approximately:

In case of the concentration condition: $\lambda_c = 0.3$ m
In case of the gradient condition: $\lambda_c = 0.9$ m

5.8 Bed topography

The stationary bed topography in the 180 degree bend is depicted in fig. 5. A maximum of the transversal bed slope occurs at cross sections 15 to 17. At this location a point-bar is present in the inner part of the bend. A pool is present in the outer part of the bend. Further downstream the transversal bed slope increases again, up to cross-section 45, which is also the end of the bend. The bed topography of the bend is characterized by a slowly damped oscillation of the transversal bed slope in downstream direction. The bed topography is comparable with run no.1 (Talmon and Marsman, 1988). Some slight differences are noticed however. At cross-section 25-30, where the transversal bed slope is minimal, a somewhat larger transversal slope is measured in run no. 1. At cross-section 42-45 the transversal bed slope of run no. 1 is somewhat steeper.

An analytical approximation the bed topography can be formulated by:

$$\frac{a'}{a_0} = (\hat{a}e^{iks} - i|\hat{a}|)e^{ik_b n} \qquad (5.14)$$

with: $\hat{a}$ complex amplitude (including a phase shift of the harmonic oscillation with regard to the bend entrance)
s coordinate in streamwise direction
n coordinate in transversal direction
$k_b = \pi/W$ wave number in transversal direction
k complex wave number

The $-i|\hat{a}|e^{ik_b n}$ term yields the axi-symmetrical bed topography (sinusioidal). Fitting equation (5.14) to the measured bed topography (cross section 14...45) yields:

$$re(k) = \frac{2\pi}{8.6} = 0.73 \qquad im(k) \approx 0.085 \qquad |\hat{a}| = 0.17 \text{ m}$$

im(k) and $\hat{a}$ are difficult to estimate, consequently the accuracy is limited. These results indicate a wave length of oscillation of 8.6 m, and 63% damping (e^{-1}) at s = 12 m.
These results are close to the wave length and damping of run no 1. (difference: ≈ 20 %).

5.9 Concentrations in cross-section 40

The concentration data at cross-section 40 is given in fig. 11a and fig. 11b. The iso-concentration contour line representation, fig. 11c. will be used to discuss the relevant physics.
In a straight reach the balance is between vertical turbulent diffusion and the fall velocity, while boundary conditions determine the concentration levels. At cross-section 40 the secondary flow and main flow convection gradients are factors affecting the concentration field. Main flow convection gradients are presumably small because changes of the bed topography in main flow direction are small.
In the inner part of the bend the concentrations are expected to be low because of smaller bed shear stresses. The results depicted in fig. 11c confirm this. In the outermost part of the bend, beyond Y/W=0.8, the concentrations decrease as well in the upper as the lower part of the flow. The decrease of concentrations could be caused by an additional secondary flow (Taylor-Gortler) cel due to the presence of the convex wall. The same effect is noticed in run no. 2.

5.10. The depth averaged concentration field

The depth averaged concentration field is given in fig. 12. The depth-averaged concentration field displays large variations.
The suspended sediment concentration on which the data in fig. 12 is normalized is the concentration $\bar{c}_s$ in the entrance section of the bend.
The depth averaged concentration field displays the following features, fig. 12:

- In the inner part of the bend, downstream of the point bar until bend exit, concentrations are low: ≈ 50 % of the value in the entrance section.

- Except near the pool and point-bar the concentration in the outer part of the bend is about 20 % larger than at the centerline.

6 CONCLUSIONS

The bed topography and sediment concentrations have been measured in a 180 degree curved flume.

The main features of the experiment are:

- The stationary bed topography displays over- and undershoot effects due to the abrupt change of curvature at the bend entrance.
- The bed topography is characterized by a slowly damped oscillation of the radial bed slope. The topography is very similar to that of run no. 1 in which the same sediment is used. The water depth is nearly the same, but the sediment transport rate in run no. 1 is 6 times larger.

The following parameters characterize the experiment.

- The Chézy value is about: $C = 20\ m^{0.5}/s$
- With the aid of curve fitting the Z parameter of the equilibrium concentration profile is estimated to be: $Z = 0.33$
- Due to the exaggerated bed form dimensions the reference height should be chosen within: $0.1 < z_r/a < 0.2$
- The bed forms are classified as ripples. The bed forms in the previous experiments, run no. 1 and run no. 2 are also to be classified as ripples
- The percentage suspended sediment transport is about 75 % .

In view of an analytical and numerical simulation of the experiment the following has been investigated:

- Transport formulae are applied, they fail to predict the total transport rate. This could be due to an erroneous estimate of the ratio of friction drag and total drag.
- Adaptation lengths of flow velocity, bed level and concentration have been calculated.
- The measured bed topography is approximated by an analytical expression incorporating harmonic oscillation and damping.
- The depth-averaged concentration field is calculated. In the inner part of the bend the concentrations are about half the concentration in the outer part of the bend.

REFERENCES

Ackers, P. and W.R. White, 1973, Sediment transport: a new approach and analysis, Journal of the Hydraulics Division, ASCE, vol. 99, no. HY11, pp. 2041-2060

ASCE, 1966, Task force on bed forms in alluvial channels, Nomenclature for bed forms in alluvial channels, Journal of Hydraulic Engineering, Vol 92, HY3, pp. 51-64

Barton, J.K. and P.N. Lin, 1955, A study of the sediment transport in alluvial channels, report no. 55JRB2, Colorado Agricultural and Mechanical College, Civil Engineering Department, pp. 50

Brownlie, W.R., 1981, Prediction of flow depth and sediment discharge in open channels, W.M. Keck Laboratory of Hydraulics and Water Resources, California Institute Of Technology, Pasadena California, rep. no. KH-R-43A

Coleman, N.L., 1970, Flume studies of the sediment transfer coefficient Water Resources, Vol 6, no 3.

Csanady, G.T., 1973, Turbulent diffusion in the environment, D. Reidel Publishing Co., Dordrecht, the Netherlands

Delft Hydraulics, 1986, Optical concentration meter, model OPCON, Technical manual

Engelund, F. and E. Hansen, 1967, A monograph on sediment transport in alluvial streams, Teknisk Forlag, Copenhagen, Denmark, pp. 62

Guy, H.P., D.B. Simons and E.V. Richardson, 1966, Summary of alluvial channel data from flume experiments, 1956-1961, Geological Survey Professional Paper 462-I, Washington, D.C. pp. 93

Hino, M., 1969, Equilibrium range spectre of sand waves forming by running water. Journal of Fluid Mechanics, vol. 34, part 3

Hinze, J.O., 1959, Turbulence, McGraw-Hill, New York

Mantz, P.A., 1977, Incipicient transport of fine grains and flakes by fluids - extended Shields diagram, Journal Hydraulics Div. ASCE, Vol. 103, no. HY6, pp. 601-615

Olesen, K.W., Bed topography in shallow river bends
Doctoral thesis Delft University of Technology, 1987
(also: ISSN 0169-6548 Communications on Hydraulic and Geotechnical Engineering, Delft University of Technology, Faculty of Civil Engineering)

Rijn, L.C. van, 1984a, Sediment transport, part I: bed load transport, Journal of Hydraulic Engineering, Vol 110, no. 10, pp. 1431-1456

Rijn, L.C. van, 1984b, Sediment transport, part II: suspended load transport, Journal of Hydraulic Engineering, Vol 110, no. 11, pp. 1613-1641

Rijn, L.C. van, 1984c, Sediment transport, part III: bed form and alluvial roughness, Journal of Hydraulic Engineering, Vol 110, no. 12, pp. 1733-1754

Rijn, L.C. van, 1987, Mathematical modelling of morphological processes in the case of suspended sediment transport
Doctoral thesis Delft University of Technology, 1987
(also: Delft Hydraulics Communication no. 382)

Simons, D.B. and E.V. Richardson, 1961, Forms of bed roughness in alluvial channels, Journal of Hydraulic Engineering, Vol 87, no. HY3, pp. 87-105

Simons, D.B. and E.V. Richardson, 1966, Resistance to flow in alluvial channels, Geological Survey Professional Paper 422-J, Washington, D.C.

Slot, R.E., 1983, Terminal velocity formula for spheres in a viscous fluid. Delft Univ. of Techn., Dept. Civil Engrg., Laboratory of Fluid Mechanics, rep. no. 4-83,

Slot, R.E. and H.J.Geldof, 1986, An improved settling tube system for sand. ISSN 0169-6548, Communications on Hydraulics and Geotechnical Engineering, Delft University of Technology, Faculty of Civil Engineering, rep. no. 86-12,

Struiksma, N.; K.W. Olesen, C. Flokstra and H.J. de Vriend, 1985, Bed deformation in alluvial channel bends. IAHR, Journal of Hydraulic Research, vol. 23, no. 1, pp. 57-79

Talmon, A.M., 1989a, Suspended-load experiments in a curved flume, run no.2, Delft Univ. of Techn., Dept. Civil Eng., rep. no. 4-89

Talmon, A.M., 1989b, A theoretical model for suspended sediment transport in river bends, ISSN 0169-6548, Communications on Hydraulic and Geotechnical Engineering, Delft University of Technology, Faculty of Civil Engineering, rep. no. 89-5

Talmon, A.M., J.M.G. Kunen and G. Ooms, 1986, Simultanious flow visualization and Reynolds-stress measurement in a turbulent boundary layer. Journal of Fluid Mechanics, vol. 163,

pp. 459-478

Talmon, A.M. and E.R.A. Marsman, 1988, Suspended-load experiments in a curved flume, run no.1, Delft Univ. of Techn., Dept. Civil Eng., rep. no. 8-88

Vanoni, V.A., 1977, Sedimentation Engineering, ASCE-manuals and reports on engineering practice-no.54. pp. 745

Vanoni, V.A. and N.H. Brooks, 1957, Laboratory studies of the roughness and suspended load of alluvial streams, Rep. no. E-68, Publication no. 149, California Institute of Technology Pasadena, California, pp. 121

White, W.R., 1972, Sediment transport in channels: a general function, rep. INT 104, Hydraulics Research Station, England

Yalin, M.S., 1964, Geometric properties of sand waves, Journal of Hydraulic Engineering, Vol 90, no. HY5

Yalin, M.S., 1977, Mechanics of Sediment transport. Pergamon Press, Oxford

Yalin, M.S., 1984, On the determination of ripple geometry, Journal of Hydraulic Engineering, Vol 111, no. HY8, pp. 1148-1155

Yalin, M.S., 1988, On the formation mechanisme of dunes and ripples, bericht no. 59, Oskar v. Miller-institut, Obernach, Technical University Munchen, pp. 81-93, (also Euromech 215, 1987 Genua)

Yalin, M.S., and H. Scheuerlein, 1988, Friction factors in alluvial rivers, bericht no. 59, Oskar v. Miller-institut, Obernach, Technical University Munchen, pp. 59

Appendix A: Ensemble averaged water depths.

In this appendix the ensemble averaged relative water depths of the 10 measurements are tabulated.

Discharge 0.0050 m^3/s. Sediment transport 1.9 kg/h dry sand.

Relative mean water depth a/a_0. (a_0 = 0.051 m.)

from inner side of bend	CS01	CS02	CS03	CS04	CS05	CS06	CS07
0.05	1.01	0.98	1.00	0.97	0.96	0.94	0.90
0.10	1.09	1.05	1.03	1.01	0.94	0.90	0.98
0.15	1.04	1.00	1.03	0.98	0.99	1.00	0.88
0.20	1.04	0.96	1.00	0.99	0.98	0.96	0.97
0.25	1.04	1.02	0.97	0.88	0.99	1.00	1.06
0.30	1.06	0.98	0.92	1.01	1.04	1.05	1.10
0.35	1.07	0.98	0.95	1.01	1.02	0.98	1.05
0.40	1.03	0.98	0.95	1.04	0.96	0.99	0.93
0.45	1.00	0.99	0.98	1.11	0.94	1.06	0.97

from inner side of bend	CS08	CS09	CS10	CS11	CS12	CS13	CS14
0.05	0.79	0.74	0.68	0.57	0.42	0.35	0.32
0.10	0.86	0.80	0.76	0.61	0.58	0.43	0.39
0.15	0.92	0.88	0.84	0.70	0.67	0.64	0.59
0.20	0.91	0.84	0.87	0.83	0.74	0.74	0.69
0.25	0.96	0.95	0.98	0.95	0.96	0.94	0.89
0.30	0.99	1.10	1.07	1.11	1.16	1.08	1.17
0.35	1.02	1.13	1.15	1.21	1.26	1.12	1.31
0.40	1.14	1.15	1.26	1.32	1.42	1.30	1.42
0.45	1.10	1.20	1.34	1.47	1.60	1.56	1.58

from inner side of bend	CS15	CS16	CS17	CS18	CS19	CS20	CS21
0.05	0.24	0.28	0.39	0.44	0.54	0.64	0.79
0.10	0.32	0.37	0.41	0.47	0.52	0.64	0.73
0.15	0.47	0.55	0.53	0.53	0.67	0.70	0.68
0.20	0.64	0.66	0.69	0.68	0.73	0.77	0.75
0.25	0.97	0.92	1.01	0.90	0.93	0.87	0.93
0.30	1.17	1.22	1.26	1.20	1.15	1.12	1.11
0.35	1.26	1.32	1.37	1.22	1.24	1.23	1.17
0.40	1.40	1.52	1.44	1.36	1.38	1.32	1.33
0.45	1.53	1.73	1.59	1.61	1.49	1.52	1.46

Discharge 0.0050 m^3/s. Sediment transport 1.9 kg/h dry sand.

Relative mean water depth a/a_0. (a_0 = 0.051 m.)

from inner side of bend	CS22	CS23	CS24	CS25	CS26	CS27	CS28
0.05	0.73	0.83	0.80	0.87	0.79	0.85	0.87
0.10	0.78	0.76	0.88	0.85	0.84	0.94	0.78
0.15	0.77	0.74	0.90	0.80	0.79	0.85	0.86
0.20	0.88	0.92	0.84	0.84	0.91	0.88	0.86
0.25	0.99	0.92	0.95	0.84	0.90	0.98	0.89
0.30	1.15	1.14	1.05	0.97	0.98	1.07	1.01
0.35	1.18	1.09	1.07	1.00	1.03	1.13	1.01
0.40	1.17	1.15	1.20	1.08	1.08	1.10	1.09
0.45	1.27	1.32	1.26	1.26	1.13	1.18	1.18

from inner side of bend	CS29	CS30	CS31	CS32	CS33	CS34	CS35
0.05	0.84	0.75	0.76	0.83	0.71	0.78	0.65
0.10	0.85	0.77	0.81	0.87	0.75	0.83	0.73
0.15	0.87	0.85	0.88	0.89	0.84	0.90	0.79
0.20	0.90	0.88	0.92	0.94	0.90	0.85	0.88
0.25	0.93	0.98	1.02	1.08	0.99	0.91	0.99
0.30	0.94	0.95	1.02	1.02	0.99	1.09	1.08
0.35	0.98	0.95	1.06	1.07	1.10	1.15	1.15
0.40	1.03	1.02	1.16	1.14	1.14	1.20	1.24
0.45	1.20	1.22	1.15	1.20	1.20	1.30	1.28

from inner side of bend	CS36	CS37	CS38	CS39	CS40	CS41	CS42
0.05	0.74	0.64	0.71	0.68	0.62	0.58	0.63
0.10	0.77	0.71	0.82	0.73	0.79	0.69	0.70
0.15	0.75	0.85	0.85	0.78	0.77	0.76	0.72
0.20	0.94	0.91	0.89	0.83	0.87	0.87	0.88
0.25	1.01	1.01	1.04	1.07	1.08	1.04	1.05
0.30	1.09	1.10	1.15	1.21	1.15	1.08	1.14
0.35	1.10	1.14	1.24	1.19	1.16	1.19	1.14
0.40	1.19	1.27	1.22	1.17	1.28	1.29	1.24
0.45	1.36	1.36	1.25	1.23	1.44	1.34	1.30

Discharge 0.0050 m^3/s. Sediment transport 1.9 kg/h dry sand.

Relative mean water depth a/a_0. (a_0 = 0.051 m.)

from inner side of bend	CS43	CS44	CS45	CS46	CS47	CS48
0.05	0.59	0.55	0.57	0.57	0.68	0.79
0.10	0.70	0.75	0.59	0.66	0.69	0.76
0.15	0.78	0.76	0.74	0.79	0.83	0.84
0.20	0.83	0.89	0.90	0.93	0.93	0.95
0.25	0.99	1.03	1.02	1.10	1.04	1.01
0.30	1.08	1.20	1.16	1.20	1.12	1.09
0.35	1.06	1.24	1.27	1.20	1.22	1.08
0.40	1.21	1.30	1.35	1.28	1.34	1.14
0.45	1.39	1.35	1.47	1.42	1.40	1.24

Appendix B: Concentration data

Cross section 1.

location in cross-direction [y/W]	Mean water depth [mm]	Distance beneath water surface [mm]	Concentration [g/l]			
4/8	51	5	0.047	0.048	0.042	0.056
		10	0.059	0.064	0.052	0.052
		15	0.086	0.079	0.073	0.085
		20	0.087	0.073	0.074	0.089
		25	0.105	0.114	0.090	0.117
		30	0.098	0.107	0.095	0.119
		35	0.165	0.144	0.125	
		40	0.172	0.132	0.129	
		45	0.208			
		50	0.146			

Cross section 5.

Location in cross-direction [y/W]	Mean water depth [mm]	Distance beneath water surface [mm]	Concentration [g/l]					
4/8	51	5	0.035	0.029	0.061	0.038	0.028	
		10	0.065	0.043	0.045	0.074	0.063	0.090
			0.058					
		15	0.056	0.070	0.055	0.048	0.127	0.064
			0.085	0.066				
		20	0.129	0.095	0.075	0.097	0.098	0.086
		25	0.111	0.109	0.076	0.121	0.088	0.121
			0.074	0.124				
		30	0.087	0.192	0.152	0.138	0.128	0.101
		35	0.164	0.107	0.125	0.107	0.099	0.317
		40	0.152	0.169	0.117			
		45	0.162	0.154				
		50	0.215	0.211				

Cross section 10.

Location in cross-direction [y/W]	Mean water depth [mm]	Distance beneath water surface [mm]	Concentration [g/l]
2/8	41	5	0.051
		10	0.073
		15	0.075
		20	0.101
		25	0.089
		30	0.130
		35	0.106
		40	0.156

4/8	50	5	0.056	0.040
		10	0.085	0.063
		15	0.090	0.106
		20	0.108	0.092
		25	0.124	
		30	0.141	
		35	0.152	
		40	0.166	
6/8	62	5	0.041	
		10	0.071	
		15	0.056	
		20	0.095	
		25	0.098	0.072
		30	0.111	
		40	0.111	
		45	0.167	
		50	0.115	
		55	0.183	
		60	0.127	
		65	0.225	
		70	0.154	
		75	0.353	

Cross section 15.

Location in cross-direction [y/W]	Mean water depth [mm]	Distance beneath water surface [mm]	Concentration [g/l]		
2/8	20	5	0.092		
		10	0.058		
		15	0.110		
		20	0.076		
		25	0.132		
		30	0.084		
4/8	50	5	0.044		
		10	0.048		
		15	0.096	0.070	
		20	0.064		
		25	0.117	0.070	
		30	0.072	0.115	
		35	0.099		
		40	0.098	0.150	0.192
		45	0.158		
6/8	68	5	0.034		
		10	0.045		
		15	0.053		
		20	0.066		
		25	0.056		
		30	0.097		
		35	0.105		
		40	0.110		
		45	0.113		
		50	0.198		
		55	0.143		
		60	0.222		

65	0.175	
70	0.240	

Cross section 20.

Location in cross-direction [y/W]	Mean water depth [mm]	Distance beneath water surface [mm]	Concentration [g/l]		
2/8	34	5	0.035		
		10	0.022		
		15	0.044		
		20	0.042		
		25	0.070		
		30	0.053		
		40	0.155		
4/8	45	5	0.065		
		10	0.078	0.080	
		15	0.125		
		20	0.145	0.168	
		25	0.096	0.151	
		30	0.112		
		35	0.132	0.136	0.194
		40	0.185		
		45	0.254		
6/8	66	5	0.034		
		10	0.042		
		15	0.049		
		20	0.063		
		25	0.058		
		30	0.122	0.076	
		35	0.216	0.067	
		40	0.092	0.135	
		45	0.287		
		50	0.143		
		55	0.903		

Cross section 25.

Location in cross-direction [y/W]	Mean water depth [mm]	Distance beneath water surface [mm]	Concentration [g/l]		
2/8	42	5	0.020		
		10	0.022		
		15	0.034	0.024	0.052
		20	0.038		
		25	0.067	0.040	0.036
		30	0.053		
		35	0.047		
4/8	43	5	0.038		
		10	0.036	0.036	0.084
		15	0.070		

		20	0.074	0.109	0.067
		25	0.105		
		30	0.092		
		35	0.136		
		40	0.129		
6/8	53	5	0.032		
		10	0.079	0.061	
		15	0.075	0.052	
		20	0.121		
		25	0.073		
		35	0.094	0.183	
		45	0.113		

Cross section 30.

Location in cross-direction [y/W]	Mean water depth [mm]	Distance beneath water surface [mm]	Concentration [g/l]
2/8	42	5	0.028
		10	0.037
		15	0.043
		20	0.054
		25	0.056
		30	0.070
		40	0.084
3/8	45	5	0.031
		10	0.074
		15	0.058
		20	0.133
		25	0.073
		30	0.165
		35	0.097
4/8	50	10	0.063
		15	0.072
		20	0.104
		25	0.049
		30	0.127
		35	0.094
		40	0.441
		45	0.128
6/8	51	10	0.070
		15	0.102
		20	0.110
		25	0.107
		30	0.087
		35	0.120
		40	0.126
		45	0.195

Cross section 35.

Location in cross-direction [y/W]	Mean water depth [mm]	Distance beneath water surface [mm]	Concentration [g/l]	
2/8	39	5	0.027	
		10	0.038	
		15	0.053	
		20	0.048	
		25	0.076	
		30	0.072	
		35	0.115	
		40	0.094	
4/8	51	5	0.040	
		10	0.068	
		15	0.067	
		20	0.091	
		25	0.075	
		30	0.132	
		35	0.110	
		40	0.183	
		45	0.121	
		55	0.149	
6/8	61	5	0.049	
		10	0.052	
		15	0.084	
		20	0.072	
		25	0.103	0.115
		30	0.098	
		35	0.151	0.095
		40	0.125	
		45	0.113	
		55	0.151	

Cross section 40.

Location in cross-direction [y/W]	Mean water depth [mm]	Distance beneath water surface [mm]	Concentration [g/l]	
1/8	34	5	0.030	0.036
		10	0.062	0.022
		15	0.041	0.061
		20	0.096	0.048
		25	0.282	0.055
		30	0.142	0.081
		35	0.265	
2/8	40	5	0.029	0.033
		10	0.037	0.051
		15	0.046	0.050
		20	0.053	0.064
		25	0.048	0.068
		30	0.102	0.069

		35	0.093	0.063		
		40	0.180			
3/8	44	5	0.021	0.046		
		10	0.047	0.037		
		15	0.079	0.042		
		20	0.063	0.066		
		25	0.068	0.123		
		30	0.082	0.100		
		35	0.190	0.079		
		40	0.127			
4/8	55	5	0.037	0.029		
		10	0.042	0.050		
		15	0.069	0.048		
		20	0.067	0.064	0.065	
		25	0.094	0.064		
		30	0.087	0.092	0.068	
		35	0.088	0.140		
		40	0.125	0.128	0.093	
5/8	59	5	0.044	0.062		
		10	0.044	0.046		
		15	0.073	0.094		
		20	0.057	0.070		
		25	0.096	0.103		
		30	0.105	0.076		
		35	0.129	0.119		
		40	0.100	0.176		
6/8	63	5	0.045	0.038		
		10	0.048			
		15	0.054	0.073		
		20	0.073			
		25	0.104	0.074	0.090	0.074
		30	0.137	0.089		
		35	0.088	0.135	0.081	0.079
		40	0.166	0.116		
		45	0.098	0.088		
		50	0.277			
		55	0.097			
		60	0.216			
7/8	72	5	0.018	0.016		
		10	0.044	0.029		
		15	0.045	0.037		
		20	0.039	0.057		
		25	0.037	0.042		
		30	0.066	0.043		
		35	0.050	0.087	0.062	0.060
		40	0.090	0.073	0.099	0.046
		45	0.062	0.094		
		50	0.105	0.104		
		55	0.089	0.113		
		60	0.136	0.115		
		65	0.118			
		70	0.199	0.131		

Cross section 45.

Location in cross-direction [y/W]	Mean water depth [mm]	Distance beneath water surface [mm]	Concentration [g/l]	
2/8	35	5	0.020	0.024
		10	0.030	0.036
		15	0.032	0.048
		20	0.049	0.075
		25	0.040	0.054
		30	0.473	0.056
4/8	52	5	0.023	
		10	0.035	
		15	0.056	
		20	0.056	
		25	0.102	
		30	0.079	
		35	0.134	
		40	0.103	
6/8	67	5	0.031	
		10	0.068	
		15	0.082	
		20	0.109	
		30	0.114	
		35	0.133	
		40	0.135	

Cross section 48.

Location in cross-direction [y/W]	Mean water depth [mm]	Distance beneath water surface [mm]	Concentration [g/l]
4/8	52	5	0.036
		10	0.038
		15	0.059
		20	0.061
		25	0.082
		30	0.078
		35	0.107

Appendix C: Bed form height in cross section 30-45

The bed form dimensions are, at least at laboratory scale, important to the characteristics of the flow. Their shape determines the drag due to local pressure gradients. Their height yields an indication for the choice of reference level to be used for suspended sediment transport modelling.

For modelling of river bend flow and suspended sediment transport it is important how to model the spatial distribution of the bed resistance factor and the choice of reference level.

According to the similarity theory of Engelund and Hansen (1967) two flows are geometrical similar when the Froude number and the ratio of height/length of the bed forms are equal. Then the friction factors are also equal. It is tempting to apply this theory. The applied measuring method of the bed level does not incorporate longitudinal traverses, consequently no data on bed form length is available. The theory can not be applied.

The choice of reference level is to be taken near the top of the bed forms. Usually this level is modelled relative to the local water depth (Wang, 1988). To check whether this choice is correct, bed level data of run no. 2 and 3 are investigated. The region of cross section 30-45 is used. In this region the bed is axi-symmetrical in run no. 2, in run no. 3 it is not.

Two hypothesis are investigated:

A: The absolute bed form height is constant in transversal direction.

B: The relative bed form height is constant in transversal direction.

The bed form height is normalized with the local mean water depth. In fig. c1 and c2 the data is normalized with the overall mean depth to investigate hypothesis A. In fig. c3 and c4 the data is normalized with the local depth to test hypothesis B. For a hypothesis to be valid the data should be on a horizontal line. This is for neither hypothesis the case. Hypothesis A seems to be appropriate in the inner and central part of the bend; $Y/W < 0.6$. Hypothesis B on the contrary seems to be appropriate in the central and outer part of the bend; $Y/W > 0.4$.

The conclusion is that both hypothesis can neither be affirmed or rejected. A reference level which is modelled relative to the local water depth is appropriate in the central and outer part of the bend.

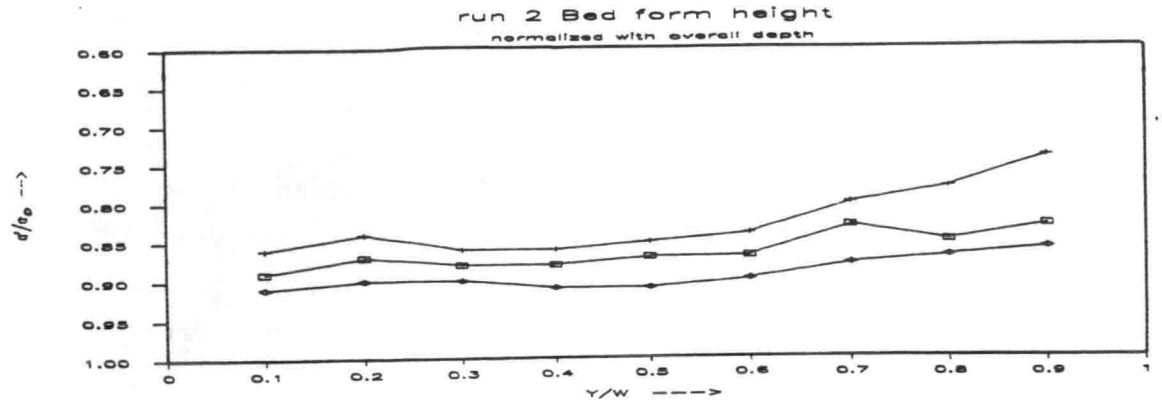

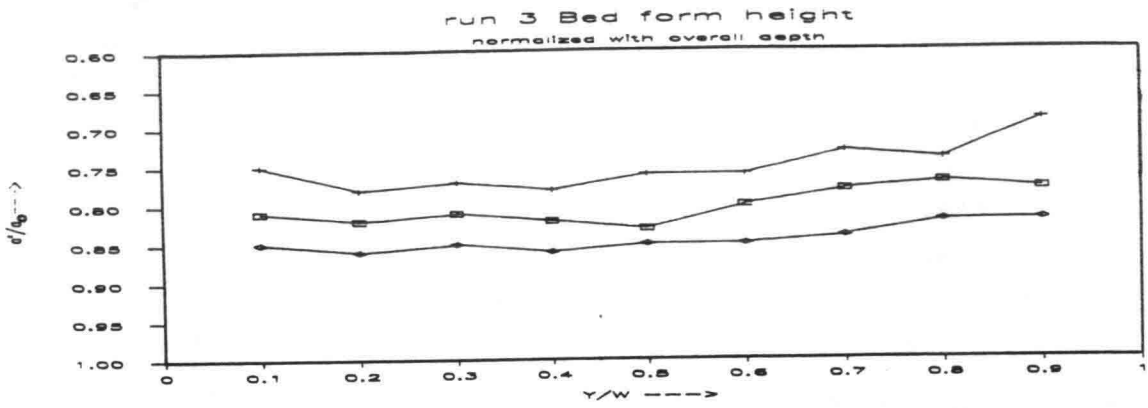

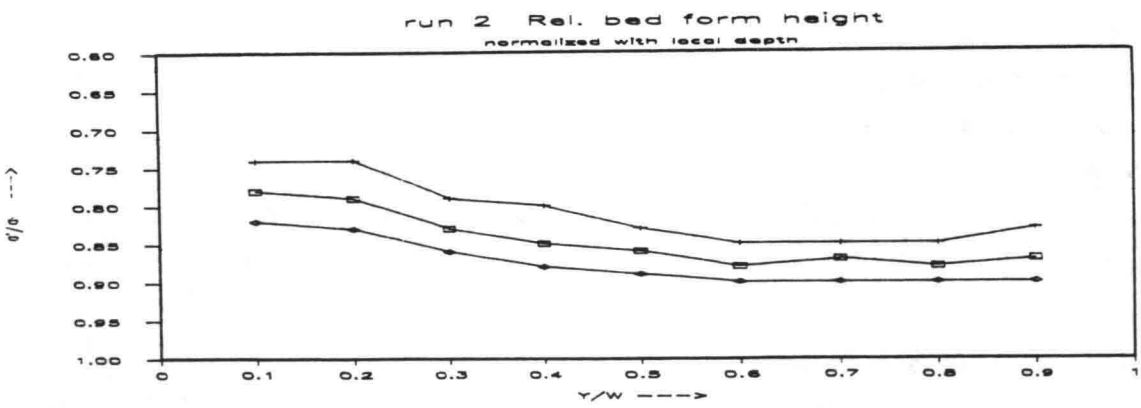

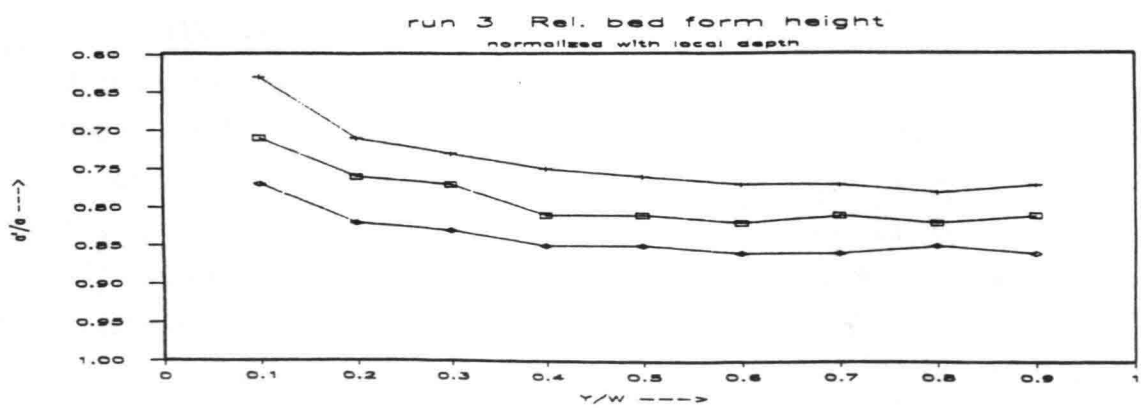

5 and 10% exceedance levels and r.m.s. value

+ 1-x(5%) □ 1-x(10%) ◇ 1-RMS

BED FORM HEIGHT IN CROSS-SECTION 30-45

FIG. C1-C4

DELFT UNIVERSITY OF TECHNOLOGY

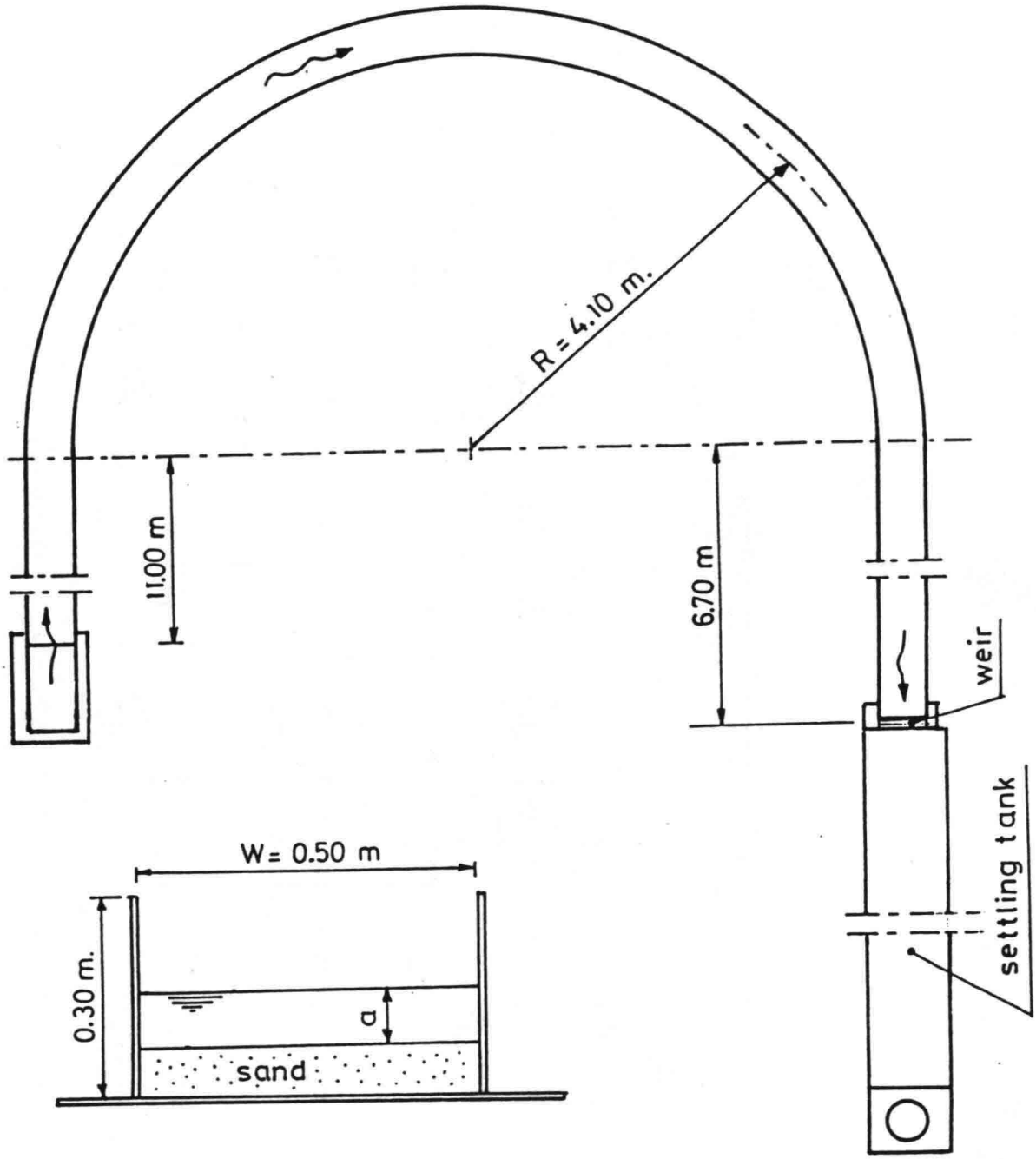

LAYOUT, LFM CURVED FLUME

FIG. 1

DELFT UNIVERSITY OF TECHNOLOGY

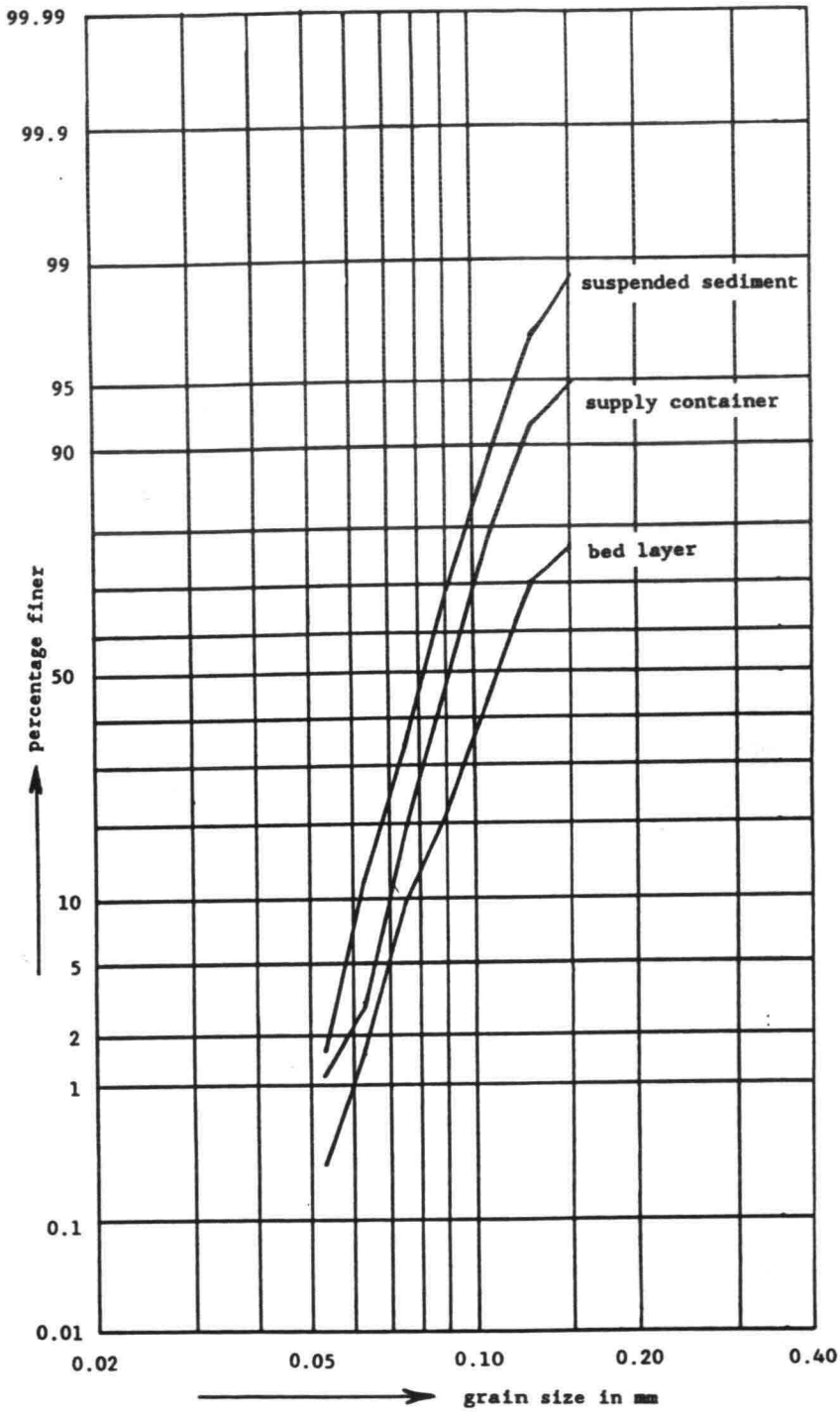

SIEVE CURVES OF SEDIMENT

DELFT UNIVERSITY OF TECHNOLOGY

FIG. 2

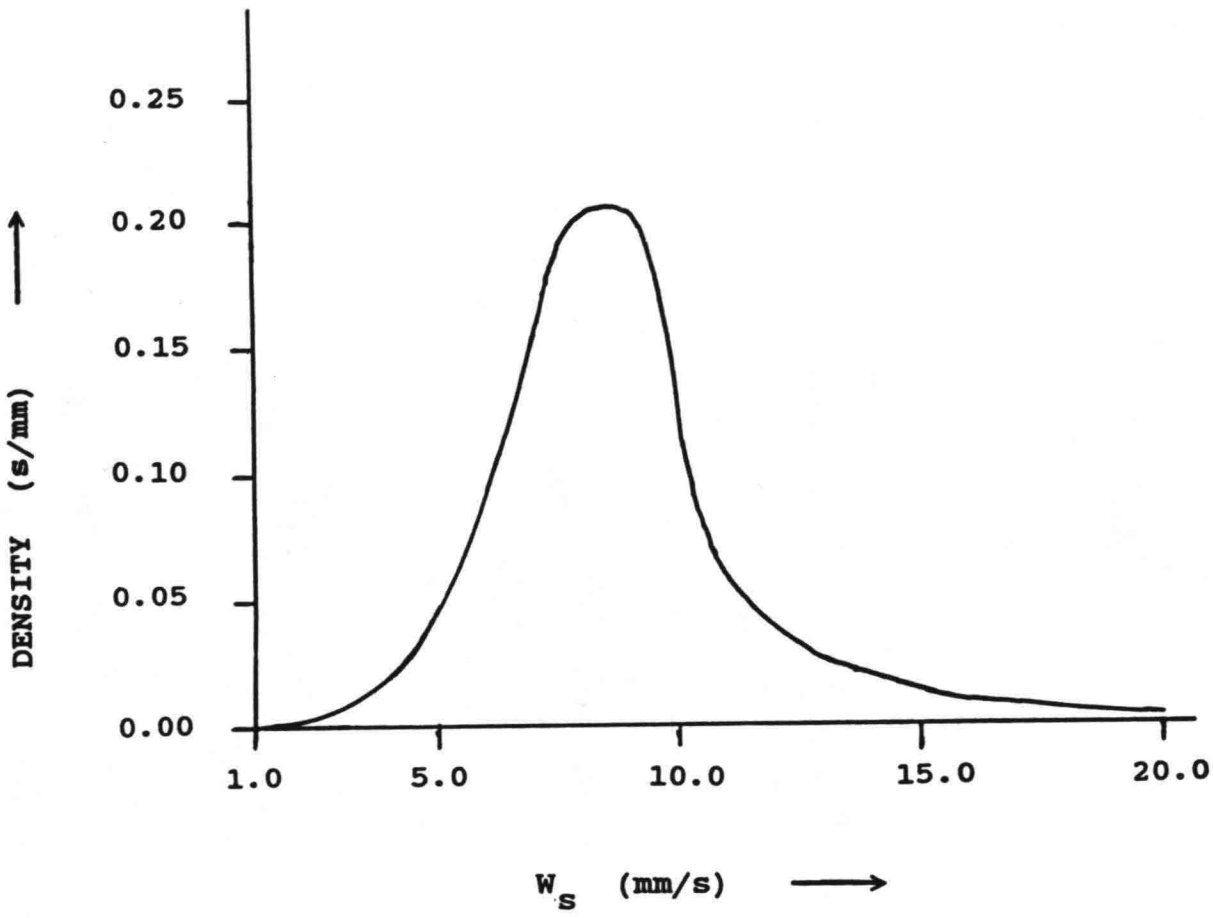

PROBABILITY DENSITY DISTRIBUTION OF FALL VELOCITY

FIG. 3

DELFT UNIVERSITY OF TECHNOLOGY

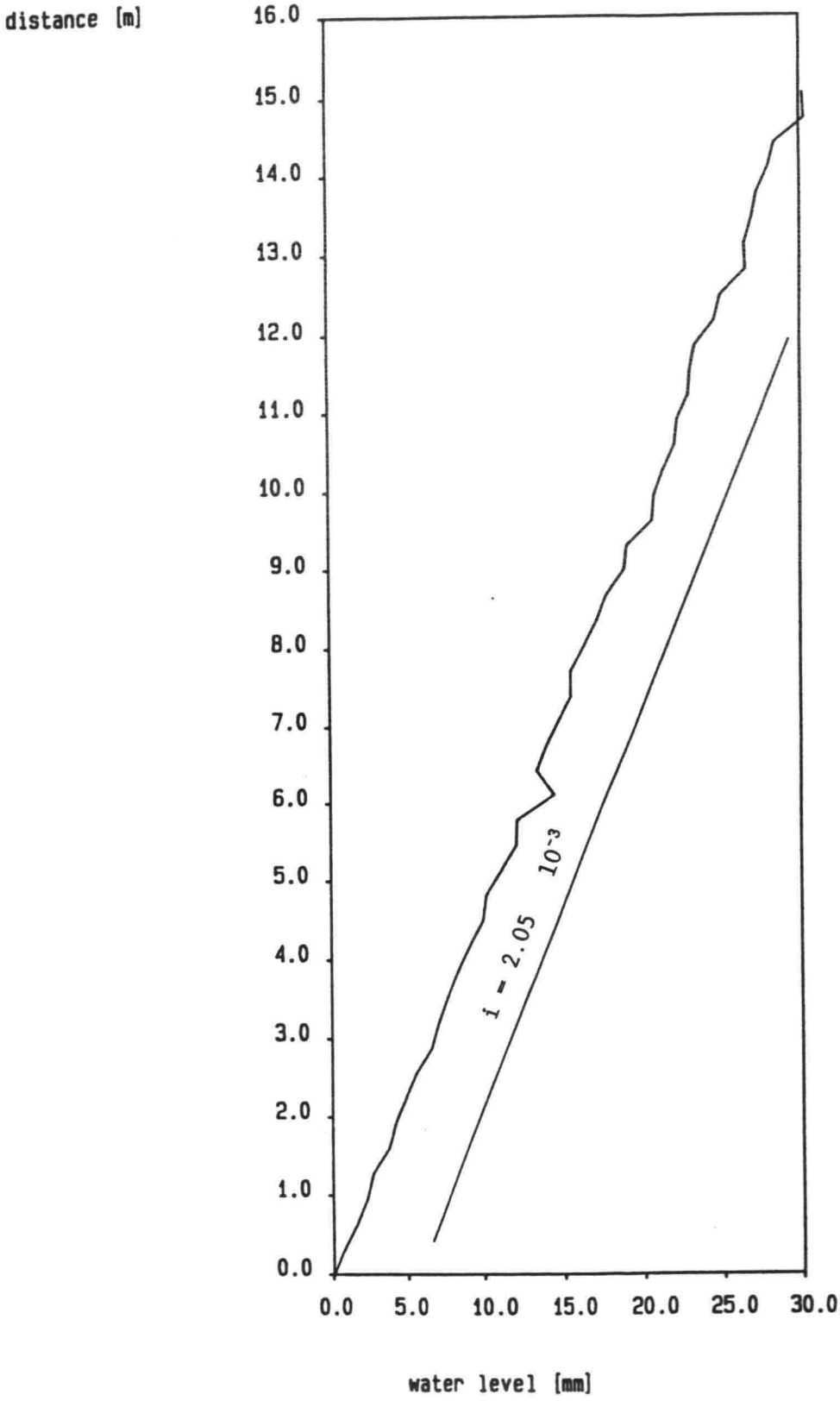

LONGITUDINAL WATER LEVEL SLOPE

FIG. 4

DELFT UNIVERSITY OF TECHNOLOGY

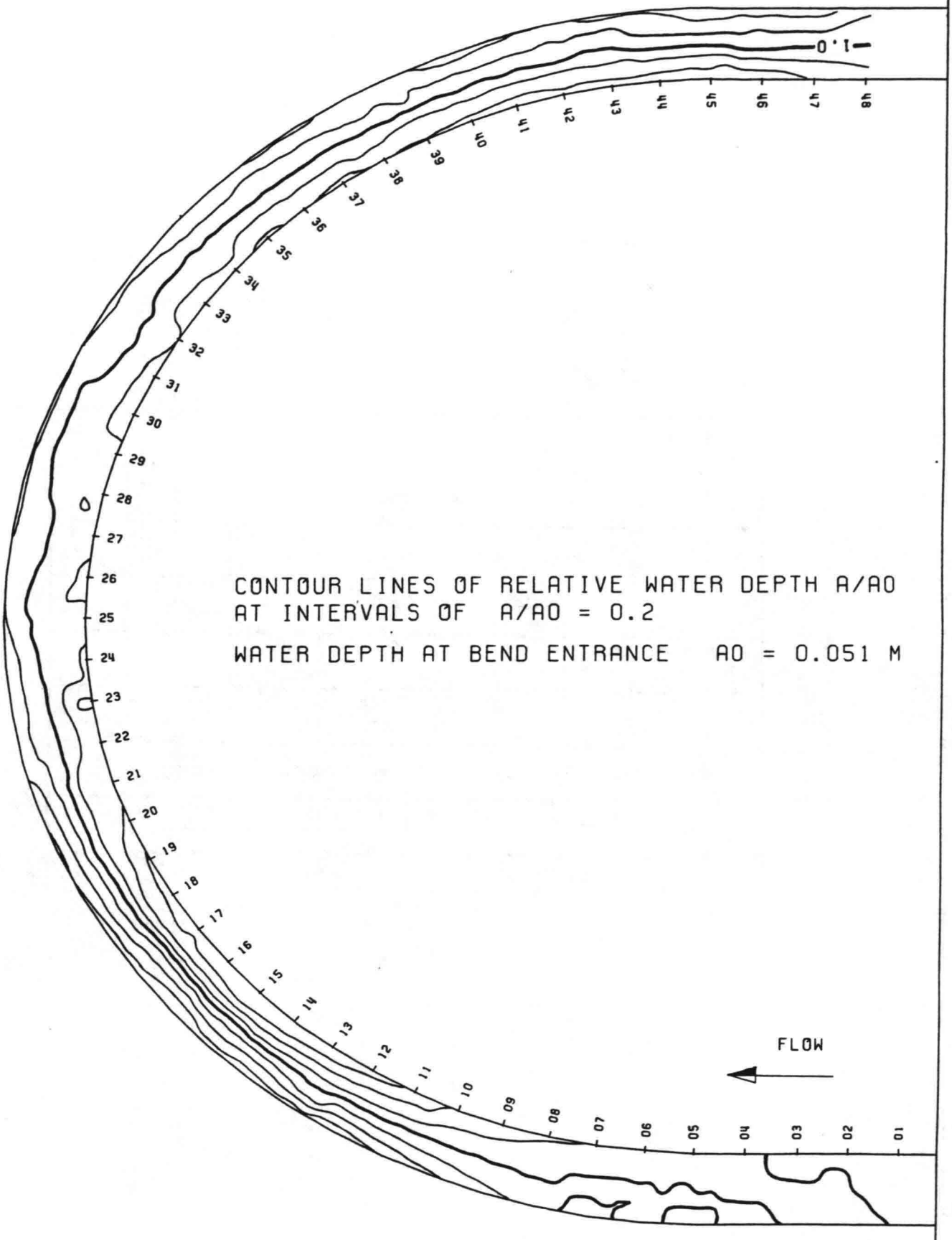

MODEL OF RIVER BEND, SUSPENDED-LOAD EXPERIMENT
ENSEMBLE MEAN OF 10 LONGITUDINAL TRAVERSES

DELFT UNIVERSITY OF TECHNOLOGY

FIG.5

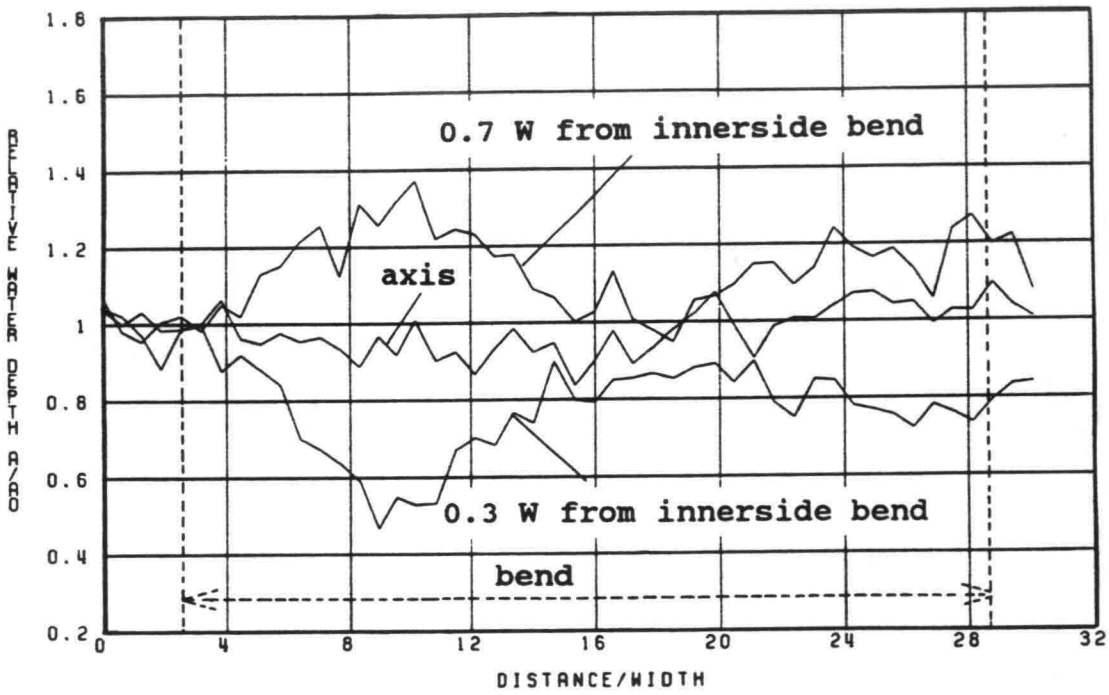

W = 0.5 M AO = 0.051 M

LONGITUDINAL PROFILE OF THE WATER DEPTH

FIG 6

DELFT UNIVERSITY OF TECHNOLOGY

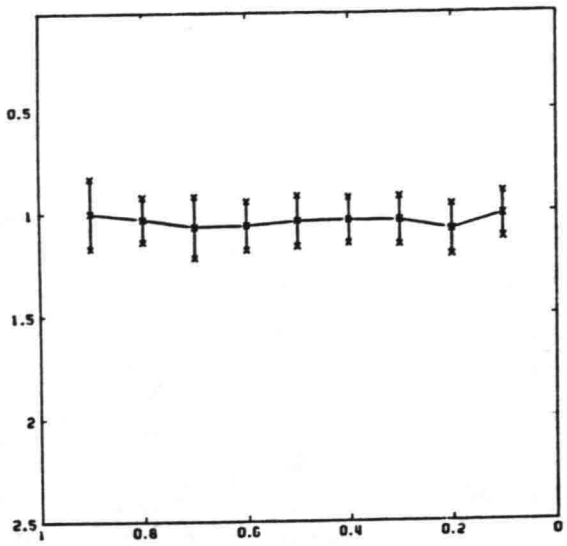

CROSS-SECTION 1

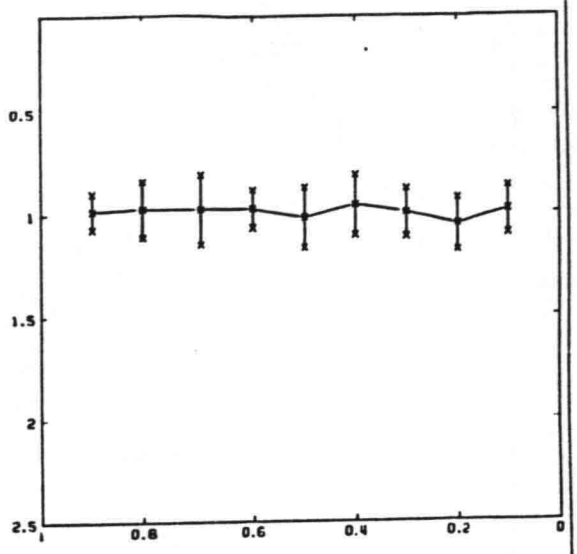

CROSS-SECTION 2

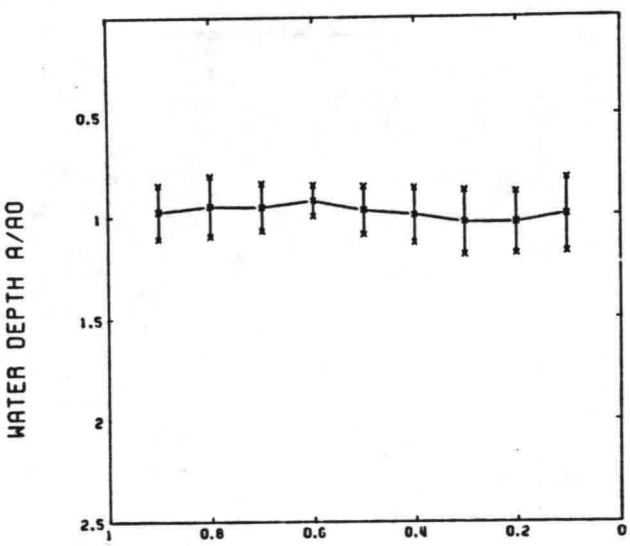

CROSS-SECTION 3

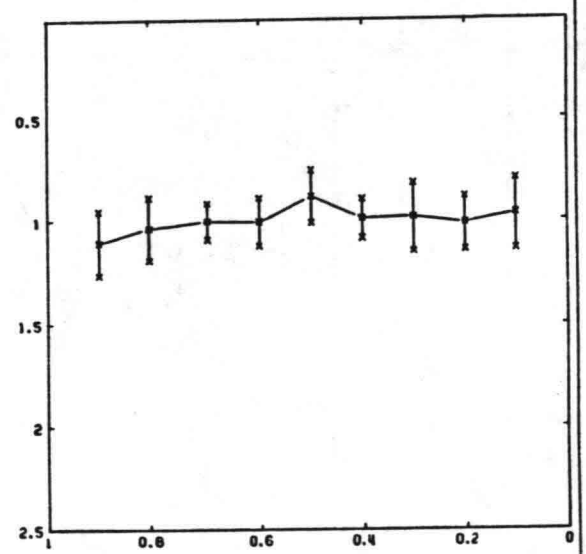

CROSS-SECTION 4

W = 0.5 M AO = 0.051 M

$\pm \sigma$ OF 10 MEASUREMENTS

WATER DEPTH IN CROSS-DIRECTION

FIG 7A

DELFT UNIVERSITY OF TECHNOLOGY

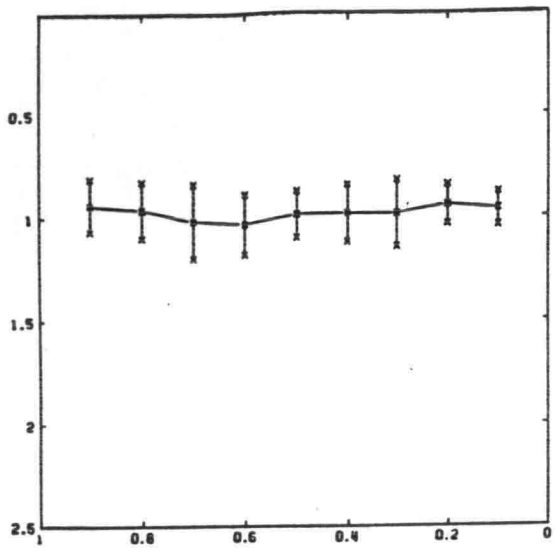

CROSS-SECTION 5

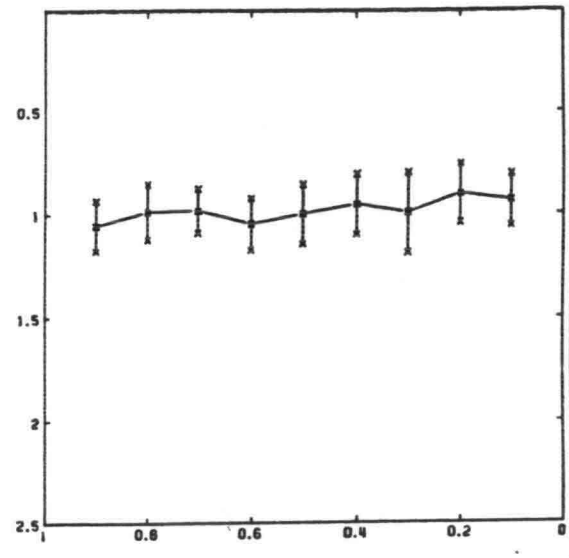

CROSS-SECTION 6

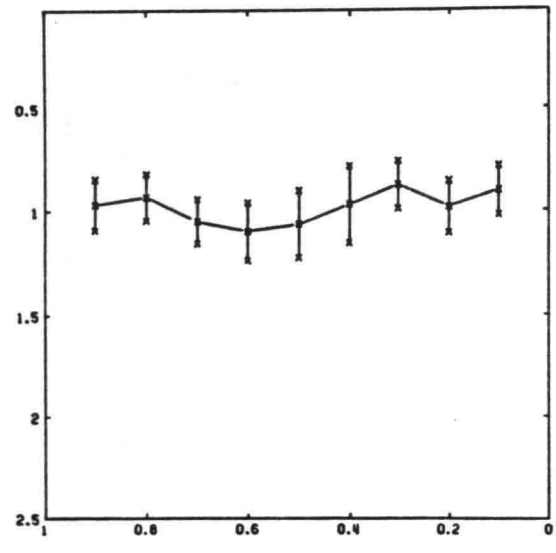

CROSS-SECTION 7

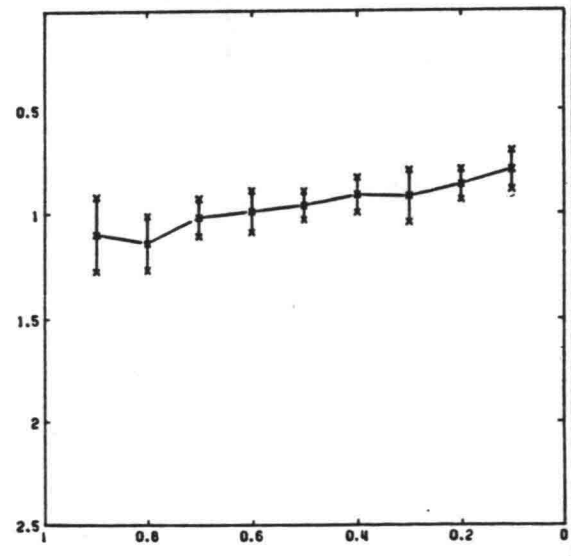

CROSS-SECTION 8

W = 0.5 M A0 = 0.051 M

± σ OF 10 MEASUREMENTS

WATER DEPTH IN CROSS-DIRECTION

FIG 7B

DELFT UNIVERSITY OF TECHNOLOGY

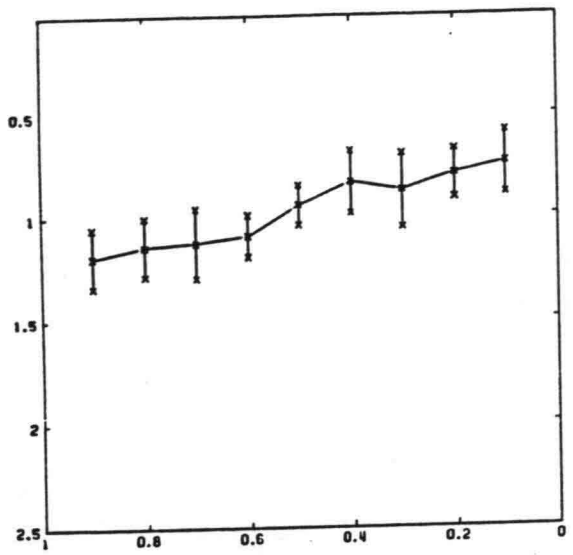

CROSS-SECTION 9

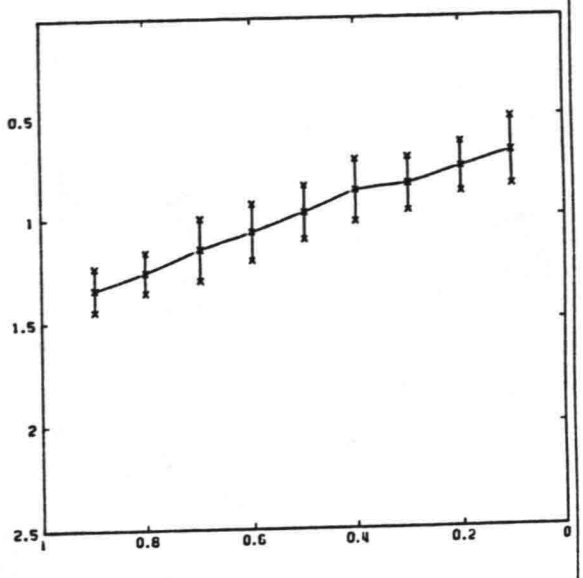

CROSS-SECTION 10

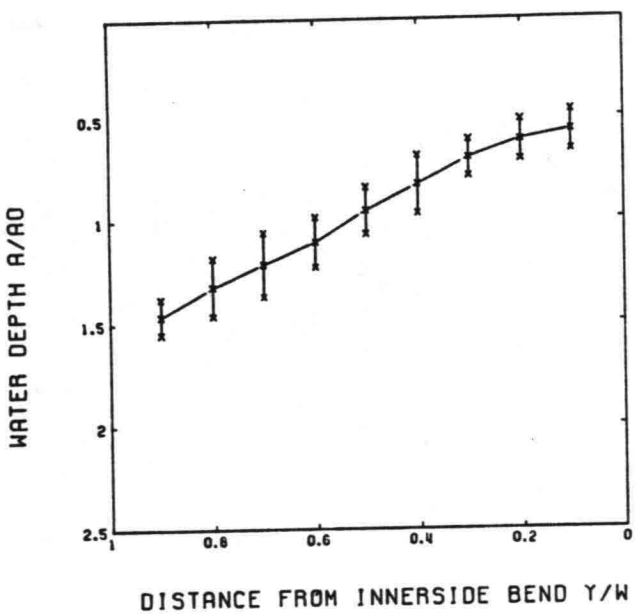

CROSS-SECTION 11

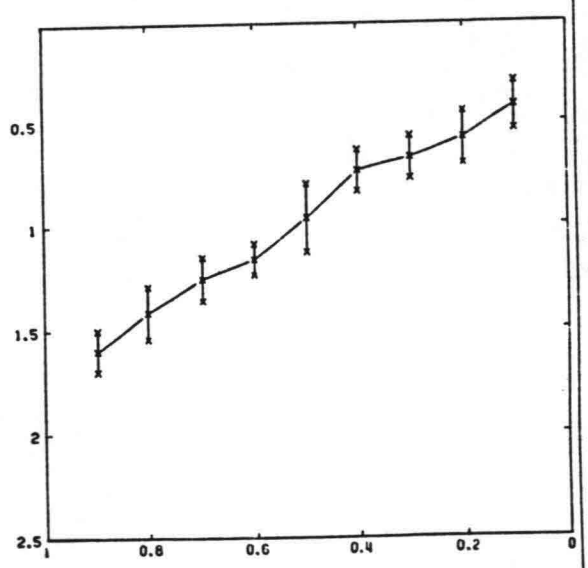

CROSS-SECTION 12

W = 0.5 M AO = 0.051 M

$\pm\sigma$ OF 10 MEASUREMENTS

WATER DEPTH IN CROSS-DIRECTION

FIG 7C

DELFT UNIVERSITY OF TECHNOLOGY

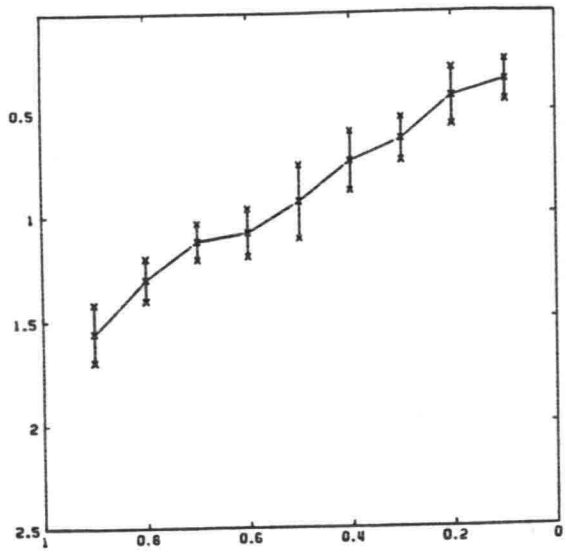

CROSS-SECTION 13

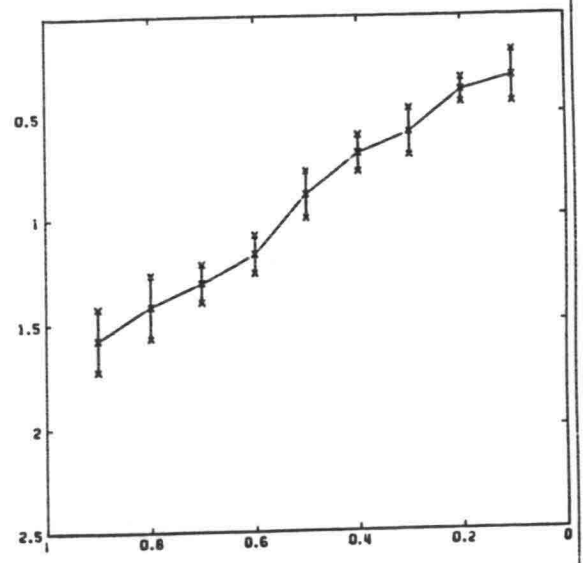

CROSS-SECTION 14

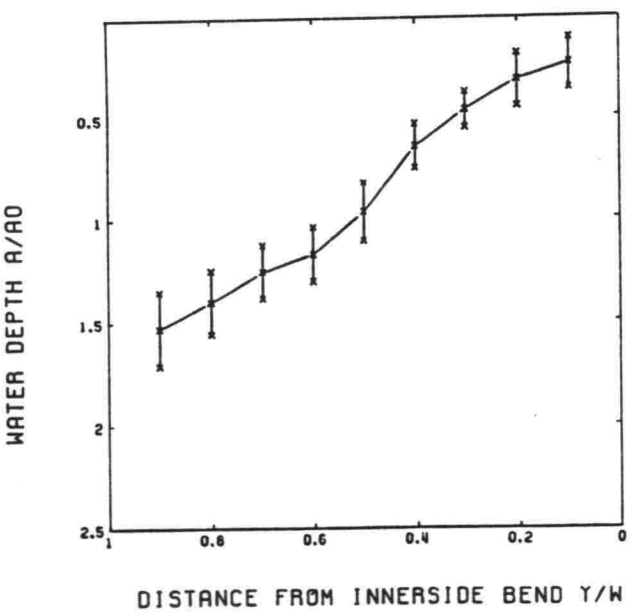

CROSS-SECTION 15

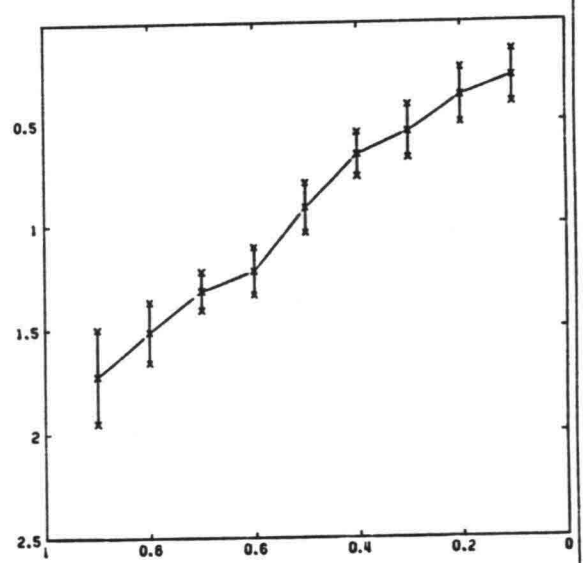

CROSS-SECTION 16

W = 0.5 M A0 = 0.051 M

± σ OF 10 MEASUREMENTS

WATER DEPTH IN CROSS-DIRECTION

FIG 7D

DELFT UNIVERSITY OF TECHNOLOGY

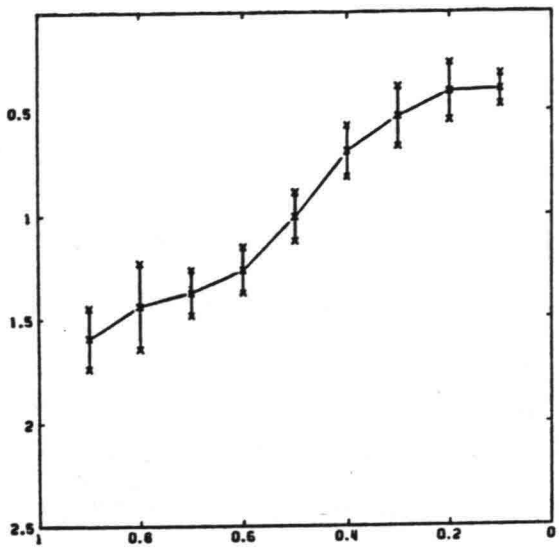

CROSS-SECTION 17

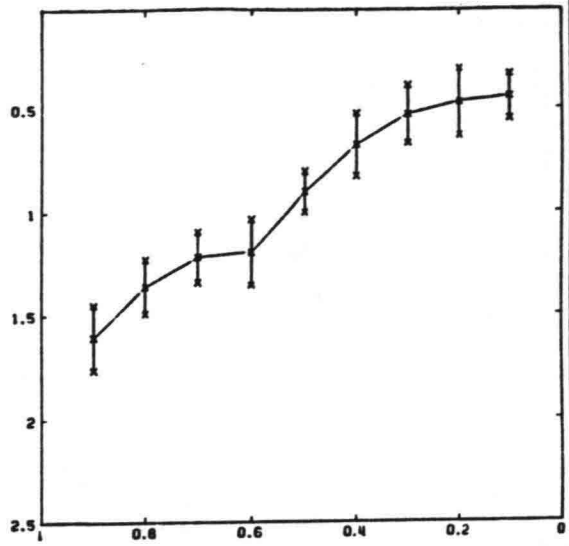

CROSS-SECTION 18

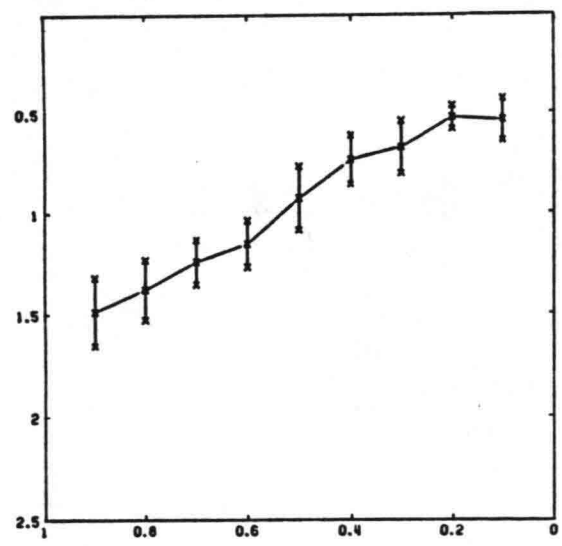

CROSS-SECTION 19

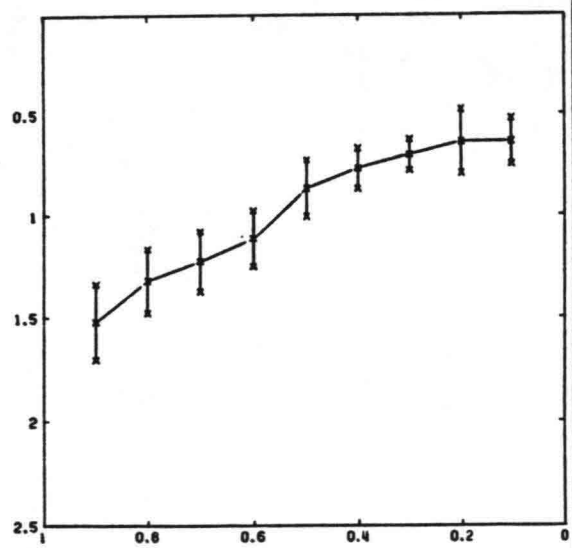

CROSS-SECTION 20

W = 0.5 M AO = 0.051 M

$\pm \sigma$ OF 10 MEASUREMENTS

WATER DEPTH IN CROSS-DIRECTION

FIG 7E

DELFT UNIVERSITY OF TECHNOLOGY

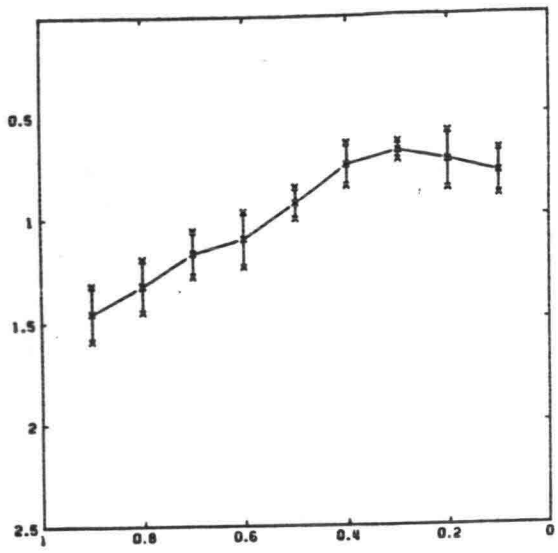

CROSS-SECTION 21

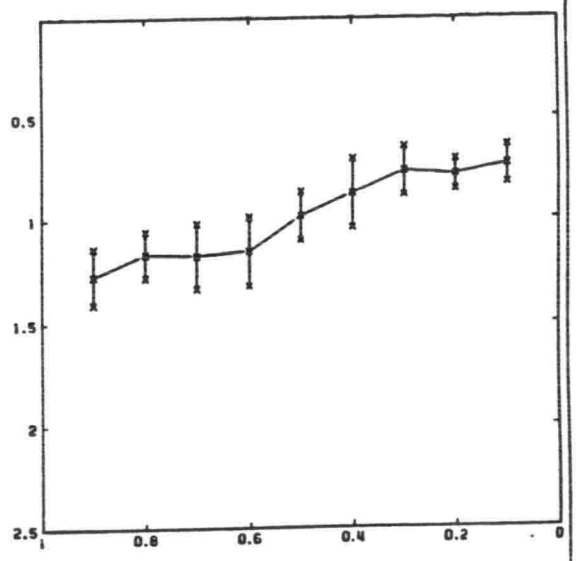

CROSS-SECTION 22

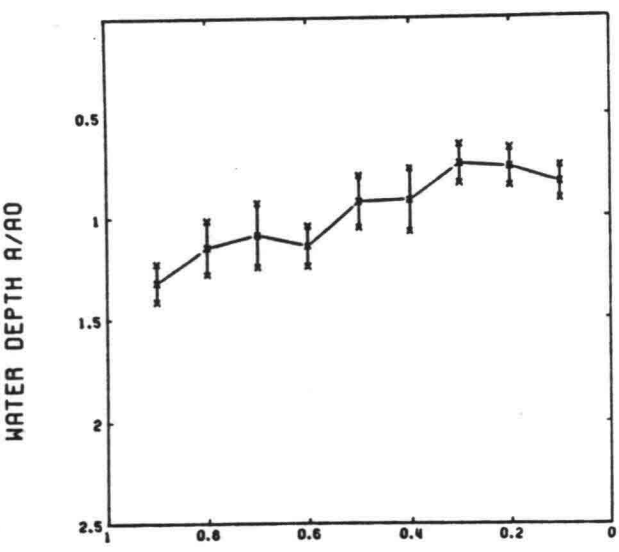

CROSS-SECTION 23

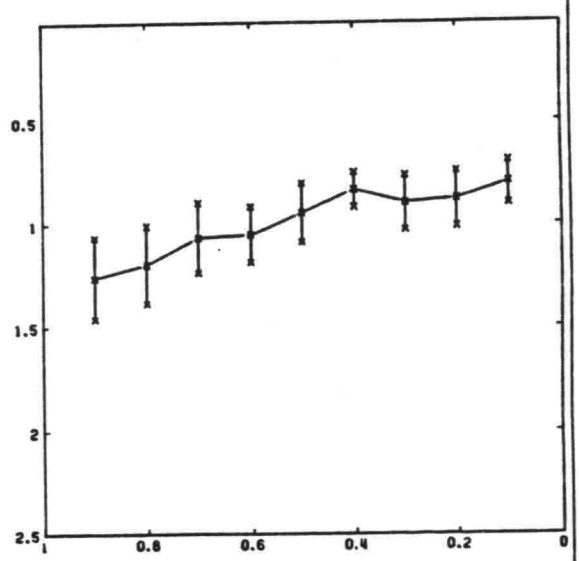

CROSS-SECTION 24

W = 0.5 M A0 = 0.051 M

$\pm \sigma$ OF 10 MEASUREMENTS

WATER DEPTH IN CROSS-DIRECTION

FIG 7F

DELFT UNIVERSITY OF TECHNOLOGY

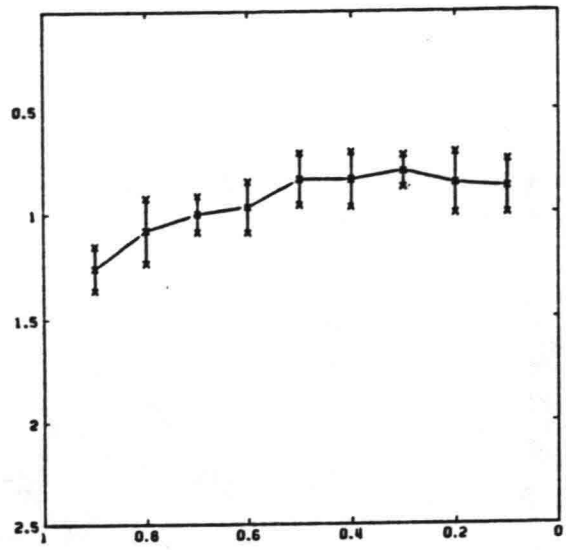

CROSS-SECTION 25

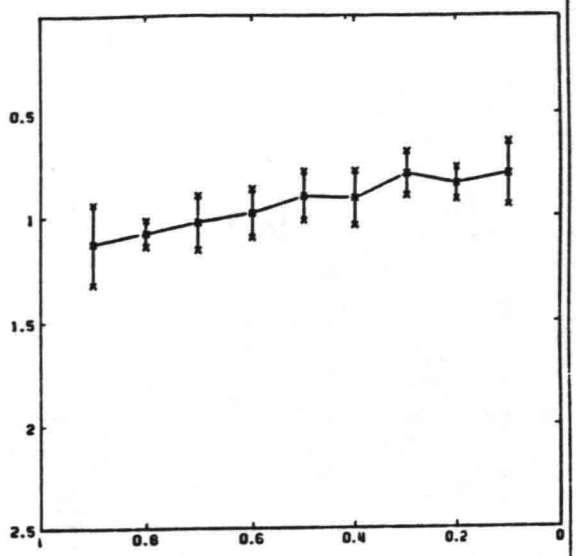

CROSS-SECTION 26

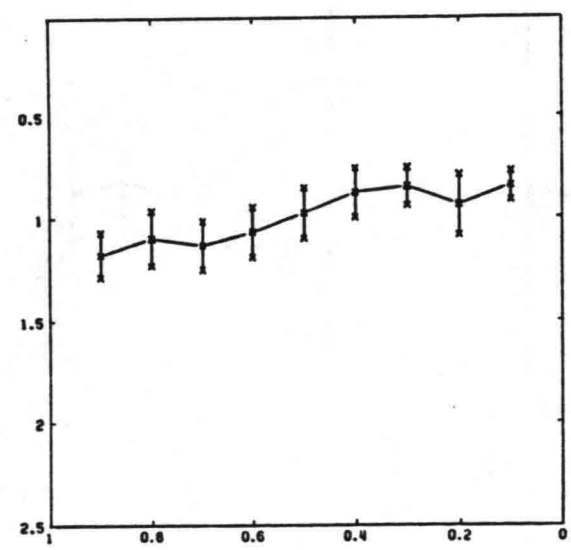

CROSS-SECTION 27

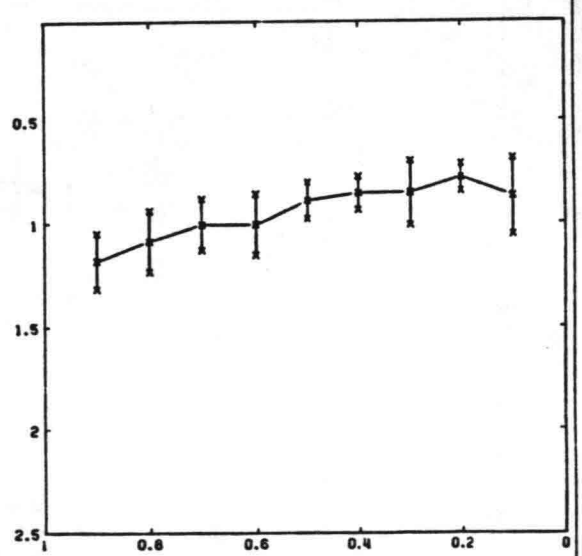

CROSS-SECTION 28

W = 0.5 M AO = 0.051 M

± σ OF 10 MEASUREMENTS

WATER DEPTH IN CROSS-DIRECTION

FIG 7G

DELFT UNIVERSITY OF TECHNOLOGY

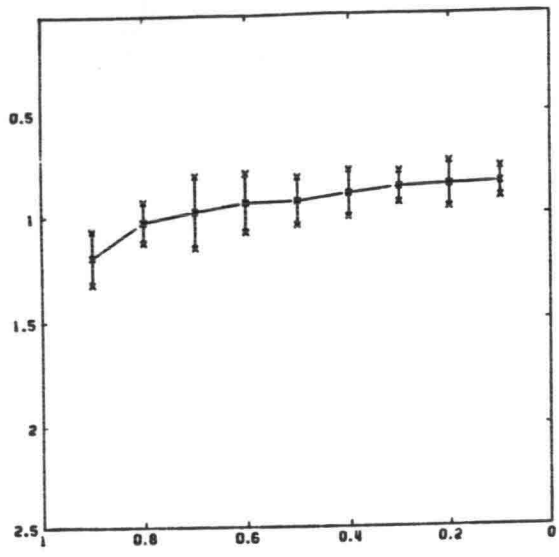

CROSS-SECTION 29

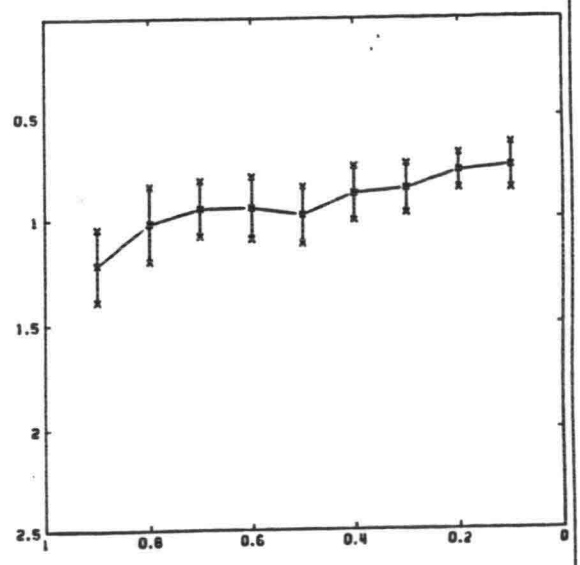

CROSS-SECTION 30

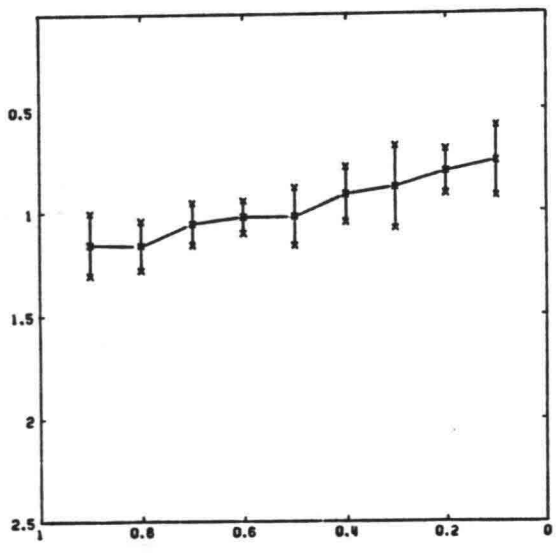

CROSS-SECTION 31

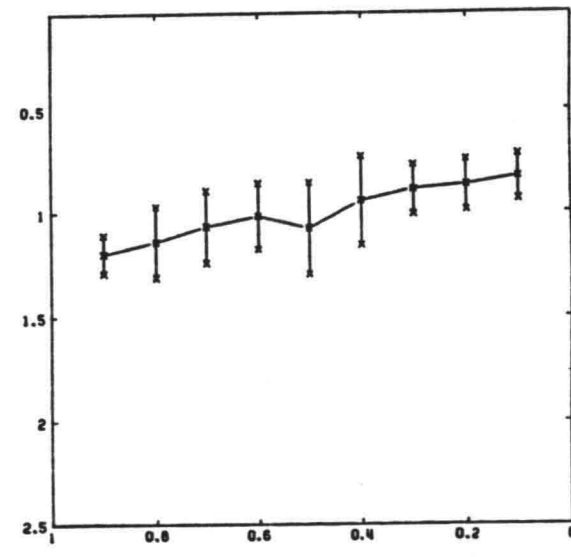

CROSS-SECTION 32

W = 0.5 M A0 = 0.051 M

$\pm \sigma$ OF 10 MEASUREMENTS

WATER DEPTH IN CROSS-DIRECTION

FIG 7H

DELFT UNIVERSITY OF TECHNOLOGY

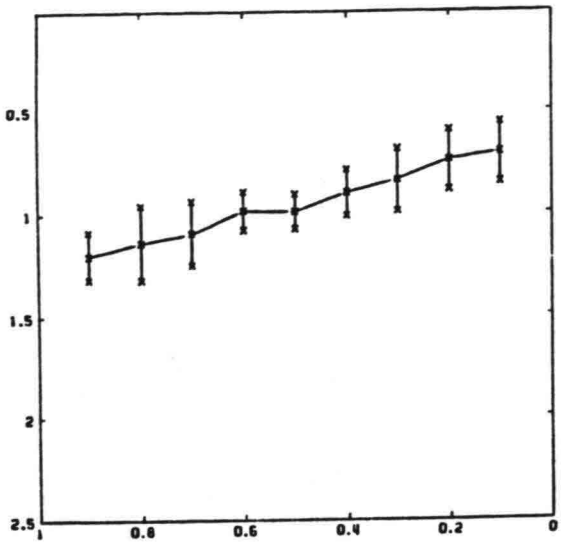

CROSS-SECTION 33

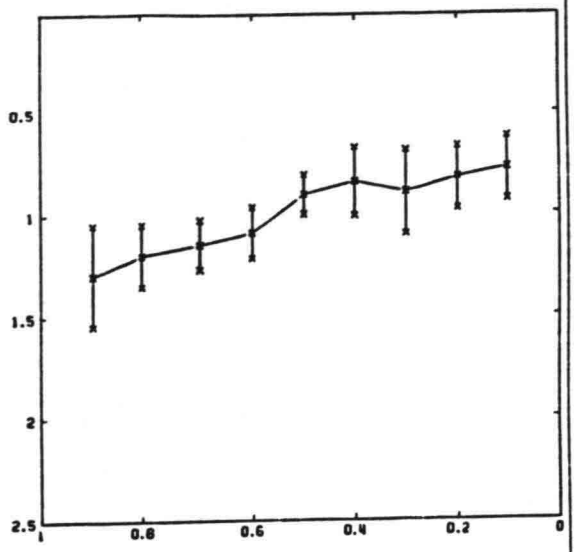

CROSS-SECTION 34

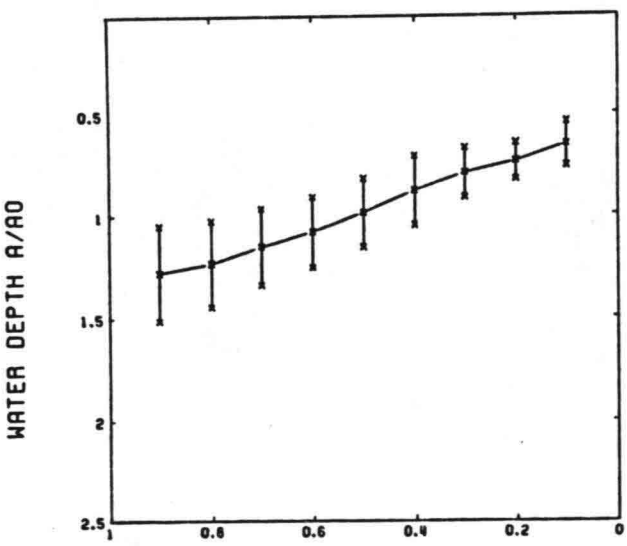

CROSS-SECTION 35

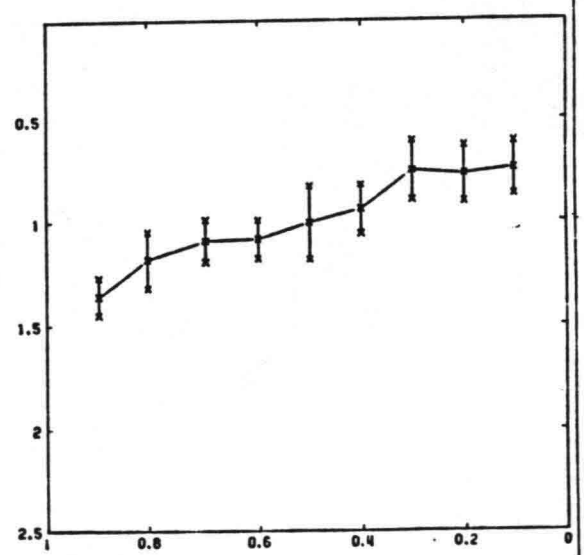

CROSS-SECTION 36

W = 0.5 M A0 = 0.051 M

$\pm \sigma$ OF 10 MEASUREMENTS

WATER DEPTH IN CROSS-DIRECTION

FIG 7I

DELFT UNIVERSITY OF TECHNOLOGY

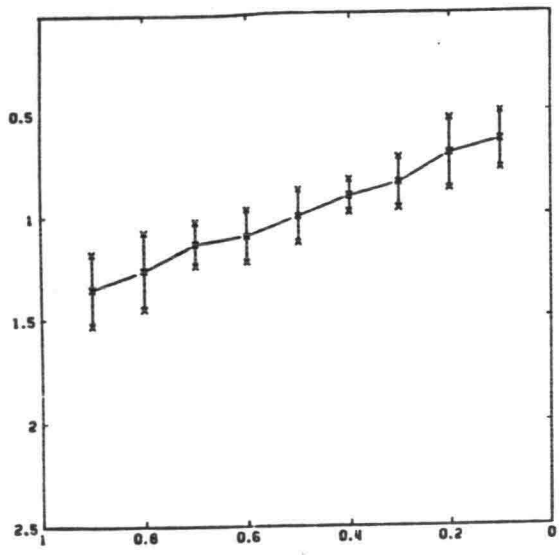

CROSS-SECTION 37

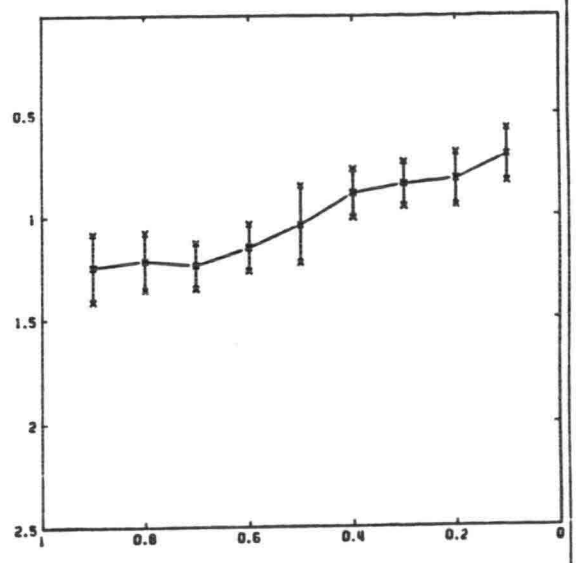

CROSS-SECTION 38

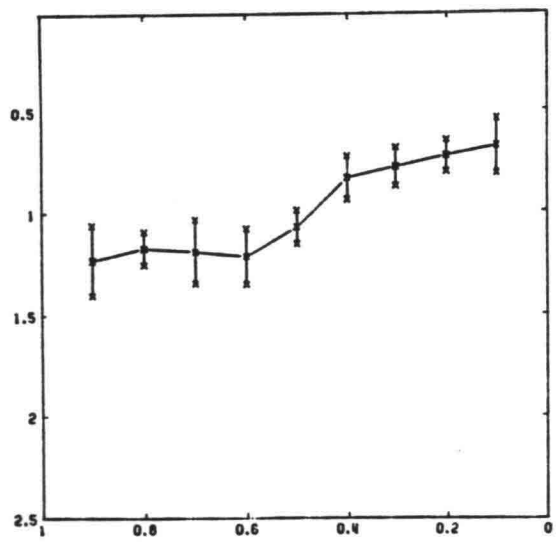

CROSS-SECTION 39

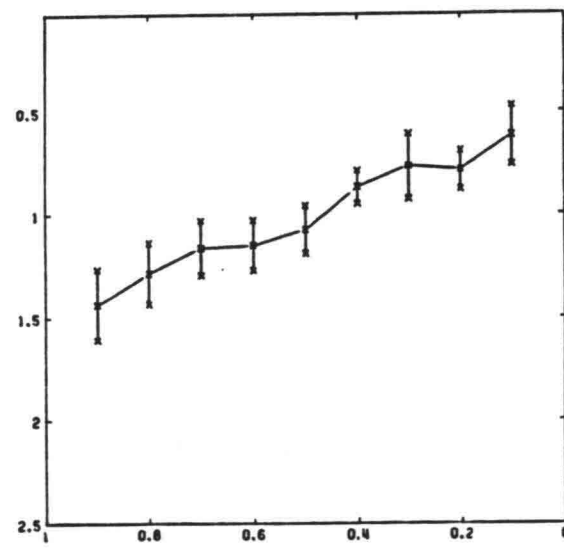

CROSS-SECTION 40

W = 0.5 M A0 = 0.051 M

$\pm \sigma$ OF 10 MEASUREMENTS

WATER DEPTH IN CROSS-DIRECTION

FIG 7J

DELFT UNIVERSITY OF TECHNOLOGY

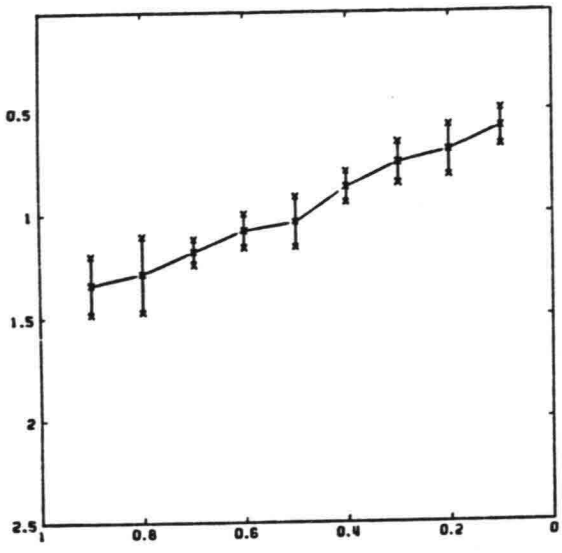

CROSS-SECTION 41

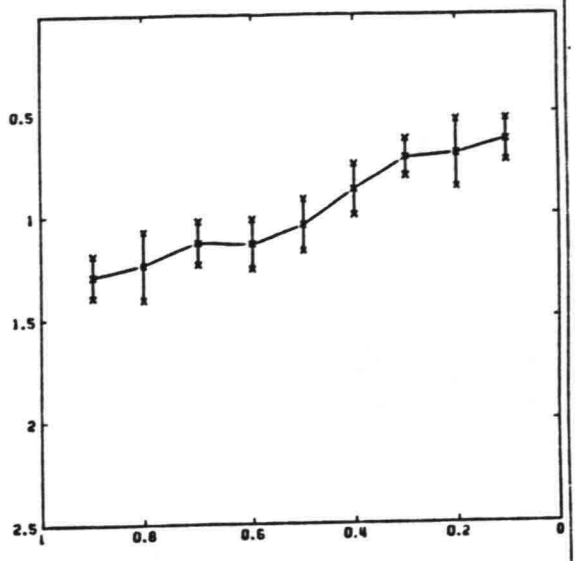

CROSS-SECTION 42

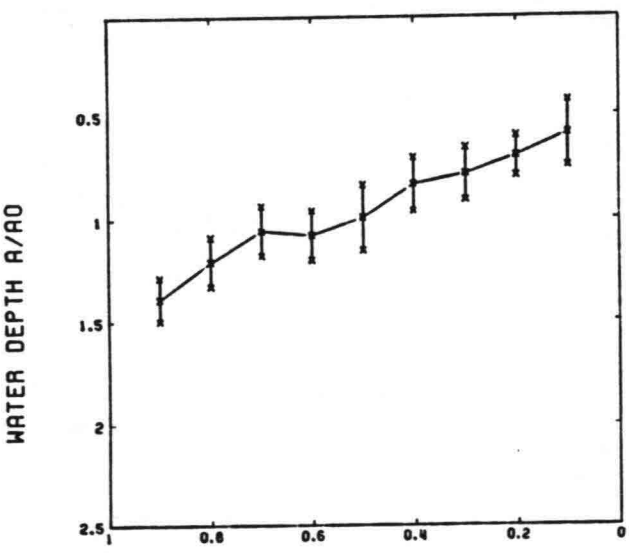

CROSS-SECTION 43

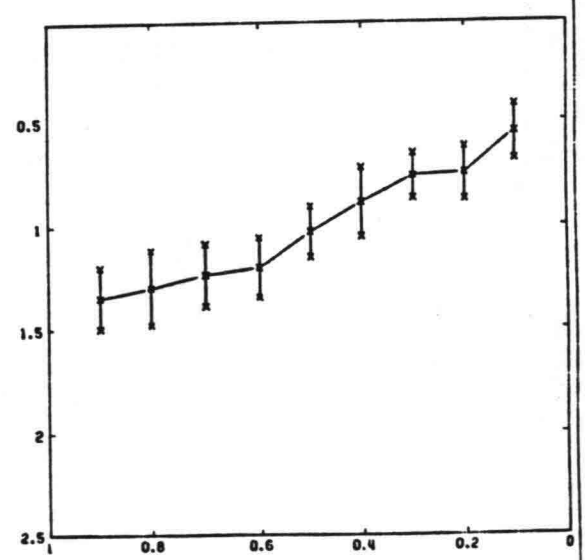

CROSS-SECTION 44

W = 0.5 M AO = 0.051 M

$\pm \sigma$ OF 10 MEASUREMENTS

WATER DEPTH IN CROSS-DIRECTION

FIG 7K

DELFT UNIVERSITY OF TECHNOLOGY

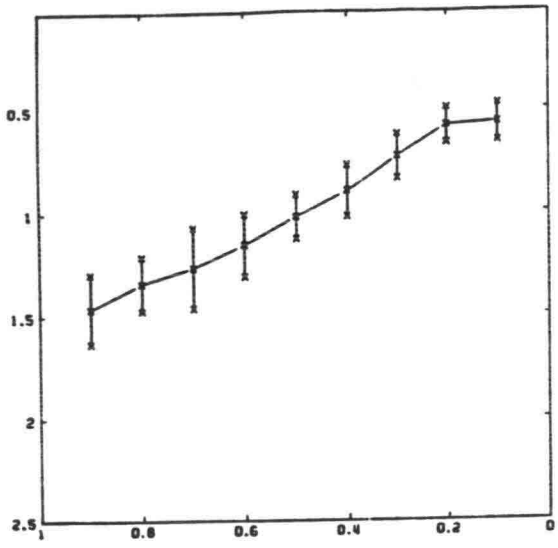

CROSS-SECTION 45

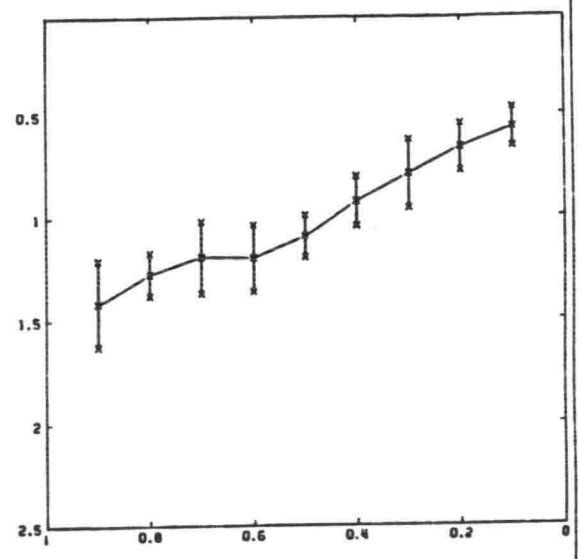

CROSS-SECTION 46

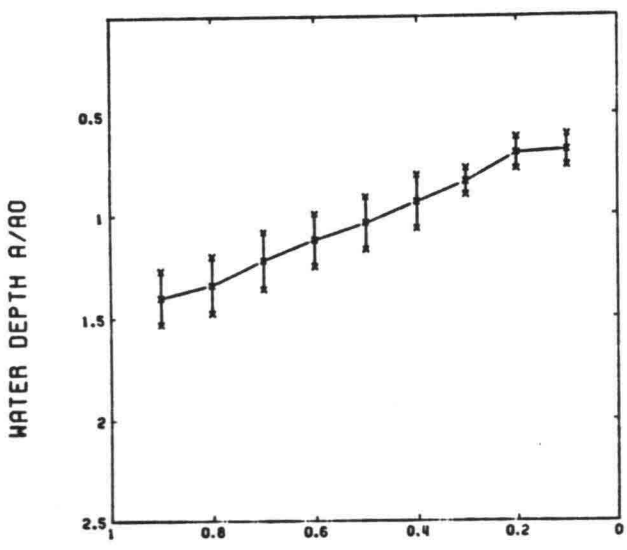

CROSS-SECTION 47

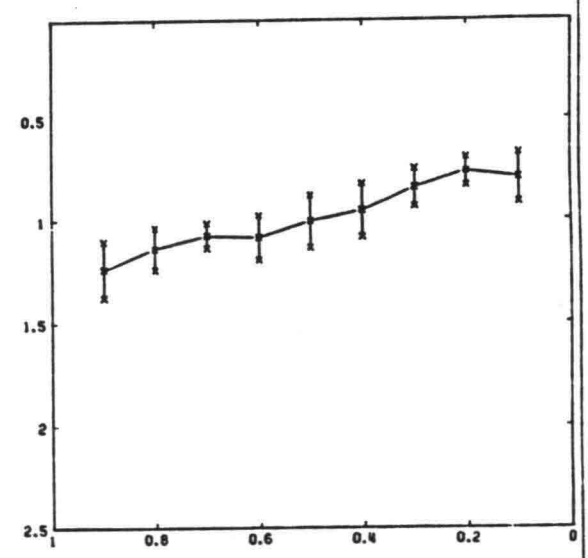

CROSS-SECTION 48

W = 0.5 M AO = 0.051 M

$\pm \sigma$ OF 10 MEASUREMENTS

WATER DEPTH IN CROSS-DIRECTION

FIG 7L

DELFT UNIVERSITY OF TECHNOLOGY

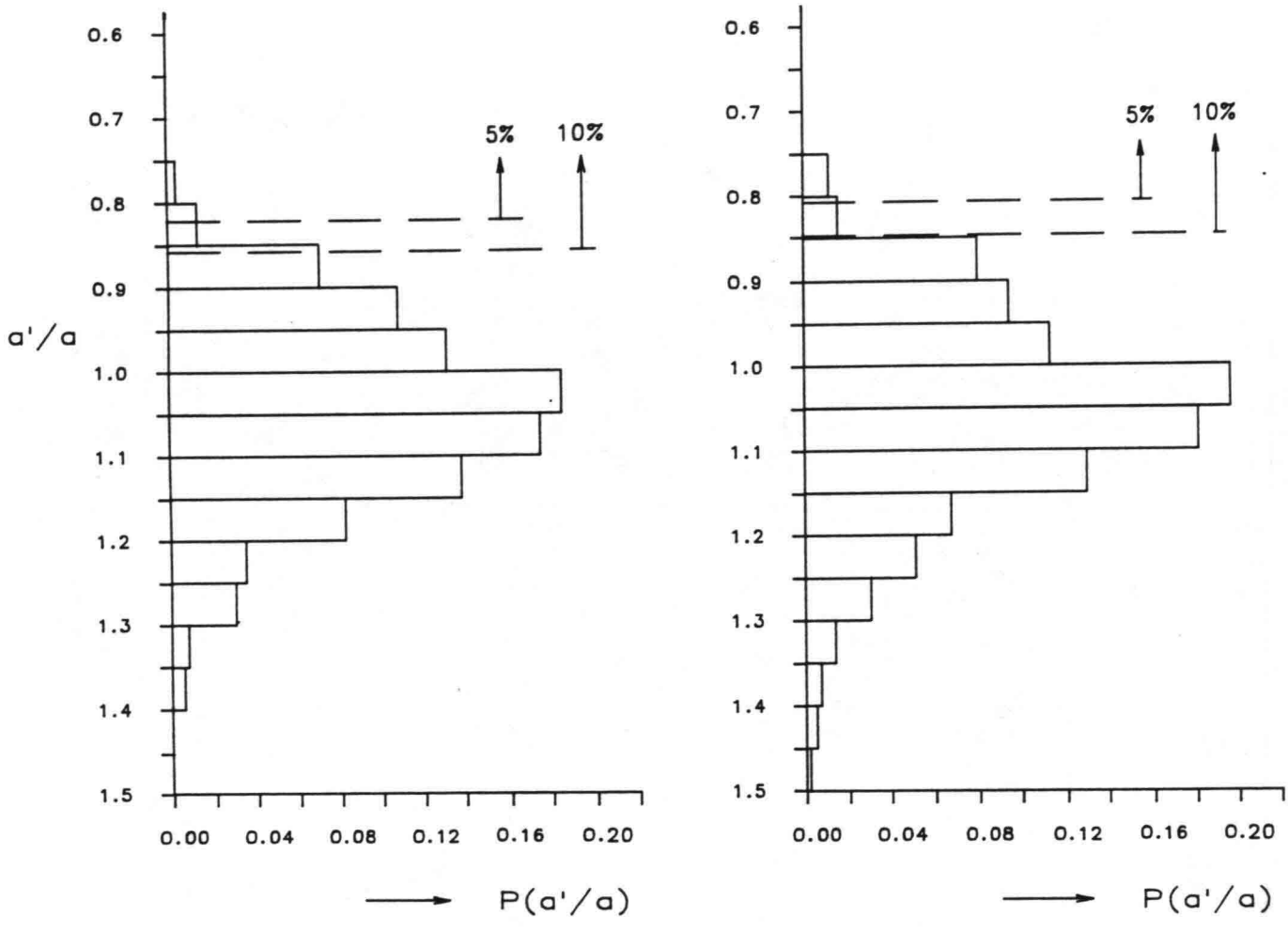

a' local water depth

a ensemble mean local water depth

PROBABILITY DISTRIBUTION OF BED LEVEL

FIG. 8

DELFT UNIVERSITY OF TECHNOLOGY

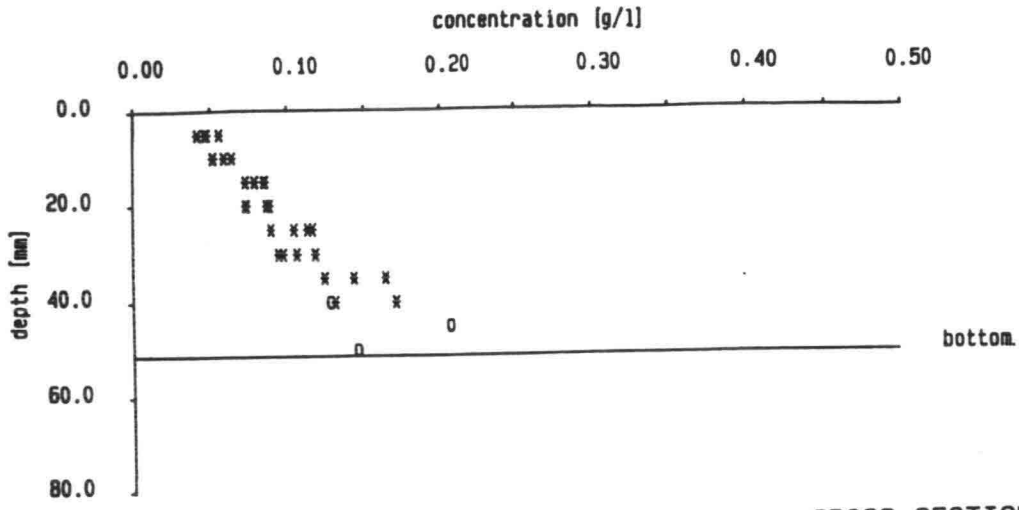

at: y=1/2 W

CROSS-SECTION 1

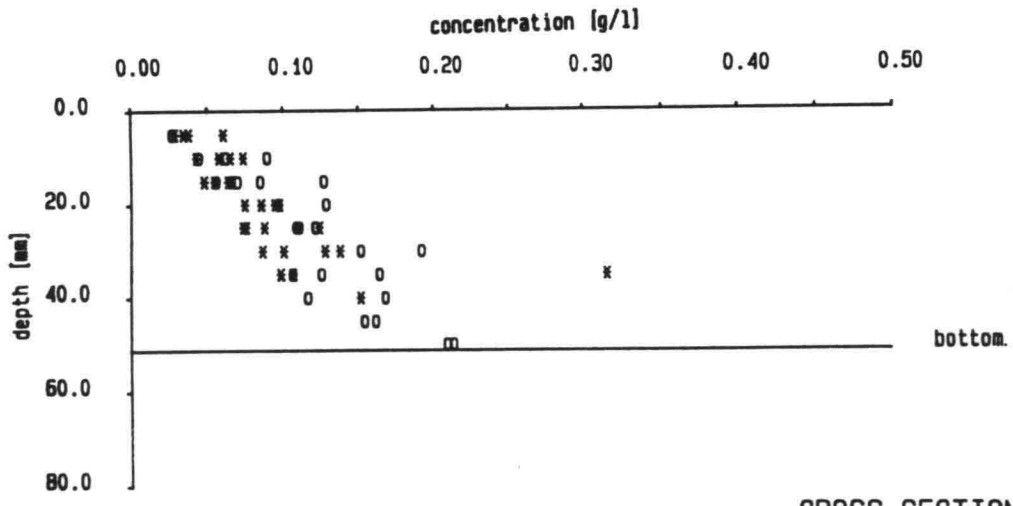

at: y=1/2 W

CROSS-SECTION 5

CONCENTRATION PROFILES
(mean water depth of 10 measurements)

FIG. 9 a

DELFT UNIVERSITY OF TECHNOLOGY

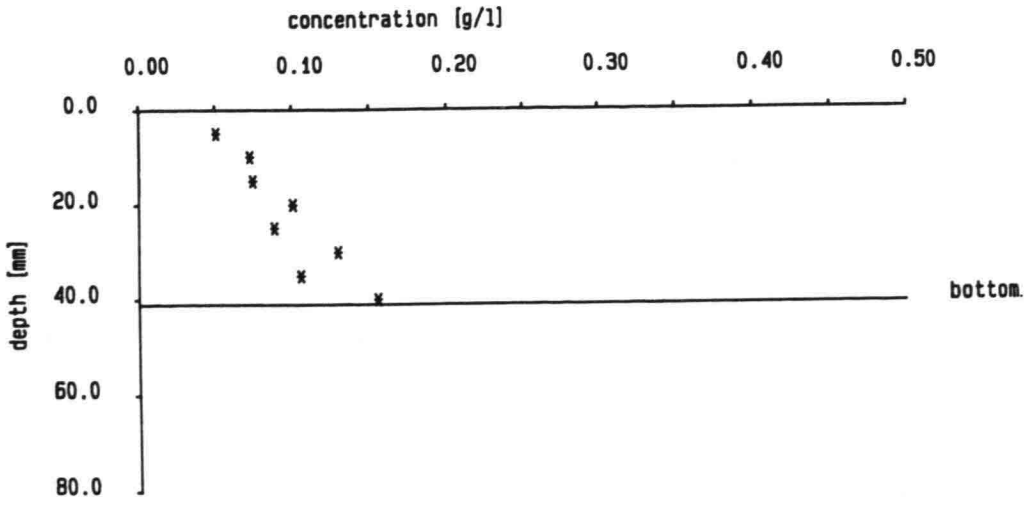

at: y=1/4 W

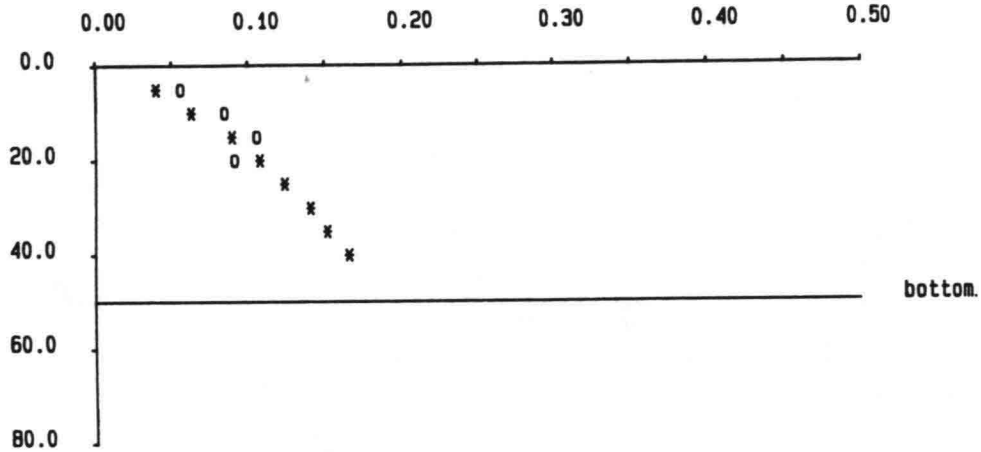

at: y=1/2 W

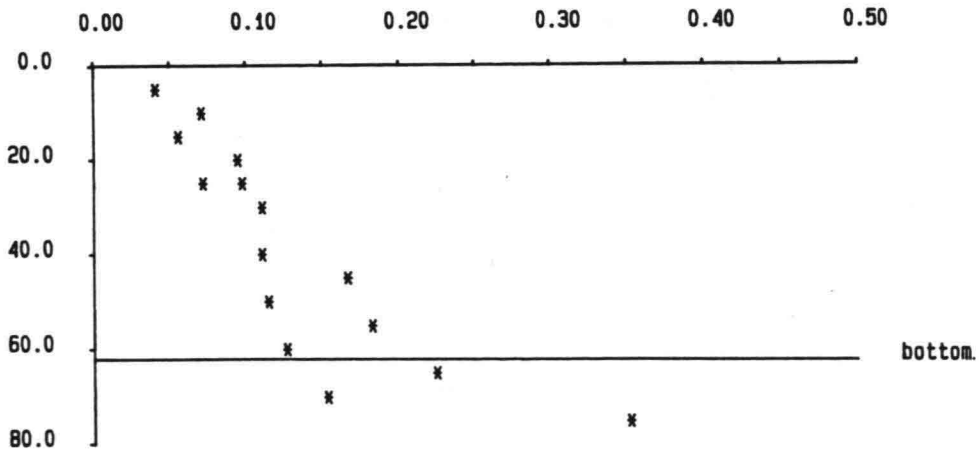

at: y=3/4 W

CROSS-SECTION 10

CONCENTRATION PROFILES
(mean water depth of 10 measurements)

FIG. 9 b

DELFT UNIVERSITY OF TECHNOLOGY

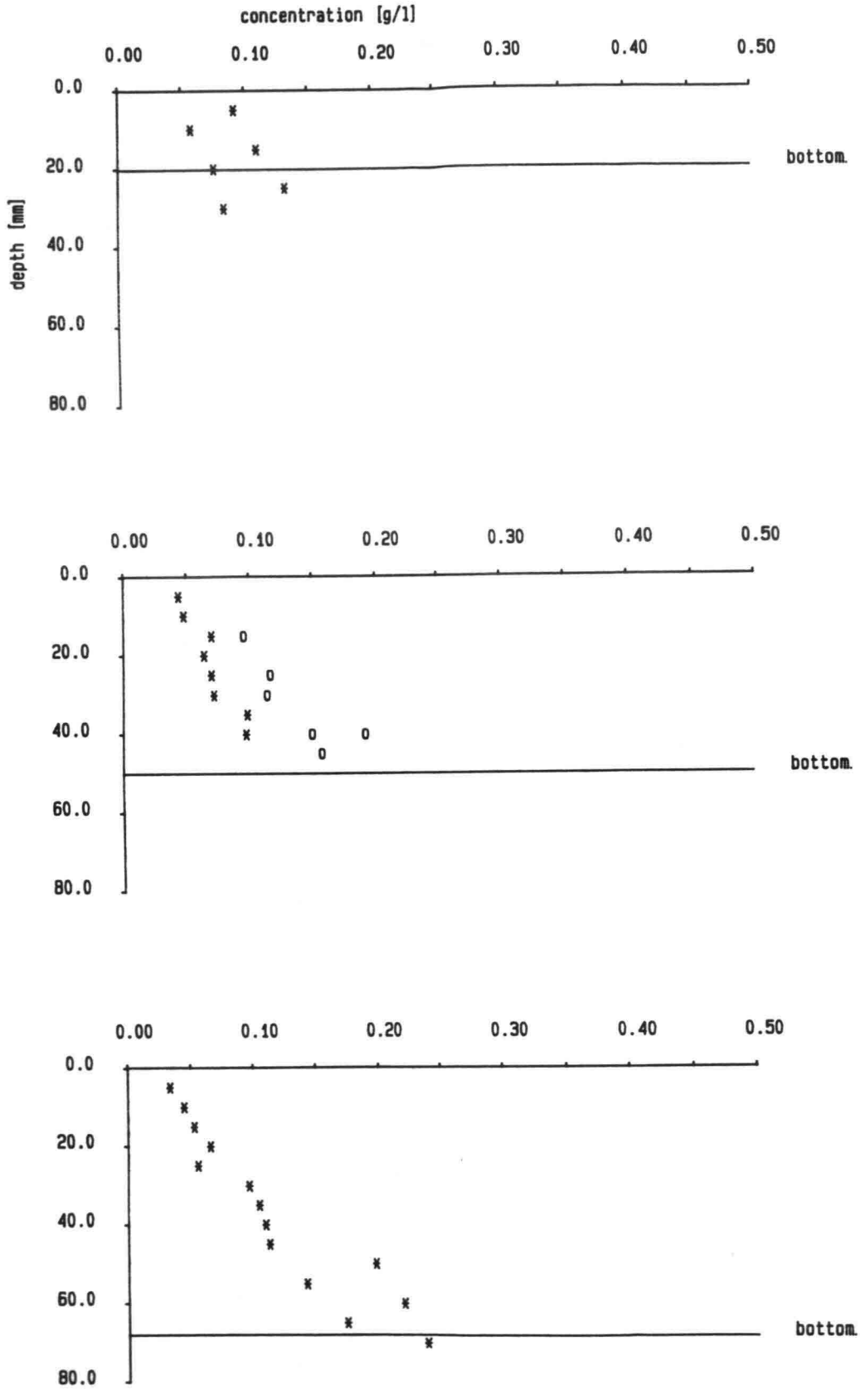

CROSS-SECTION 15

CONCENTRATION PROFILES
(mean water depth of 10 measurements)

FIG. 9 c

DELFT UNIVERSITY OF TECHNOLOGY

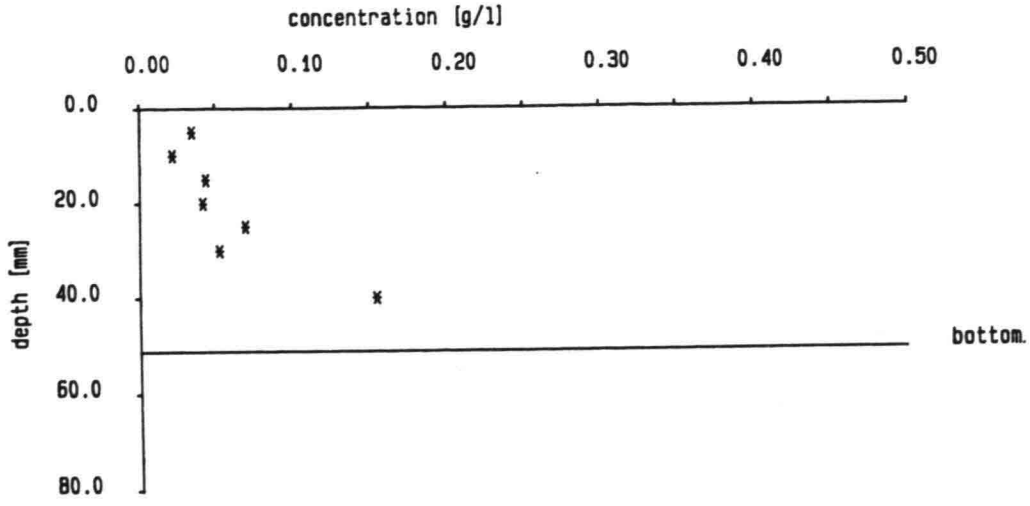

at: y=1/4 W

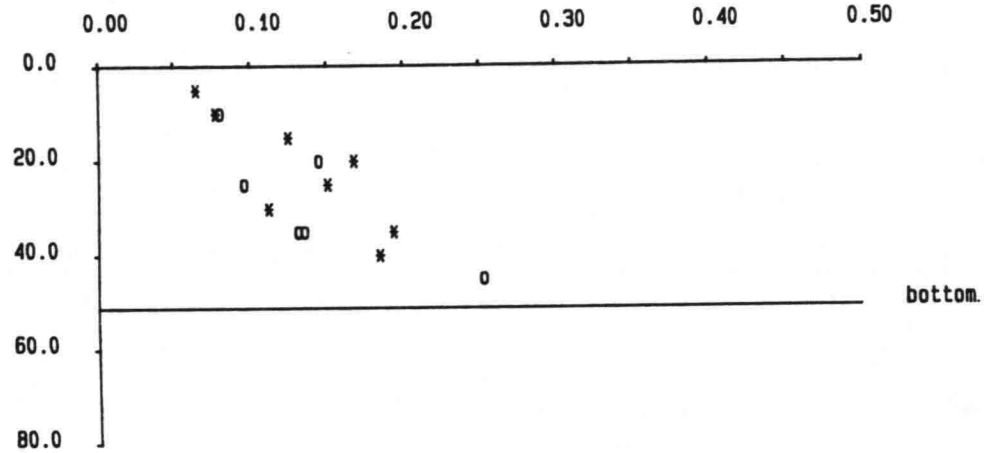

at: y=1/2 W

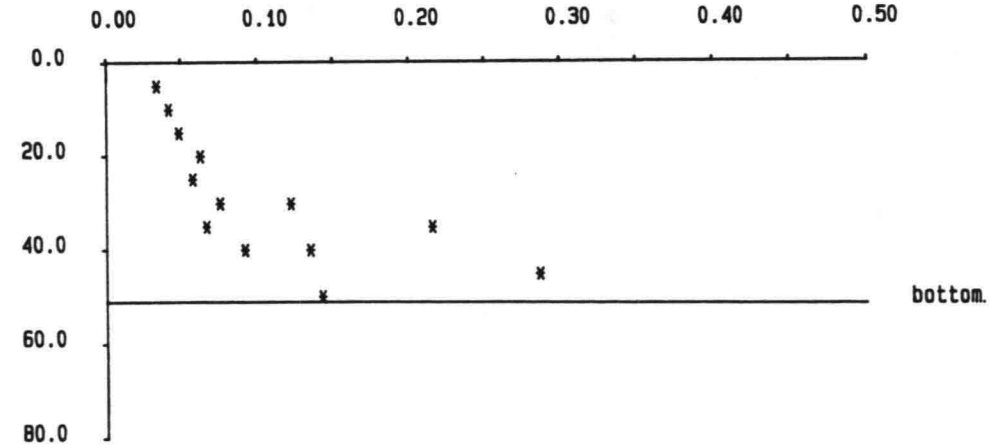

at: y=3/4 W

CROSS-SECTION 20

CONCENTRATION PROFILES
(mean water depth of 10 measurements)

FIG. 9 d

DELFT UNIVERSITY OF TECHNOLOGY

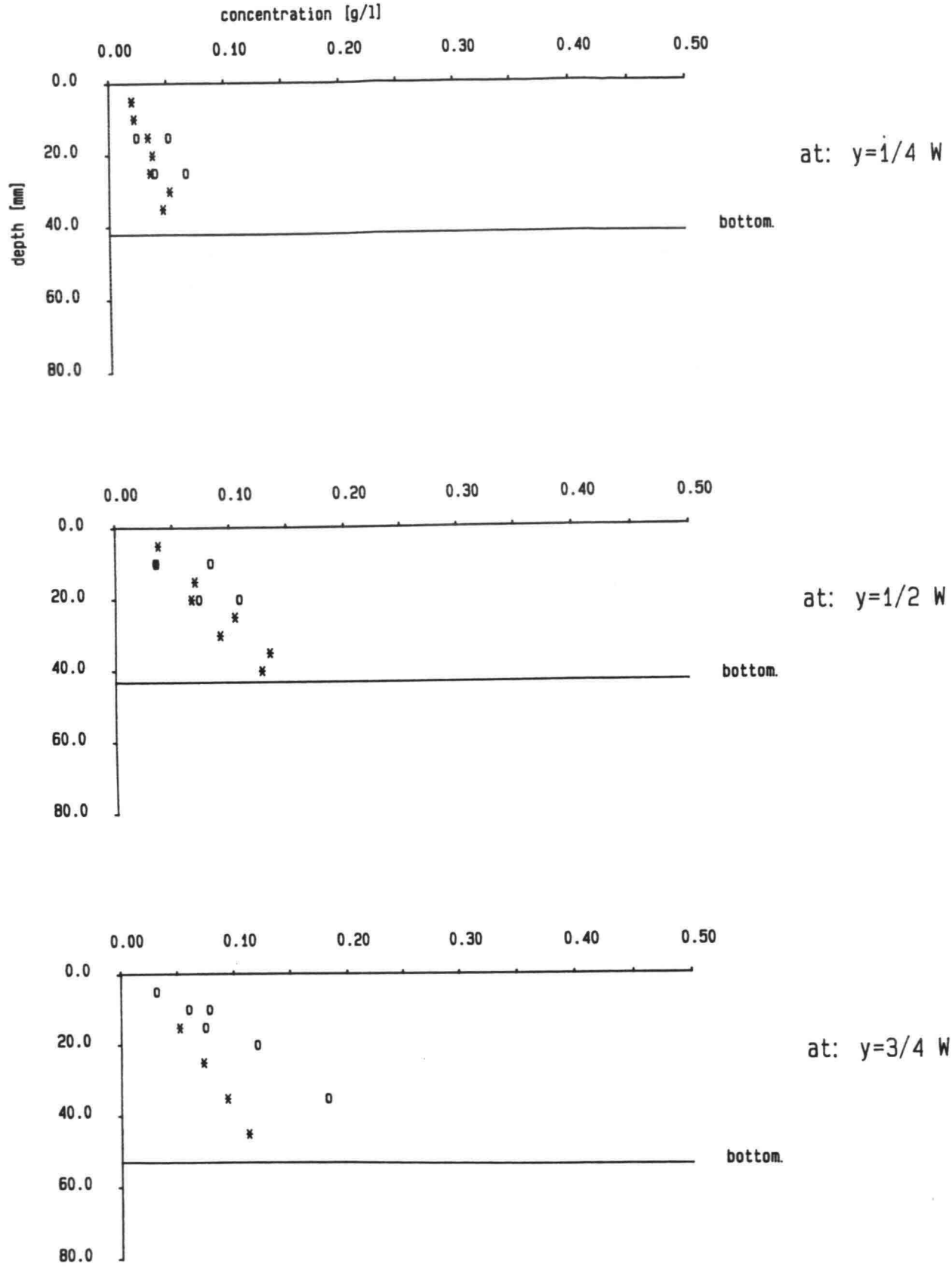

CROSS-SECTION 25

CONCENTRATION PROFILES
(mean water depth of 10 measurements)

FIG. 9 e

DELFT UNIVERSITY OF TECHNOLOGY

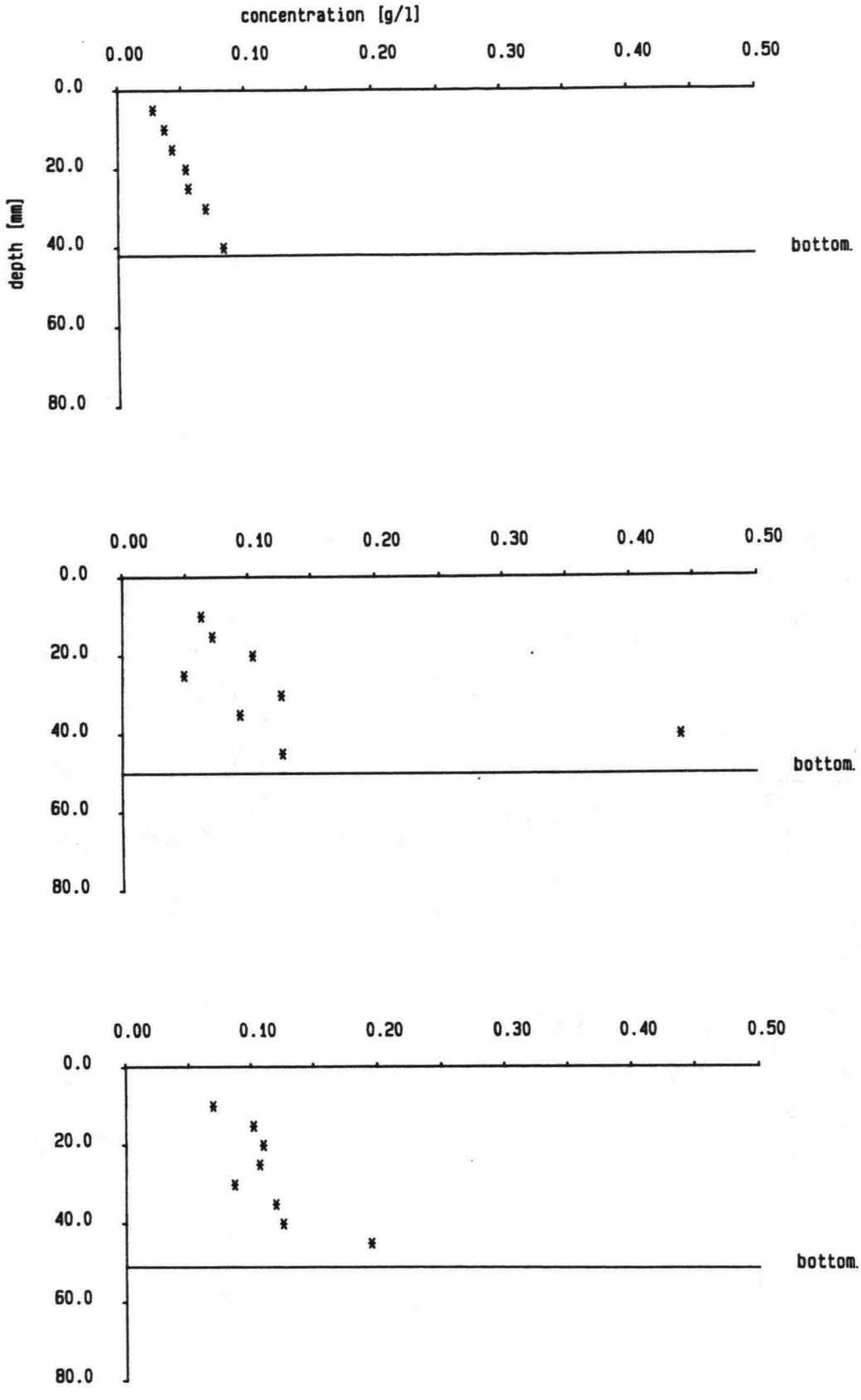

CROSS-SECTION 30

CONCENTRATION PROFILES
(mean water depth of 10 measurements)

FIG. 9 f

DELFT UNIVERSITY OF TECHNOLOGY

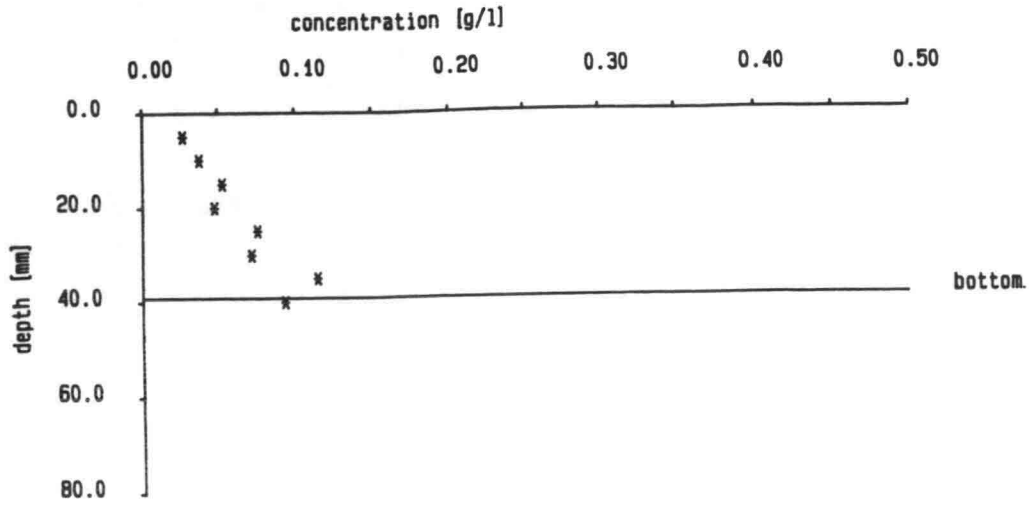

at: y=1/4 W

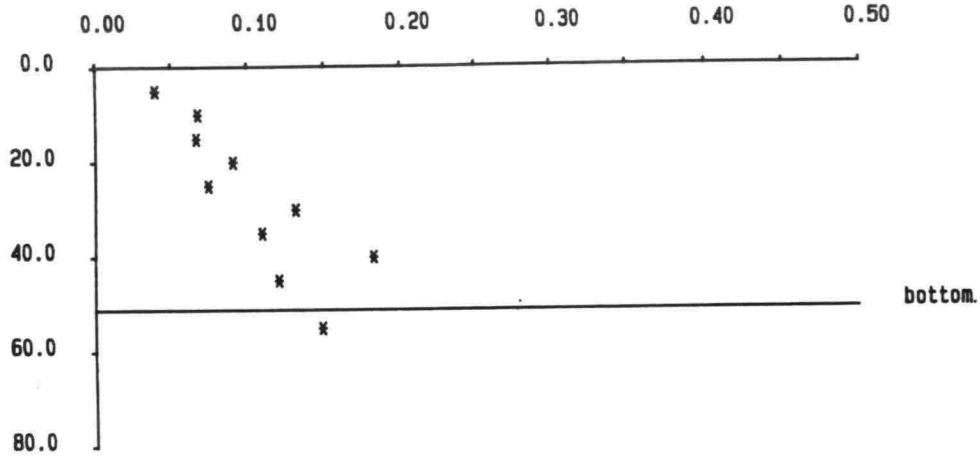

at: y=1/2 W

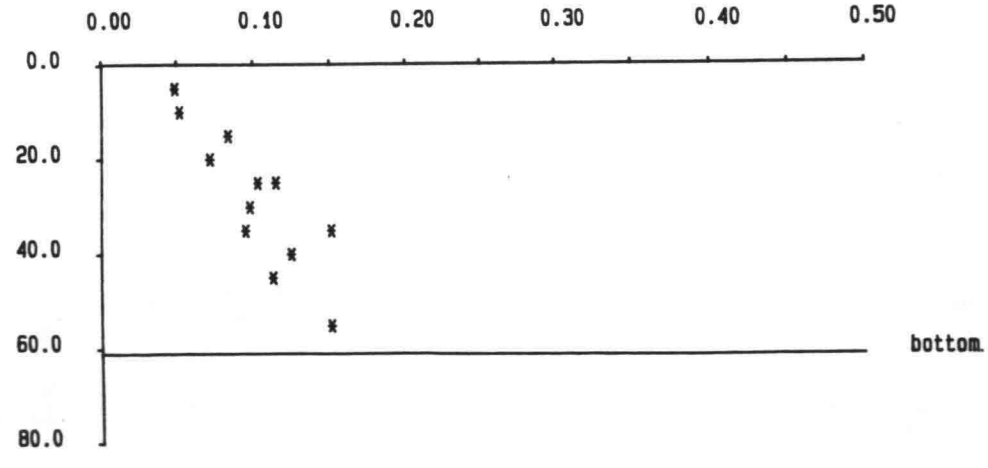

at: y=3/4 W

CROSS-SECTION 35

CONCENTRATION PROFILES
(mean water depth of 10 measurements)

FIG. 9 g

DELFT UNIVERSITY OF TECHNOLOGY

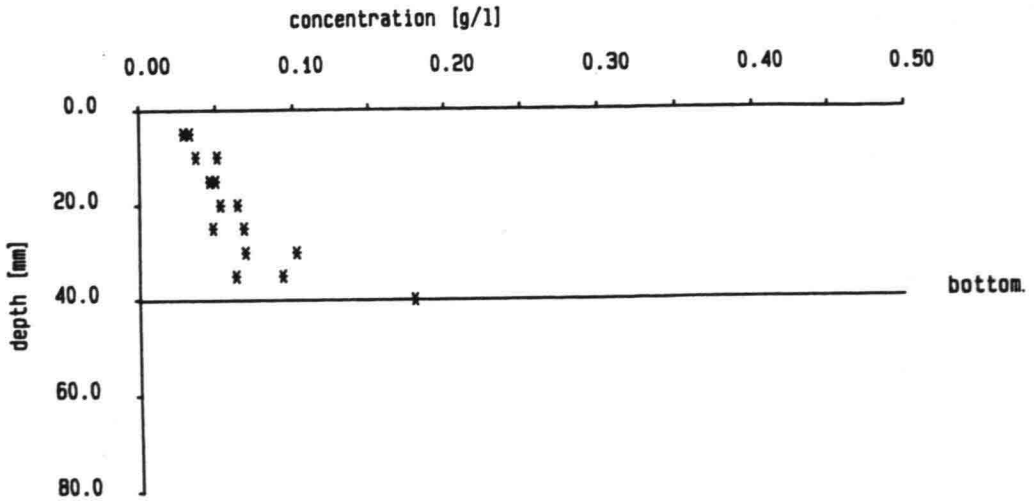

at: y=1/4 W

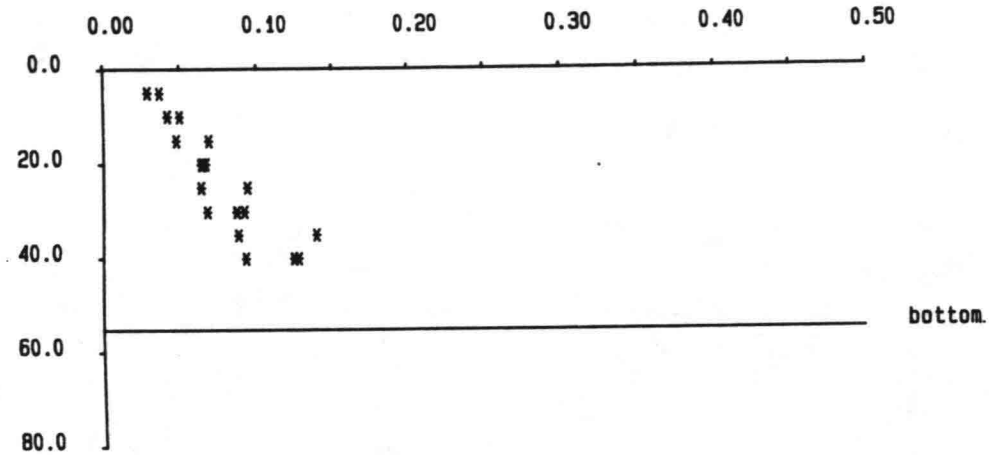

at: y=1/2 W

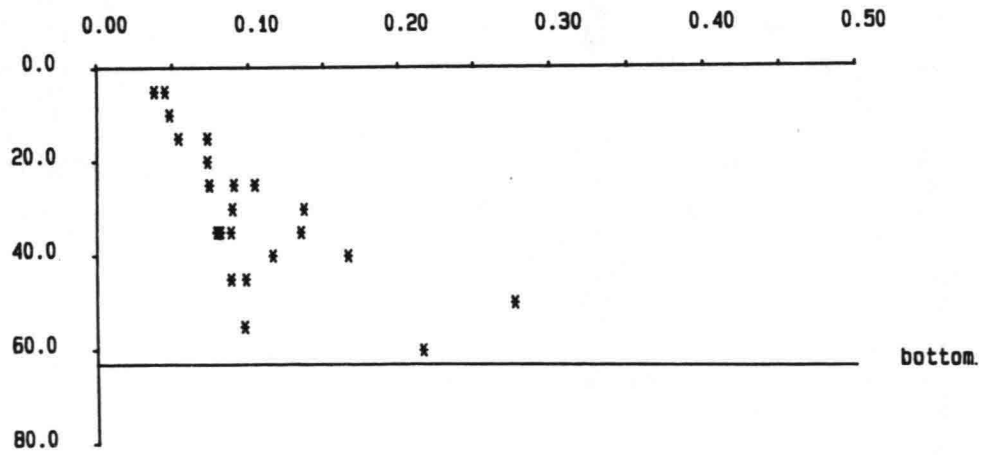

at: y=3/4 W

CROSS-SECTION 40

CONCENTRATION PROFILES
(mean water depth of 10 measurements)

FIG. 9 h

DELFT UNIVERSITY OF TECHNOLOGY

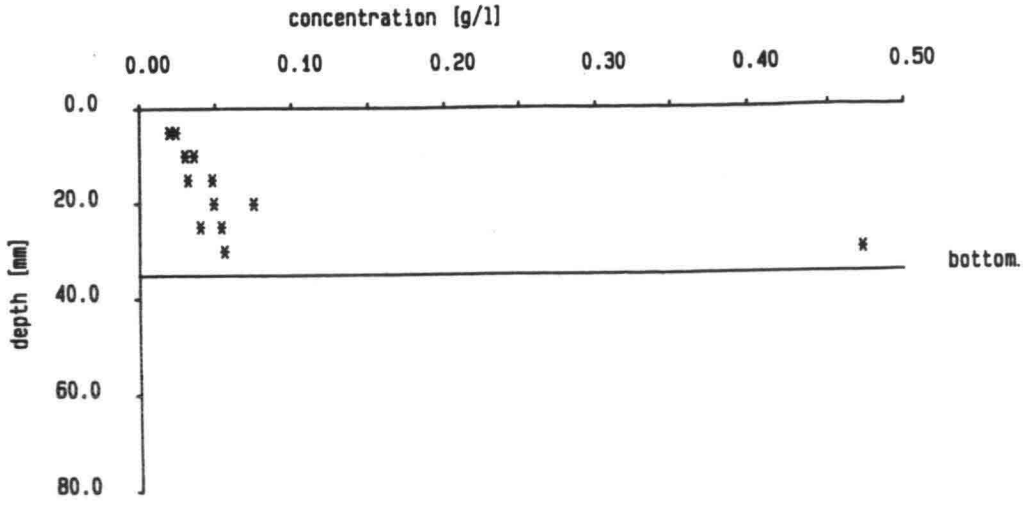

at: y=1/4 W

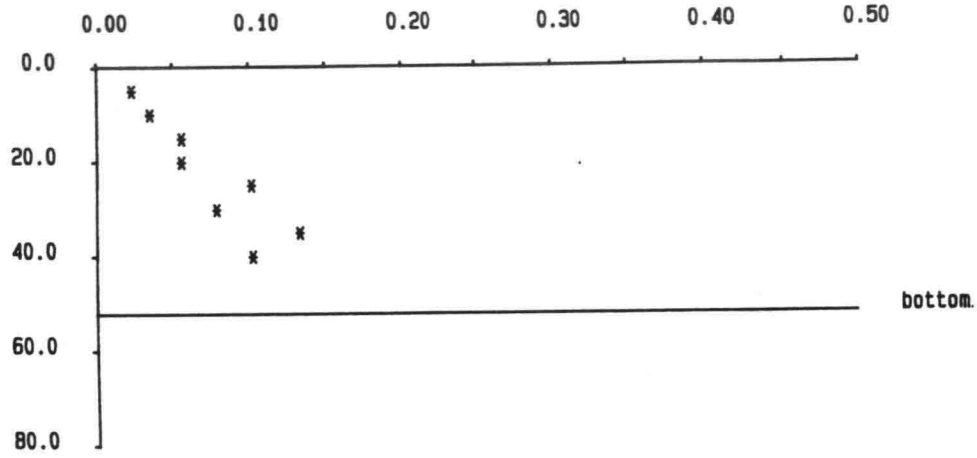

at: y=1/2 W

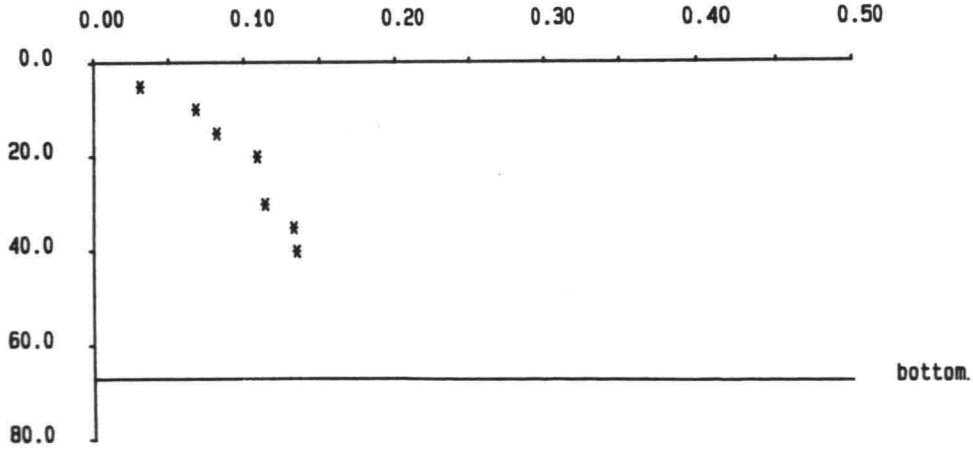

at: y=3/4 W

CROSS-SECTION 45

CONCENTRATION PROFILES
(mean water depth of 10 measurements)

FIG. 9 i

DELFT UNIVERSITY OF TECHNOLOGY

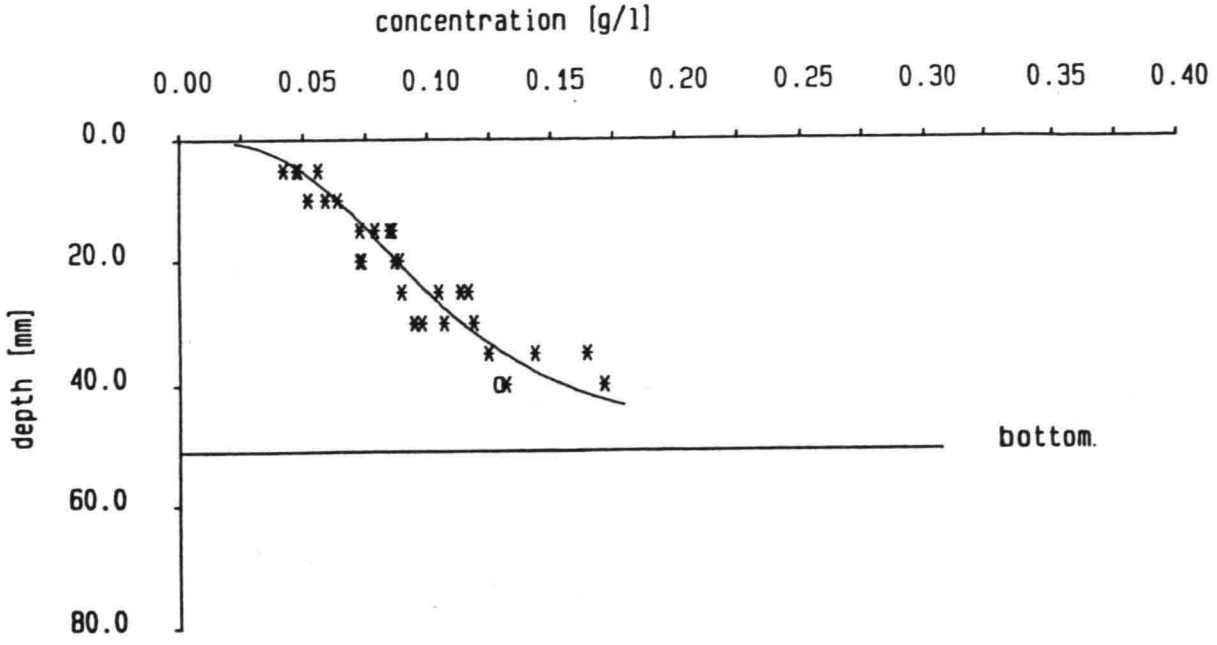

CROSS-SECTION 1

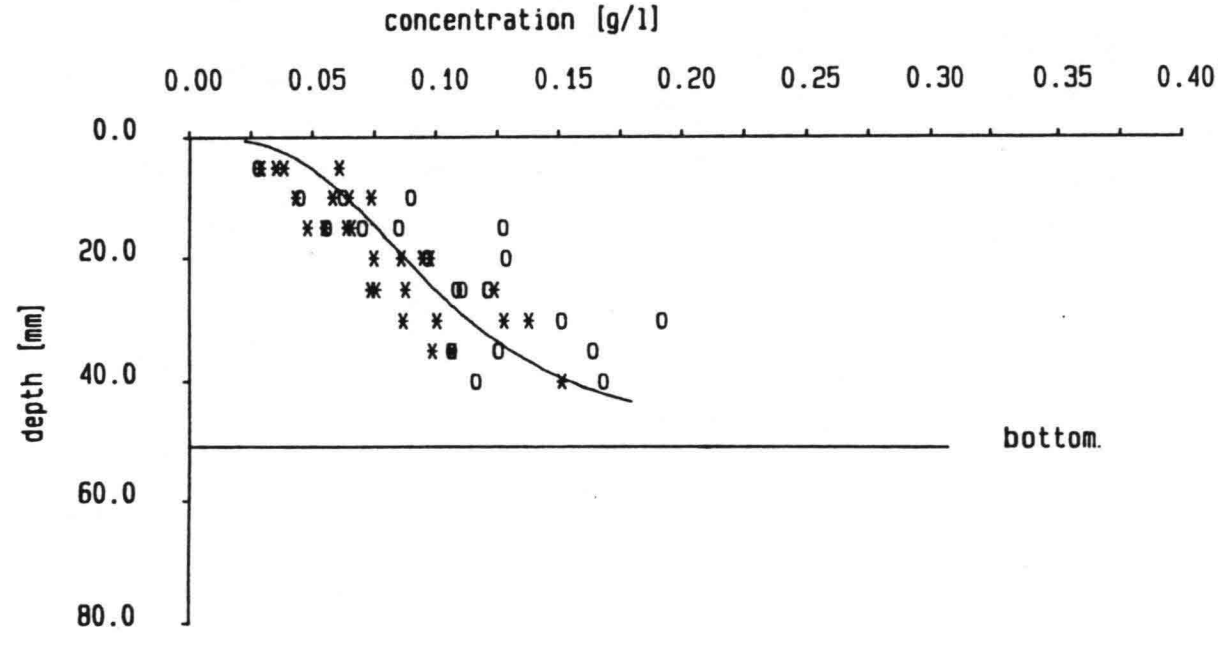

CROSS-SECTION 5

CURVE FIT OF EQUILIBRIUM PROFILE

FIG. 10

DELFT UNIVERSITY OF TECHNOLOGY

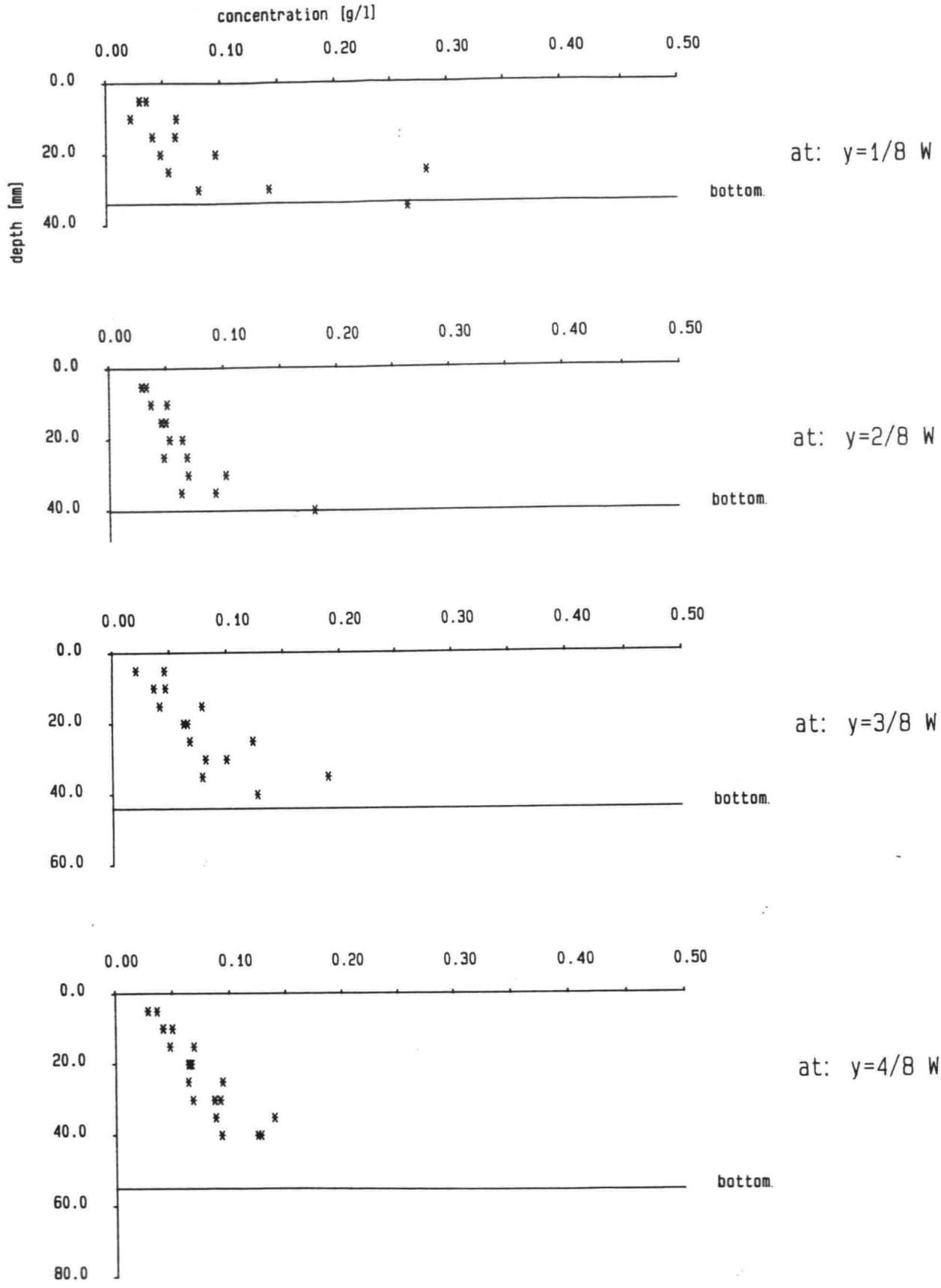

CONCENTRATION PROFILES AT CROSS-SECTION 40
(mean water depth of 10 measurements)

FIG. 11 a

DELFT UNIVERSITY OF TECHNOLOGY

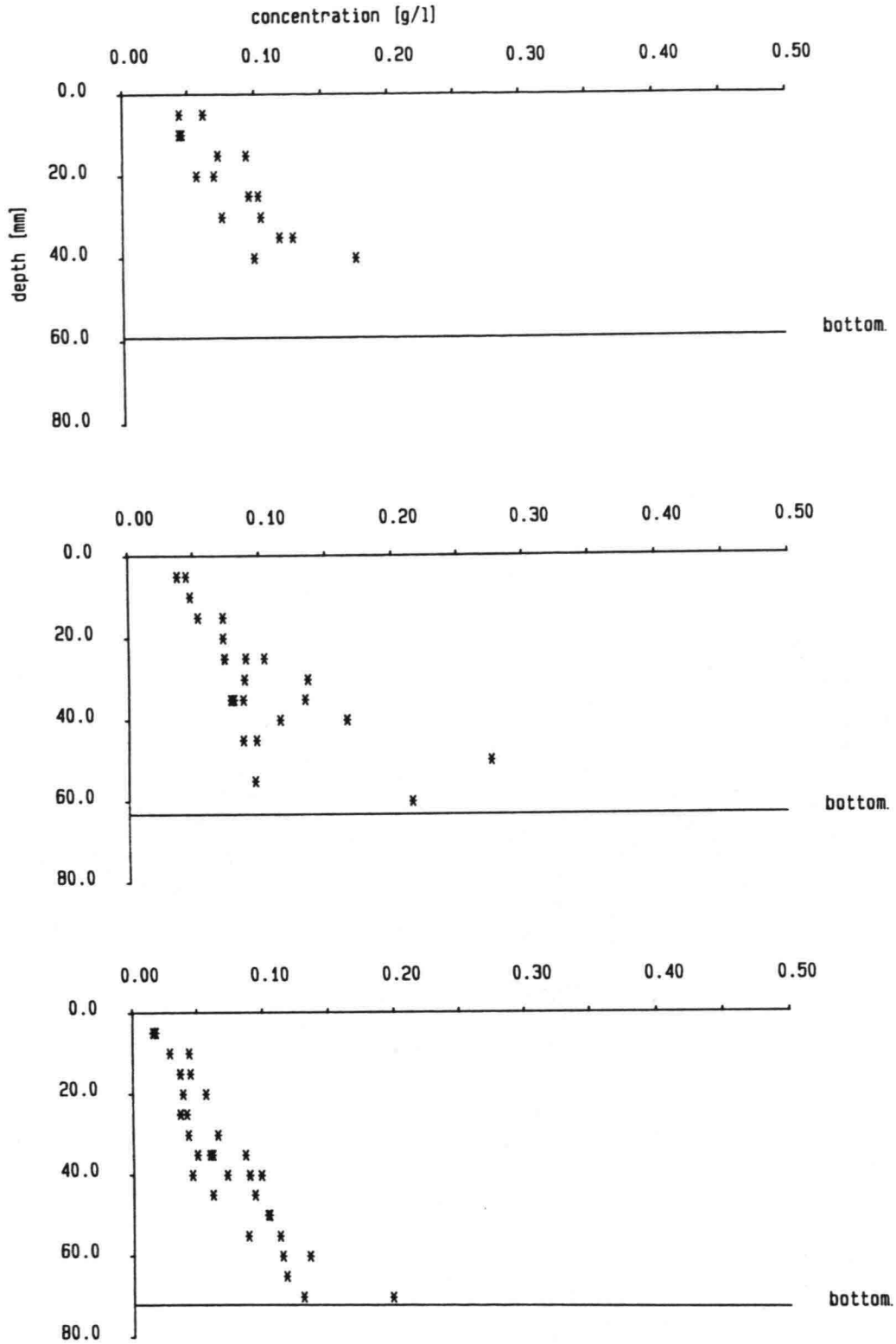

CONCENTRATION PROFILES AT CROSS-SECTION 40
(mean water depth of 10 measurements)

FIG. 11 b

DELFT UNIVERSITY OF TECHNOLOGY

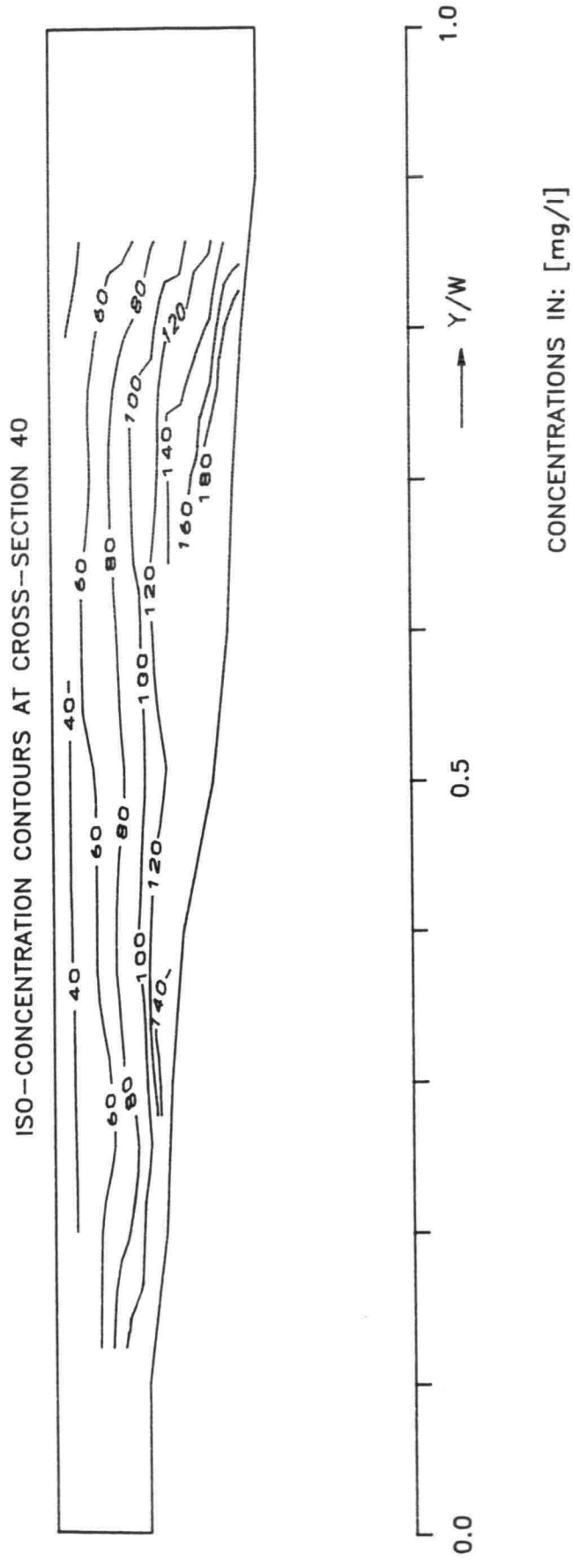

ISO-CONCENTRATION CONTOURS AT CROSS-SECTION 40

FIG. 11 C

DELFT UNIVERSITY OF TECHNOLOGY

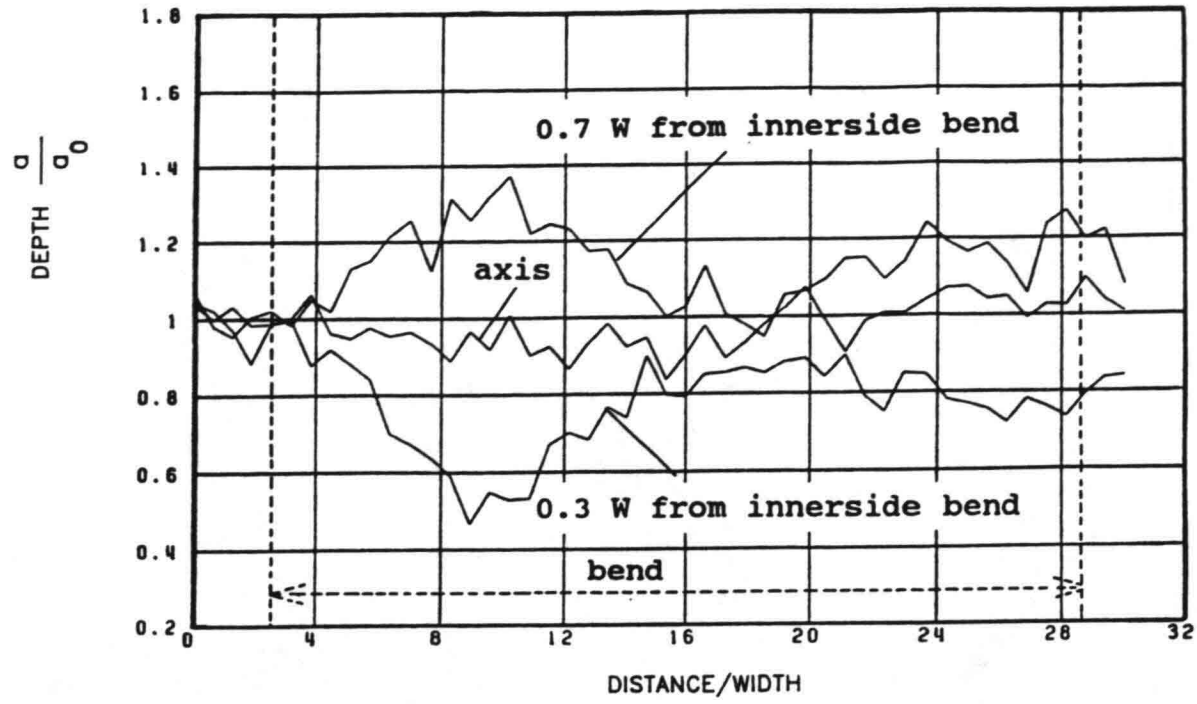

W = 0.5 M A0 = 0.051 M

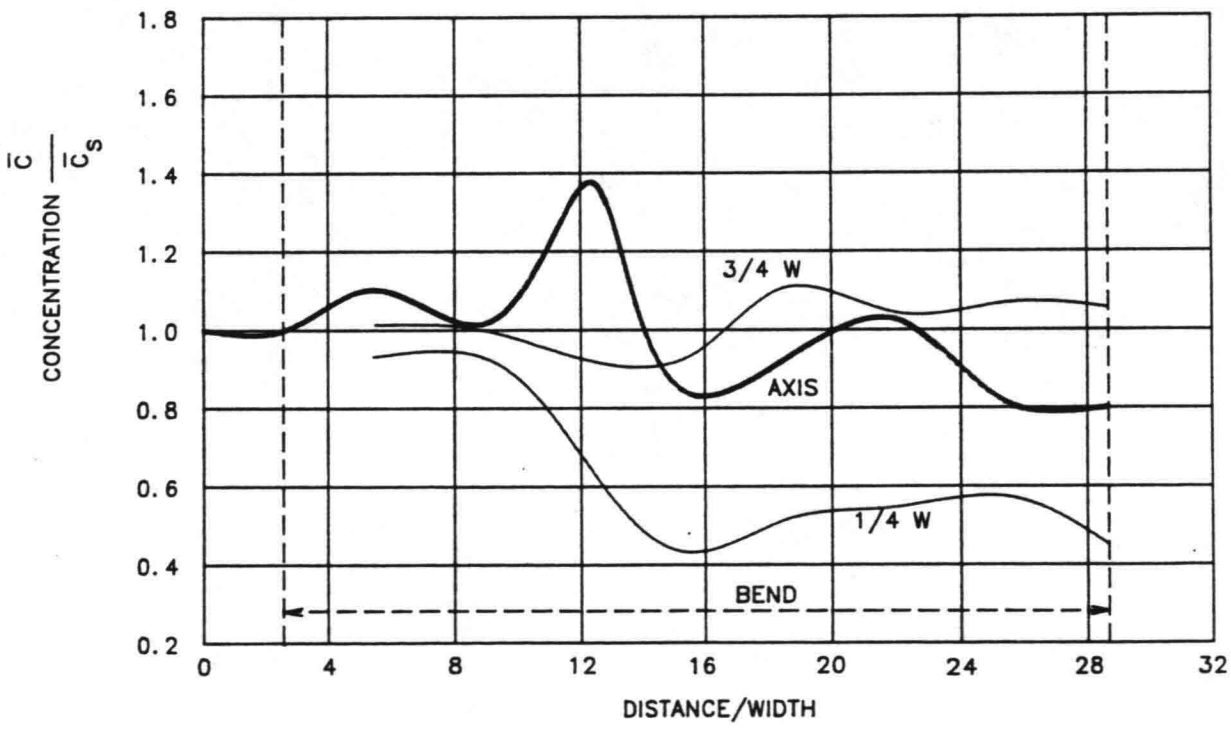

$\bar{c}_s$ = 0.093 g/l z_r = 0.15 a

DEPTH AVERAGED CONCENTRATION FIELD

FIG. 12

DELFT UNIVERSITY OF TECHNOLOGY